University of Alberta

Modeling, Measurement and Mitigation of Power System Harmonics

by

Alexandre Nassif

A thesis submitted to the Faculty of Graduate Studies and Research
in partial fulfillment of the requirements for the degree of

Doctor of Philosophy

Electrical and Computer Engineering

Fall 2009
Edmonton, Alberta

Examining Committee

Wilsun Xu, Electrical and Computer Engineering

Venkata Dinavahi, Electrical and Computer Engineering

Yunwei Li, Electrical and Computer Engineering

Ted Heidrick, Mechanical Engineering, University of Alberta

Juri Jatskevich, Electrical and Computer Engineering, University of British Columbia

Abstract

Power system harmonics and interharmonics are power quality concerns that have received a great deal of attention in recent years. These phenomena can have several adverse effects on power system operation. The main harmonic and interharmonic sources are devices based on power electronics.

An emerging class of harmonic sources is comprised of power electronic-based home appliances. These appliances are dispersed throughout the low-voltage distribution system, and their collective impact can result in unacceptable levels of voltage distortion. The characterization of home appliances based on their harmonic currents is an important step toward understanding the impact of these devices. This thesis presents an evaluation of the relative severity of the harmonic currents from these devices, and the impact of the disparity of the harmonic current phase angles.

Typically, the voltage supplied to each harmonic source is already distorted. This distortion causes a change of the harmonic current magnitudes (traditionally referred to as the attenuation effect). Common harmonic analysis methods cannot take this variation into account because they use a typical harmonic current source model specified by a supply voltage having little or no distortion. This thesis characterizes the harmonic attenuation effect of power electronic-based appliances. One of the findings is that harmonic amplification, rather than attenuation, can occur under credible voltage conditions. This finding had not been made previously. In order to include the harmonic attenuation/amplification in appliance modeling, a measurement-based harmonic modeling technique is proposed.

One of the most economic and effective ways to mitigate harmonics in power systems is through the use of harmonic shunt passive filters. These filters can be of many topologies. Selecting these topologies is a task that, today, depends on the experience and

judgment of the filter designer. An investigation is carried out on the common filter topologies, and the most cost-effective topologies for mitigating harmonics are identified.

As many of the larger harmonic loads also generate interharmonics, interharmonics have become prevalent in today's medium-voltage distribution system. Mitigation cannot be carried out until the interharmonic-source location is known. A method for interharmonic source determination is proposed and then verified through simulation and field measurement studies.

Acknowledgements

I would like to show my appreciation to Dr. Wilsun Xu. I cannot simply say that this thesis would not have been written without him; I must say that without his endless patience and tireless will to guide and supervise me, I would have never conducted this work. I will always be proud to say I had the privilege of being his student, and I hope to have learned enough to succeed in my future career.

I thank Alberta Ingenuity Fund and iCORE for their generous grants provided for more than 4 years. I am also thankful to the University of Alberta, for providing me with one year of the Provost Doctoral Entrance Scholarship, to Dr. Xu, for providing me with several terms of R.A., to the ECE department for providing me with several terms of T.A, and to GSA for providing me with a PD travel grant. This collection of financial sources made my student life a lot more enjoyable, and is very much appreciated.

I thank my parents Antonio and Yeda for supporting me in so many different ways. They supported my coming to Canada and my desire to spend another half decade in school. This is also extensive to my siblings, who have always loved me.

I am deeply obliged with my wife Michelle. Without her encouragement, I would not have continued my Ph.D. when I faced some of the major obstacles. Michelle is the person who most loved and motivated me during the past 3 years. I wish to lead our family to an eternal, healthy and fulfilling relationship. I would also like to express my gratitude to the love and support from my parents-in-law, Glen and Aline.

I am grateful to Dr. Jing Yong, for her supervision, patience, and concerns about our collaborative research. I thank Yunfei Wang, Jacek Kliber, Enrique Nino, Dr. Walmir Freitas, Hugo Ayres, Carlos Almeida, Xiaoyu Wang, Wencong Wang, Sami Abdulsalam, and Thavatchai Tayjasanant, for the friendship and fruitful discussions through many years. I want to acknowledge all the other members of the power lab as well, whose names are not mentioned here. I also recognize the assistance of Albert Terheide with numerous laboratory experiments.

Finally, I thank the committee members of this examination for the valuable comments that helped in improving the quality of this thesis: Dr. Wilsun Xu, Dr. Venkata Dinavahi, Dr. Yunwei Li, Dr. Ted Heidrick, and Dr. Juri Jatskevich.

CONTENTS

LIST OF FIGURES

LIST OF TABLES

Chapter 1

Introduction

Power system harmonics is one of the power quality concerns that have received a great deal of attention recently. The techniques for harmonics measurement and analysis have continuously evolved during the last decades, as a result of the developments in power electronic technology. Generally speaking, solid state power electronic components, which are used for industrial, commercial or residential purposes, comprise an increasingly larger portion of the total connected load [1]. This trend has increased the concern about harmonic voltage and current distortion levels, which can become considerable and exceed today's allowable distortion limits. In this introductory chapter, an overview of harmonics is presented. The chapter then discusses the scope of the thesis and presents the thesis outline.

1.1 Power System Harmonics

Power systems apparatuses are designed to operate with pure sinusoidal alternating voltages and currents at 50/60 Hz frequency. Utilities strive to provide such kind of supply to the end users. Ideally, the current flowing to the customer load and the supply voltage have waveforms of identical shapes. This ideal situation is possible only for the hypothetical case where the customer load is purely linear. In practice, generally the current drawn through the power utility service is a nonlinear function of the voltage and shows periodic distortions superimposed onto a 60Hz sinusoidal current waveshape. These distortions can be decomposed into sinusoidal components of frequencies multiple of the fundamental frequency (e.g., 180 Hz, 300 Hz, 420 Hz), which are called harmonics [2]. Conversely, harmonics, when combined with the fundamental frequency component, cause waveform distortions. Harmonics have been a concern in power systems since the adoption of alternating current for electric energy transmission. Loads that draw current waveforms that are not linearly related to the supply voltage are called nonlinear loads.

When the current waveform contains harmonics not linearly related to those presented in the supply voltage, the nonlinear load is said to be a harmonic source.

1.1.1 Harmonic Generation Process

Currently, the most common sources of harmonics are nonlinear power electronic loads based on the principle of rectification (conversion from AC to DC). This principle is responsible for the generation of several harmonics. Since the DC side is behind a thyristor bridge (see Figure 1.1), the AC current will be highly distorted, and harmonics will be present in the AC side. Figure 1.1a and Figure 1.1b show the basic configuration of a 6-pulse thyristor bridge and the AC current waveform and its spectrum in the upper and lower part, respectively.

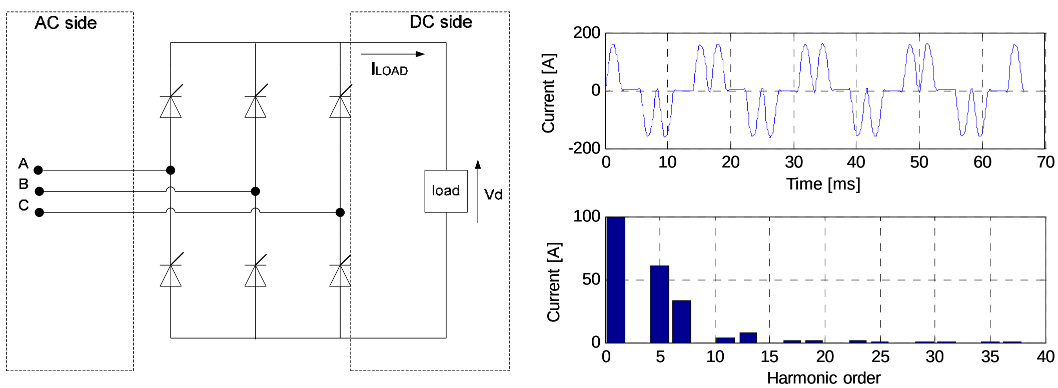

(a) (b)

Figure 1.1. Three-phase rectification: (a) 6-pulse thyristor bridge and (b) AC side current and current spectrum

The typical spectrum of the current drawn by a 6-pulse diode bridge contains the following harmonics:

$$n = 6k \pm 1, \tag{1.1}$$

where n is the harmonic order, and k is any integer 1, 2, 3, etc. The mathematical basis of harmonics is provided next.

1.1.2 Mathematical Basis of Harmonics

Power systems are designed to supply and operate undistorted sinusoidal voltage and current waveforms. In reality, however, power systems do not do so. Large deviations from ideal supply conditions are commonly experienced. Nonlinear loads draw currents that are not linear with the supply voltage, and these currents are usually polluted with distortions that can be represented mathematically as sine waves that repeat themselves with a frequency that is an integer multiple of the fundamental frequency, thereby resulting in the flow of harmonic currents [3], [4].

Harmonics are a mathematical way of describing a steady-state nonsinusoidal voltage or current waveform [5]. Under periodic conditions, distorted voltage and current waveforms can be expressed in terms of a Fourier series. The Fourier series for a periodic function *f(t)* with a fundamental angular frequency ω can be represented as [6]

$$f(t) = a_0 + \sum_{h=1}^{\infty}\left[a_h \cos(h\omega t) + b_h \sin(h\omega t)\right], \tag{1.2}$$

where the angular frequency is $\omega = 2\pi/T$, and T is one fundamental-frequency period. The coefficients a_0, a_h and b_h are defined as

$$a_0 = \frac{1}{2\pi}\int_{-\pi}^{\pi} f(\omega t)\, d(\omega t), \tag{1.3}$$

$$a_h = \frac{1}{\pi}\int_{-\pi}^{\pi} f(\omega t)\cos(h\omega t)\, d(\omega t), \tag{1.4}$$

$$b_h = \frac{1}{\pi}\int_{-\pi}^{\pi} f(\omega t)\sin(h\omega t)\, d(\omega t). \tag{1.5}$$

The root mean square (RMS) value of *f(t)* is defined as

$$RMS = \sqrt{a_0^2 + \sum_{h=1}^{\infty}\left(\frac{\sqrt{a_h^2 + b_h^2}}{\sqrt{2}}\right)^2}. \tag{1.6}$$

When the fundamental frequency component is defined as a cosine, the combined waveforms containing harmonics will show even symmetry. A function f is said to be an *even* function if for any number x, $f(-x) = f(x)$. As a result, the Fourier series can be simplified as

$$a_h = \frac{4}{T}\int_0^{T/2} f(t)\cos\left(\frac{2\pi ht}{T}\right)dt, \tag{1.7}$$

$$b_h = 0. \tag{1.8}$$

Harmonics are combined so that the resulting waveform is no longer undistorted. Figure 1.2 presents a typical current waveform generated by a harmonic-producing load in power systems of 60 Hz fundamental frequency. The figure depicts the decomposed fundamental and 5th harmonic components of this waveform.

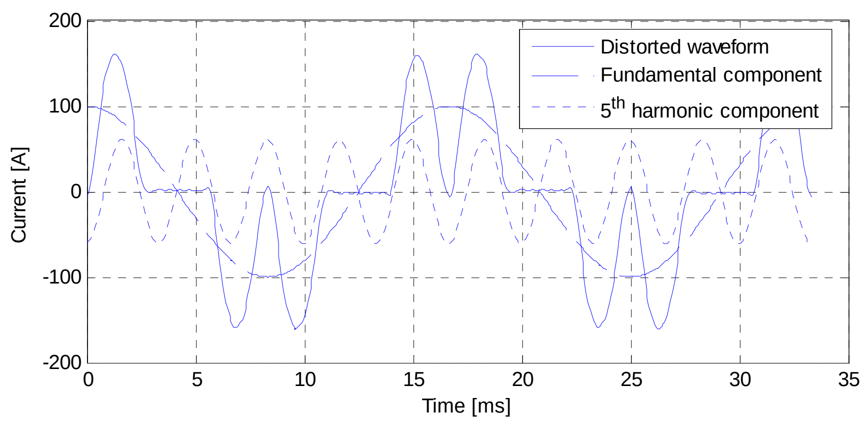

Figure 1.2.Typical distorted current waveform in electric power systems

1.1.3 Harmonic Indices

The most common index to measure the waveform harmonic distortion is called Total Harmonic Distortion (*THD*), which quantifies the harmonic content of the voltage and current waveforms relative to the fundamental frequency component. For the determination of the voltage and current *THD*, the IEEE definition [3] is adopted in this thesis:

$$THD_V\left(\%\right)=\frac{\sqrt{V_2^2+V_3^2+\ldots+V_h^2}}{V_1}\times 100, \tag{1.9}$$

$$THD_I\left(\%\right)=\frac{\sqrt{I_2^2+I_3^2+\ldots+I_h^2}}{I_1}\times 100, \tag{1.10}$$

where V_1 and I_1 are the RMS value of the fundamental, and V_h and I_h are the RMS value of the h-order harmonic component.

The current *THD*, however, is a measure of the current harmonic distortion relative to the fundamental harmonic current. This index, therefore, is not the most appropriate one to use for our purposes because it is not able to measure the harmonic injections from a single customer into the utility grid. A more appropriate index is called Total Demand Distortion (*TDD*), which is defined as [3]

$$TDD\left(\%\right)=\frac{\sqrt{I_2^2+I_3^2+\ldots+I_h^2}}{I_L}\times 100, \tag{1.11}$$

where I_L is the maximum load demand.

According to [3], for a voltage level of less than 69 kV, the voltage *THD* standard limit is 5%. The current *TDD* standard limit depends on the ratio of the short circuit current level available at the point of common coupling to the maximum load current (I_{sc}/I_L). For a voltage level between 120 V and 69 kV, the current *TDD* limit varies between 5% and 20% for a I_{sc}/I_L ratio less than 20 and greater than 1000, respectively.

In the presence of harmonics, the total power factor (*PF*) is calculated as [7], [8]

$$PF=\frac{P_{rms}}{S_{rms}}=\frac{P_1+P_H}{V_{rms}\times I_{rms}}, \tag{1.12}$$

where

$$P_H = \sum_{h \neq 1} V_h I_h \cos\theta_h, \tag{1.13}$$

and θ_h is the angular difference between the harmonic voltage and current.

When $THD_V < 5\%$ and $THD_I > 40\%$,

$$PF = \frac{P_{rms}}{S_{rms}} = \frac{P_1 + P_H}{S_{rms}} \approx \frac{1}{\sqrt{1 + THD_I^{\,2}}} \times FPF, \tag{1.14}$$

where FPF is the 60 Hz power factor given by $FPF = P_1/S_1 = cos(\theta_1)$, and P_{rms} and S_{rms} are the total real and apparent powers including the harmonics.

Several other indices are explained in [3], such as the Telephone Influence Factor (*TIF*), which is used to measure the telephone interference, and the *K*-factor index, which is used to describe the impact of harmonics on losses and to de-rate equipment such as transformers [5].

1.1.4 Sources and Effects of Power System Harmonics

Prior to the commercialization of power semiconductors, the main sources of harmonics were arc furnaces, the accumulated effect of fluorescent lamps, and, to a lesser extent, electrical machines and transformers [5]. The increasing use of power electronic devices has recently increased the concern about waveform distortion. Typical harmonic sources are now adjustable speed drives (ASDs), personal computers (PCs), compact fluorescent lamps (CFLs), and electronic-ballasted regular fluorescent lamps, televisions, and many other devices that use AC/DC conversion. Common harmonic sources can be categorized as follows [5], [9]:

- Power electronic devices: the main purpose today for using switching power electronic devices in common loads is the capability for drawing current during a portion of a fundamental frequency cycle. This switching provides an increase on the load efficiency and controllability. Although beneficial for the load, this effect is detrimental for the power system, as the immediate side effect is an increase in the harmonic levels in the utility grid. The main power electronic-based harmonic sources are single-phase converters, three-phase converters, and some types of Flexible AC Transmission Systems (FACTS) devices. The term converter is used throughout this thesis to denote a broad range of devices with many topologies. Single-phase converters, for example, are the AC-DC interface of almost all electronic home appliances, computers, televisions, electronic-ballasted discharge lamps, etc.

- Arcing devices: harmonics from arcing devices are generated as a result of the nonlinear relationship between the voltage and current due to the physical nature of the electric arc. The main harmonic sources in this category are the electric arc furnace, discharge-type lighting with magnetic ballasts, and arc welders.
- Electromagnetic saturable devices: harmonics from electromagnetic saturable devices are generated due to the nonlinearity of the magnetic core caused by the electromagnetic saturation. This phenomenon occurs mainly in power transformers.

Each power system apparatus has a distinct sensitivity to harmonics, and therefore the harmonics flowing in power systems affect each type of apparatus differently. Harmonic distortion may have several effects including the following:

- Stress on cables: harmonics cause voltage and current stress on power cables and lead to dielectric failure [3].
- Shortening of capacitor life: power factor correction capacitors provide low shunt impedance for high-order harmonics. Harmonic currents flowing through capacitor banks can increase the dielectric loss and thermal stress. When excessive, the capacitor can be overloaded, and damage may occur [9].
- Amplification due to resonance: amplification of harmonic levels resulting from series and parallel resonances can occur as capacitors are added to the power system. If voltage amplification occurs, magnified harmonic currents will also exist in the resonant circuit [10].
- Premature ageing: the insulation of electrical plant components can age prematurely [7].

- Losses and pulsating torque on electrical machines: in rotating machines, losses increase due to harmonics, and overheating may happen as a result [12]. Pulsating torques can be produced, resulting in a higher audible noise [5].
- Transformer overheating: in transformers, the primary effect is the additional heat generated by the losses caused by the harmonic content of the load current. Delta-connected windings can be overloaded by the circulation of zero-sequence harmonic currents [11]-[13].
- Telephone interference: harmonic effects have also been observed to degrade communication system performance due to interference caused by power system harmonics with the communication system frequency [5].
- Malfunction of electronic loads: power electronic loads that are sensitive to AC supply voltage characteristics, such as zero crossing, can malfunction [10], [13].
- Metering errors: metering and instrumentation can be affected by harmonic components [3], [13].

1.1.5 Power System Interharmonics

IEC-61000-2-2 defines power system interharmonics as the frequencies that occur "[b]etween the harmonics of the power frequency voltage and current" and "which are not an integer of the fundamental" [14]. Furthermore, these frequencies "can appear as discrete frequencies or as a wide-band spectrum" [14]. A more recent draft re-defines interharmonics as "[a]ny frequency which is not an integer multiple of the fundamental frequency" [15]. Interharmonics, therefore, are spectral components of frequencies that are non-integer multiples of the system fundamental frequency. Interharmonic generation from interharmonic-producing loads can be explained by using a current-source inverter ASD as an example. An ASD converts a 60-Hz input into an output with a different frequency as shown in Figure 1.3.

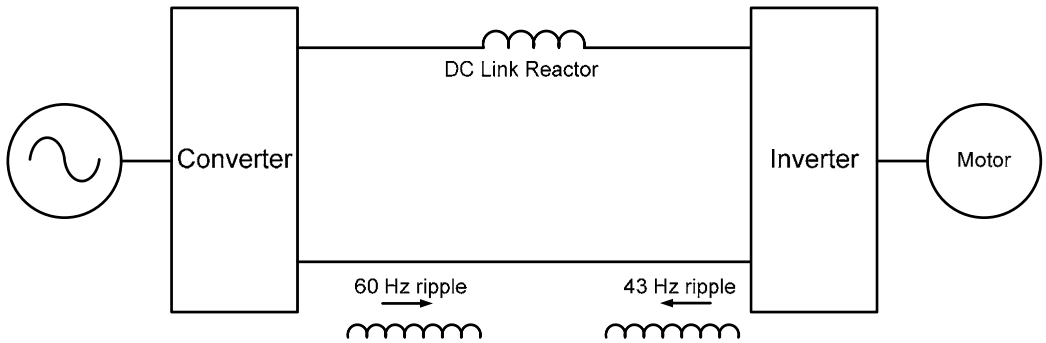

Figure 1.3. Generation of Interharmonics from an ASD

If the motor is running at 43 Hz, this frequency will be seen at the DC link as a ripple of 43 Hz times the pulse number of the inverter. As a result, the current of the DC link actually contains both 60 Hz (due to the supply voltage) and 43 Hz caused ripples (due to the motor voltage). Since the supply side current is related to the DC link current through the converter, the 43 Hz caused ripples will penetrate into the supply side and present themselves as interharmonics because $43\times(\text{pulse number})$ is not an integer multiple of 60 Hz. To illustrate the effect of interharmonics on a sample waveform, a simulated case of a current waveform is shown in Figure 1.4, along with its spectrum. In this case, one 130 Hz interharmonic of a relative magnitude of 20% is superimposed onto the fundamental frequency current, as

$$i(t)=\cos(2\pi\times 60t)+0.2\times\cos(2\pi\times 130t). \tag{1.15}$$

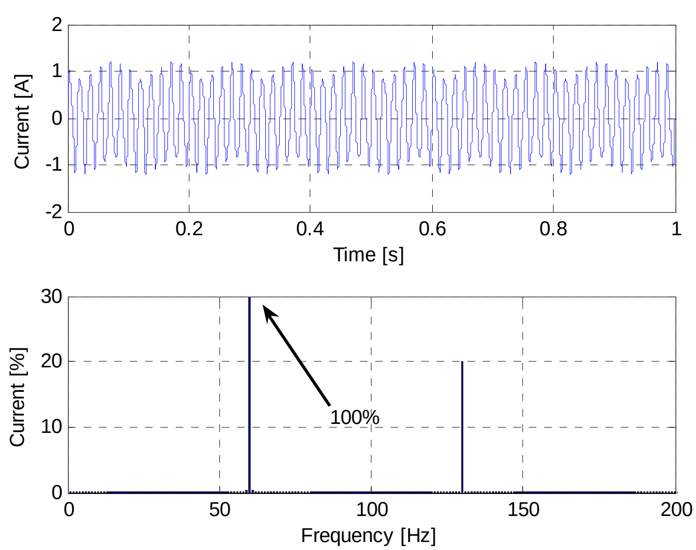

Figure 1.4. Simulated waveform containing interharmonics.

Harmonics and interharmonics do not share the same meaning and definitions, but can originate from the same sources and have similar effects. In other words, some of the harmonic sources also generate interharmonics, and most of the harmonic effects are also interharmonic effects. The main sources of interharmonic are static frequency converters, cycloconverters, fluctuating loads, arc furnaces, and ASDs [16]-[20]. In addition to the typical harmonic effects, interharmonics can also cause torsional oscillations, voltage and light flicker, and interference with control signals, even for low-amplitude levels [21]-[23]. Interharmonics also increase the difficulties in modeling and measuring distorted waveforms [16].

The interharmonic generation characteristics of ASDs with a p_1-pulse rectifier and a p_2-pulse inverter are expressed as [18]

$$f_{IH} = \left| \left(p_1 m \pm 1 \right) f \pm p_2 n f_z \right|, \quad m = 0,1,2...; \quad n = 1,2,3..., \tag{1.16}$$

where f and f_z are the fundamental and drive operating frequency, respectively. This equation shows that the frequencies characterizing the interharmonics are non-integer multiples of the fundamental frequency. Therefore, to characterize distortions of a waveform containing interharmonics, a long window for the Fourier analysis must be used to obtain adequate resolution. If the length of the data is selected as N cycles ($N>1$) of the fundamental frequency, the frequency resolution will be

$$\Delta f = \frac{1}{N \times T} = \frac{f}{N}. \tag{1.17}$$

For example, if $N = 12$, the frequency resolution is 5Hz, and the spectrum results will show components of 5Hz, 10Hz, 15Hz… To detect the interharmonics existing in the signal, the width of the window should be chosen to allow the frequency resolution to be the common divider of all frequency content contained in the signal [16].

1.2 Thesis Scope and Outline

The scope of this thesis is the study of harmonics and interharmonics in power systems. Most of the past research on power system harmonics has focused on systems with few large harmonic loads. In these typical systems, high harmonic distortion levels could be observed. Currently, however, power electronic-based harmonic sources of small ratings have proliferated for two main reasons: (1) these loads' decreased cost have increased adoption by all levels of customers, and (2) power electronics are one way to improve the use of energy by these devices. For example, most energy-saving devices save energy by using power electronics. This mass penetration of power electronic loads results in more harmonics being injected into the electric distribution grid.

At the residential level, many types of harmonic-generating home appliances are present, but the study of this new scenario is relatively new and challenging. Each of the numerous types of home appliances has its own characteristics. In order to understand the harmonic impact of the collective load of home appliances installed on a large scale, these appliances' current harmonics must be completely understood. Chapter 2 of this thesis presents a study of the current harmonics from single-phase harmonic-generating modern home appliances. In this chapter, developed indices are used to compare the magnitudes and phase angles of the harmonic currents. The indices dealing with the harmonic current magnitudes can be used to benchmark the harmonics from home appliances, whereas those dealing with the harmonic current phase angle can be used to understand the harmonic cancellation due to phase angle disparity. This study provides insight into the relative severity of the harmonic currents of these devices and also into the harmonic cancellation of an aggregation of appliances.

The harmonic current characteristics of power electronic-based home appliances depend on the voltage supply conditions. This effect is traditionally called the attenuation effect and generally means that a supply voltage waveform containing high harmonic content causes the load to produce less harmonic current. The traditional way of modeling harmonic loads, namely the constant current-source model, does not consider the attenuation effect. This limitation could result in current harmonic estimations that are too conservative to be useful [4]. Ever since the attenuation effect was first characterized, it has been given increasing importance in harmonic studies [24]. To achieve accurate characterization of power electronic-based devices, therefore, the attenuation effect must be included in the nonlinear load modeling. Chapter 3 of this thesis presents a characterization of the harmonic attenuation effect of single-phase power electronic-based home appliances. The study is conducted by using measurements and analytical results. Chapter 4 introduces a frequency-domain measurement-based harmonic modeling technique for home appliances. The technique is based on least-squares data fitting and is used for determining a harmonic model that is functional for a practical range of supply voltage conditions. This model considers the harmonic attenuation effect and therefore is more accurate than the traditional constant current injection model.

With many sources of harmonics dispersed throughout the power system, harmonic voltage levels can be in excess of the limits imposed by international standards [3], so harmonic mitigation schemes become imperative. Shunt passive filters are the most widely employed solution for harmonic mitigation because of their low cost, reliability and simplicity [5], [10], [25]. For a utility, an important consideration when planning to use harmonic filters is the voltage level of the buses where the filter should be installed. Several studies have shown that installing medium-voltage filters provides a better solution than installing multiple low-voltage filters [26]-[28]. Filters have several topologies that give different frequency response characteristics. The current industry practice is to combine filters of different topologies to achieve different harmonic filtering goals. However, information is lacking on how to select the topologies. Currently, their selection is based on the experience of the filter designers. Chapter 5 presents research results on the effectiveness and cost of various filter topologies for harmonic mitigation and recommends using the best passive filter topologies to strike a balance between performance and cost.

Due to the widespread use of ASDs and static frequency converters, interharmonics have also become a power quality concern in medium-voltage distribution systems. The cause of a problem cannot be identified, and mitigation schemes cannot be designed until the interharmonic source has been identified. No practical and reliable algorithms to determine the source of interharmonics have been developed. Chapter 6 of this thesis approaches the problem of interharmonic source identification and introduces a method for interharmonic source determination. The proposed method overcomes some of the practical limitations of traditional source detection methods and is able to determine the direction of an interharmonic source.

The main conclusions from this work, and suggestions for future studies and improvements are presented in Chapter 7.

Chapter 2

Current Harmonics from Modern Home Appliances

Currently, most home appliances in modern houses are based on power electronics. Single-phase power electronic-based devices convert the AC current into a DC current. In order to obtain a DC current, a rectifier is needed. Through the use of power electronic switches, this rectifier is able to draw the AC current during part of a 60 Hz fundamental cycle. For this reason, many home appliances draw AC currents that are pulse-shaped or triangular-shaped. As a result, power electronic loads generally inject relatively large harmonic currents into the utility grid. The collective effect of multiple harmonic loads represents a power quality concern in distribution systems [4]. Collectively, CFLs, laptops, desktops, microwave ovens, ASD-driven washers and furnaces can contribute considerably to the harmonic currents injected into the distribution feeder. Therefore, it is important to study and characterize common home appliances.

This chapter presents a study of the harmonic current characteristics of harmonic-generating modern home appliances. These characteristics are compared to show the main differences among these devices. Two approaches are proposed to perform this assessment. Firstly, magnitude-related indices are introduced to make a consistent comparison of the harmonic impacts of the various appliances and to evaluate their relative severity. Secondly, phase angle-related indices are introduced to study the diversity of the current harmonics phase angle among the devices and to understand its effect on the harmonic cancellation.

2.1 Introduction

In the past, most of the residential customer loads were typically linear, and the harmonics coming from these loads were not a significant concern. Currently, however, power electronic-based home appliances have proliferated, partly because of the need to utilize energy efficiently. For example, in the past, lighting loads were predominantly resistive, and heating/ventilation/air-conditioning were mostly a combination of resistive and motive; today, the former are being gradually replaced by CFLs and the latter are being gradually replaced by Variable Speed Air Conditioning (referred to as HVAC – Heat, Ventilation and Air Conditioning) [30]. Even though being power electronic-based and being energy-efficient are not synonymous, most of the energy-efficient loads are based on power electronics. In general, these appliances consume considerably less power than their older counterparts [29]-[32].

Among the loads typically present inside a residential customer's home, the lighting load represents a significant portion of the total power consumed by the house. Surveys conducted by the International Energy Agency (*IEA*) reveal that the average number of lamps inside an average residential customer's home is 25, and that this number is higher in North American houses (Canadian houses have an average of 27-30 lamps, and US houses have an average of 30 [33]-[34]). If the lighting load consists mainly of incandescent lamps, it may account for a significant share of a customer's energy bill. The associated lighting consumption can be reduced by 75-80% when fluorescent lamps replace incandescent lamps [35]. Today, it is estimated that 25% of the residential installed lamps are CFLs [36]. As this relative amount increases, the impact of the current harmonics from the collective load of mass-installed CFLs may become noticeable [37]-[38]. Notably, the CFL has been the focus of most of the studies of home appliances.

The literature has documented the measurement of CFLs, TVs, PCs, and air conditioners, as well as their measured or estimated harmonic effects on medium-voltage distribution feeders [39]-[42]. However, the question "Which are the most significant home appliances from the perspective of harmonics currents?" has not been addressed, as no comparative study of home appliances harmonics has been published. In this chapter, a comparison of the harmonic currents from popular home appliances is provided. This subject is important because it has been claimed that the harmonics from mass-deployed

CFLs are likely to be one of the main power quality concerns in residential areas in the near future [35], [37]-[38], for incandescent lamps are being banned in many countries.

In order to address this question, two studies of the appliances' harmonic currents are conducted in this chapter. The first study deals with the magnitudes of the harmonic currents and ranks the harmonic pollution of the home appliances. Since the comparison uses the current magnitudes only, the phase angles are not considered. In order to address more accurately the impact of a collective load of appliances, the harmonic current angles should be considered in order to predict how much harmonic cancellation can occur. Therefore, the second study tackles the phase angle issue. In both studies, indices are proposed to assess the current harmonics of the home appliances.

2.2 Characteristics of Common Home Appliances

The aim of this section is to present the characteristics of the measured common appliances. In order to record the appliances' voltages and current waveforms, the measurement set-up presented in Figure 2.1 was used. The measurements were made by using a Data Acquisition NI 6020E. This instrument has eight channels for simultaneous recording with an adjustable sampling rate. The voltage and current waveforms are measured by using voltage and current probes. The waveform data can be acquired by connecting the recorder to a laptop via a USB interface. The features and accuracy of the instruments are described in Appendix C.

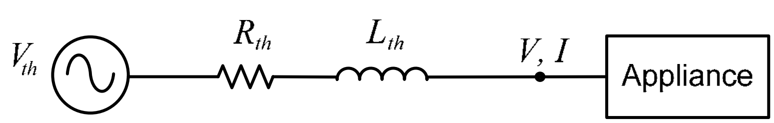

Figure 2.1. Measurement set-up to measure the home appliances

The measured appliances are explained in Table 2.1. Codes are assigned to them for easy identification in the figures and tables shown later. This table also identifies the number of measured appliances of each type. The incandescent lamp and the regular laundry dryer are not significant sources of harmonics, but were analyzed in this study for further information.

Table 2.1. Measured Home Appliances

Appliance type	**Code**	**# Tested**
Compact Fluorescent Lamp	CFL	12
Electronic-Ballast Fluorescent Lamp	EBL	3
Magnetic-Ballast Fluorescent Lamp	MBL	1
Incandescent Lamp	INC	1
Desktop PC	PC	5
LCD Computer Monitor	LCD	5
Laptop	LAP	5
LCD High-Definition Television	LCD TV	4
CRT Television	CRT TV	1
Microwave oven	MW	3
ASD-based Fridge	ASD FR	3
Regular Fridge	R FR	2
ASD-based Washer	WSH	2
ASD-based Dryer	ASD DRY	1
Regular Dryer	DRY	2
Furnace	FUR	1

Detailed results for all measured appliances are presented in Appendix A along with the data-processing methods. As shown in Table 2.1, more than one piece of equipment of the same type was measured for most of the appliances. The typical waveforms and spectra used to carry out the studies in this chapter were obtained for each type of appliance as described in Appendix A.

Table 2.2 shows the main electric results obtained for the various measured appliances. Those results include the fundamental power factor (*FPF*) and total power factor (*PF*), which were calculated by using the IEEE definition [7]-[8]. Some appliances have different operating cycles that exhibit different power consumption and harmonic current characteristics. For example, a washing machine can have washing, rinsing and spinning cycles. Other appliances, such as the CFLs, exhibit almost constant power consumption. In order to provide representative results, various operating cycles were measured. Table 2.2 presents the characteristics for the full load under normal operating conditions. The column of “Operating Power” shows the power consumption under normal operating condition. Therefore, for some appliances, the operating power is less than the rated power. For example, a washing machine may be rated as 500W but actually draws power of 180W during normal operation. In the same example, the washing machine operates most of the time in the washing condition, which is the condition corresponding to the full-load under normal operating conditions, and is also the condition in which the device draws the most distorted current.

The measured appliances are available in a variety of ratings. The tested CFLs are rated 5W-30W, and the tested LCD TVs are rated 75W-300W. The shape of the current waveforms and spectra are, however, similar. A representative rating for each appliance was obtained from survey studies. The most common rating of CFLs was identified as 15W [43]-[44], and therefore this amount of power was adopted as the operating power for this device. Table 2.2 shows that the regular fridges have current harmonic distortion higher than those of the ASD-based fridges, a fact that contradicts the expected results. Extensive measurements conducted in this thesis indeed confirm this fact, as shown in the Appendix A; the measured ASD-based fridges seem to feature harmonic distortion compensation. More details on how to use the operating power to determine the appliance parameters are presented in Appendix A. Table 2.2 confirms that most electronic home appliances are harmonic producers. Many of the electronic appliances such as CFLs, desktop PCs and computer monitors have a THD_I higher than 100%. Table 2.2 also shows that most of the appliances have reasonably high fundamental frequency power factors, and some of them have a leading power factor (indicated by "*" in the table).

Table 2.2. Harmonic Characteristics of the main Home Appliances

Appliance	THD_I [%]	FPF	PF	Operating power [W]	I_{rms} [A]	I_1 [A]
CFL	120	0.9*	0.6	15	0.24	0.15
EBL	140	0.96*	0.56	15	0.24	0.14
MBL	8	0.38	0.38	33	0.73	0.73
PC	112	1	0.69	100	1.30	0.88
LCD	110	0.96*	0.64	40	0.48	0.34
LAP	130	0.96*	0.58	75	1.14	0.68
LCD TV	10	0.99*	0.98	300	2.59	2.58
CRT TV	145	1	0.56	70	1.00	0.57
MW	41	0.99*	0.9	1200	11.08	10.49
ASD FR	7	0.92	0.91	170	1.6	1.6

R FR	16	0.94	0.93	150	1.30	1.27
WSH	75	0.45	0.35	180	4.20	3.36
ASD DRY	55	0.98	0.86	1000	4.90	4.30
FUR	11	0.84	0.84	500	4.85	4.82

The appliances' current phasors at harmonic orders 3rd-13th are shown in Figure 2.2. The phasors use the supply voltage angle as a reference, setting the phase angle of the fundamental frequency voltage to zero. The currents are normalized to emphasize the current harmonic angles and to improve visualization. This figure reveals the potential harmonic cancellation that might occur when 2 or more appliances are operated together. For example, the 3rd harmonic current of the LCD monitor is about *180°* out of phase with that of the furnace. Conversely, the 3rd harmonic of the desktop PC is almost in phase (*0°*) with that of the CRT TV. These two cases are shown in Figure 2.3, which presents the decomposed 3rd harmonic current of these appliances and illustrates the angle displacement and relative magnitudes.

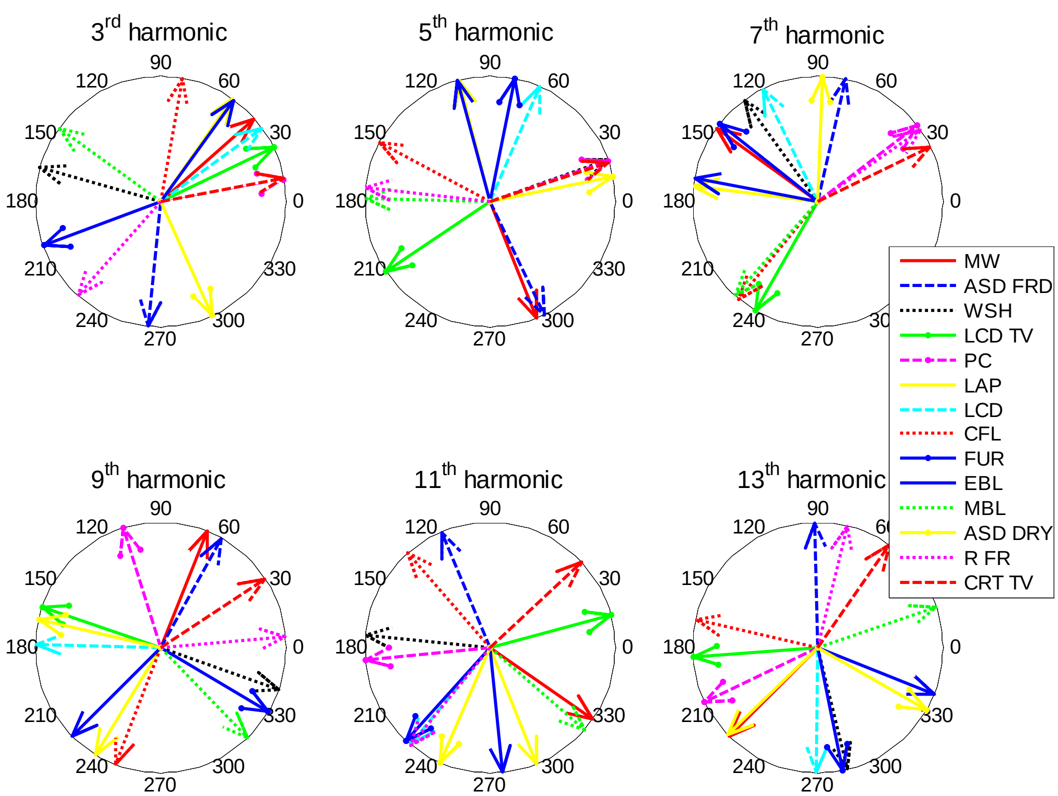

Figure 2.2. Normalized harmonic currents of all appliances using the fundamental voltage phase angle as a reference

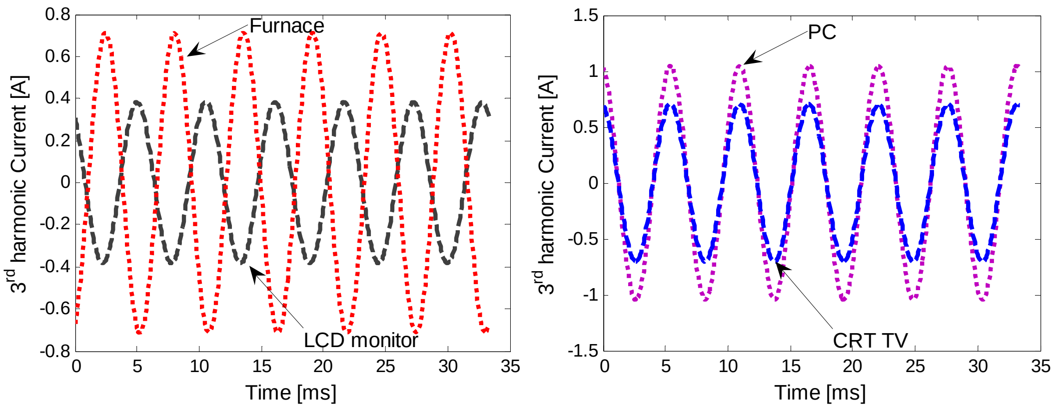

Figure 2.3. Off-phase and in-phase 3rd harmonic currents (decomposed) of selected appliances

In order to deal with the diversity of the magnitudes and phase angles of the various appliances, two studies are proposed. The severities of the harmonic currents are studied by using the Equivalent-CFL index and the harmonic decline rate, as introduced in section 2.3. The harmonic compatibility index is proposed to study the harmonic currents cancellation due to phase angles disparity, and is introduced in section 2.4.

2.3 The Harmonic Magnitude Study

The first part of this section introduces the Equivalent-CFL index to assess the relative severity of the current harmonic magnitudes of the home appliances. In order to provide a consistent comparison, the index is initially calculated based on an appliance template. Of all the power electronic-based home appliances, the CFLs have been most often studied in order to characterize them and determine their harmonic current effects [35], [37]-[38], [45]. Since CFLs have been extensively studied and characterized, it is reasonable to use their current harmonics as a "relative harmonic injection benchmark" for comparing the harmonic injections from the other home appliances. A second study of the current magnitudes is conducted by comparing the current spectrum decline rate (as the harmonic order increases). The harmonic decline rate study provides an indication of the harmonic pollution of each appliance by characterizing its spectra.

2.3.1 Magnitude-Based Equivalent-CFL Index

The Equivalent-CFL index is introduced to provide a quantitative comparison of the harmonic impacts of the appliances. This index quantifies each appliance in terms of its harmonic impact expressed as the number of CFLs it is equivalent to.

This index is defined as follows:

1. For each type of appliance measured, a representative harmonic current of that type is established. This representative current magnitude is obtained from a weight average of the measurements of several types of each of the various appliances. This procedure is explained in Appendix A. Two examples are shown in Figure 2.4: the representative desktop PC and the representative CFL. The operating power of the representative appliances is shown in Table 2.2.

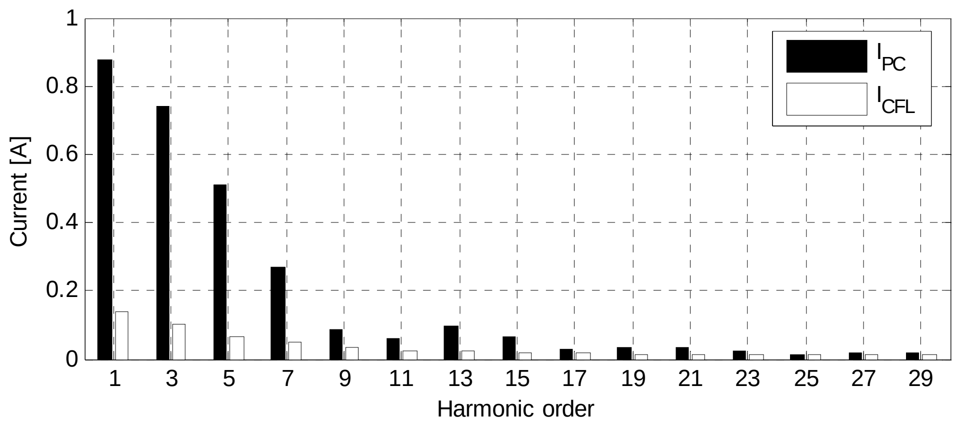

Figure 2.4. Harmonic currents produced by a desktop PC and a CFL

2. For each harmonic order *h*, the ratio of the appliance's current to that of the representative CFL current is determined by using the following equation:

$$Ratio_{h\_Appliance} = \frac{I_{h\_appliance}}{I_{h\_CFL}}, \tag{2.1}$$

where $I_{h\_appliance}$ is the appliance's harmonic current at order *h*, and I_{h_CFL} is the representative CFL harmonic current at order *h*.

For example, a $Ratio_h$ of 2 implies that the appliance generates twice as much harmonic current at order h as the representative CFL. Figure 2.5 shows the ratios for the desktop PC.

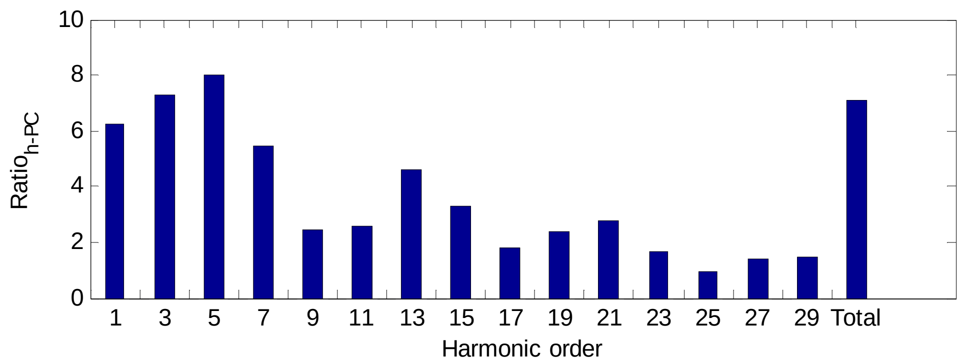

Figure 2.5. Harmonic current ratios of a desktop PC with respect to a CFL

3. In order to obtain a single index and compare the appliance with a representative CFL, the ratios of different harmonic orders are aggregated into one value by using a weighted average as follows:

$$\text{Equivalent-CFL}_{Appliance} = \sqrt{\sum_{h=3}^{H} \left(w_h \times Ratio_{h\_Appliance} \right)^2} = \tag{2.2}$$

$$= \sqrt{\sum_{h=3}^{H} \left(\frac{I_{h\_CFL}}{\sqrt{\sum_{h=3}^{H} I_{h\_CFL}^2}} \times Ratio_{h\_Appliance} \right)^2} = \sqrt{\frac{\sum_{h=3}^{H} I_{h\_Appliance}^2}{\sum_{h=3}^{H} I_{h\_CFL}^2}}.$$

The weighting factor w_h is the individual harmonic distortion of the CFL current. This weighting factor is used because if a CFL produces more harmonics at h, the harmonics from other appliances will also be treated with more significance at the same order. The last bar of Figure 2.5 (labeled as Total) represents the aggregated ratio (i.e., Equivalent-CFL) of the desktop PC.

2.3.1.1 Basic Results Provided by the Magnitude-Based Index

The results obtained from the calculated individual Equivalent-CFL index of all appliances are presented in Table 2.3. The results are arranged in the ascending order of the index. This table shows that a desktop PC is equivalent to 7 CFLs in terms of harmonic current injection. A microwave oven has a harmonic impact equivalent to 26 CFLs, and a laundry washer has a harmonic impact equivalent to 16 CFLs. The table also lists the power ratios with respect to the CFL and the harmonic current ratios from the 3rd to the 13th harmonics.

Table 2.3. Comparing the harmonic impact of one unit of home appliances

Appliance type	Operating Power [W]	Power Ratio	Eq-CFL	$Ratio_3$	$Ratio_5$	$Ratio_7$	$Ratio_9$	$Ratio_{11}$	$Ratio_{13}$
MBL	30	2	0.42	0.56	0.02	0.11	0.08	0.12	0.06
CFL	15	1	1.00	1.00	1.00	1.00	1.00	1.00	1.00
ASD FR	170	11.3	1.14	1.03	0.28	2.74	1.23	0.89	0.60
EBL	18	1.2	1.15	0.99	1.39	1.69	0.60	0.46	1.10
LCD TV	300	20	1.32	1.34	1.56	0.88	0.89	0.58	0.95
R FR	150	10	1.35	1.22	1.33	1.44	1.92	2.08	1.54
LCD	40	2.67	2.35	2.04	3.30	1.24	0.23	1.92	2.43
FUR	500	33.33	2.53	2.68	2.72	1.71	1.26	1.67	1.76
CRT TV	70	4.67	5.81	4.93	6.77	7.02	7.37	7.15	4.42
LAP	75	5	6.15	5.37	5.66	5.57	7.97	11.38	11.05
PC	100	6.67	7.05	7.32	8.02	5.47	2.43	2.58	4.62
ASD DRY	1000	66.67	12.58	15.23	8.26	5.90	10.85	4.90	8.55
WSH	180	12	16.09	12.80	17.83	20.16	22.74	24.57	19.76
MW	1200	80	26.42	33.09	16.72	9.14	7.20	6.13	4.14

2.3.1.2 Comparison among Appliances

To provide a direct comparison of the harmonic currents of all appliances, the index is modified to use all appliances as the template. For each harmonic order h, the ratio of one appliance's representative current to that of the second appliance is determined by using the following equation:

$$Ratio_{h\_Appliance\_1\_2} = \frac{I_{h\_appliance\_1}}{I_{h\_appliance\_2}}, \tag{2.3}$$

where $I_{h\_appliance\_1}$ is the first appliance's harmonic current at order h, and $I_{h\_appliance\_2}$ is the second appliance's harmonic current at order h.

The calculated indices are arranged as shown in Table 2.4-Table 2.6. These tables provide a value that directly quantifies the severity of the harmonic currents of any two given appliances. The presented values are the ratios of the horizontal list element to the vertical one. For example, if the microwave oven and the CFL are compared, the relationship provided by Table 2.4 is $Ratio_{5\_MW\_MBL} = I_{5\_MW}/I_{5\_CFL} = 16.72$. The tables also indicate that the ratio can be quite large when comparing some appliances. For example, the 5th harmonic ratio $Ratio_{5\_MW\_MBL}$ of the microwave to the magnetic-ballasted fluorescent lamp is equal to 720, because the lamp has very low 5th harmonic current magnitude.

Table 2.4. Equivalent-CFL Index Results for 3rd and 5th harmonic

h = 3 / h = 5	MW	ASD FR	WSH	LCD TV	PC	LAP	LCD	CFL	FUR	EBL	MBL	ASD DR	R FR	CRT TV
MW	**1.00**	0.03	0.46	0.04	0.22	0.16	0.08	0.03	0.15	0.04	0.02	0.39	0.02	0.15
ASD FR	60.80	**1.00**	14.82	1.30	7.12	5.22	2.61	0.97	4.86	1.18	0.55	12.46	0.58	4.80
WSH	2.03	0.03	**1.00**	0.09	0.48	0.35	0.18	0.07	0.33	0.08	0.04	0.84	0.04	0.32
LCD TV	10.70	0.18	5.28	**1.00**	5.47	4.01	2.01	0.75	3.74	0.91	0.42	9.57	0.45	3.69
PC	2.09	0.03	1.03	0.19	**1.00**	0.73	0.37	0.14	0.68	0.17	0.08	1.75	0.08	0.67
LAP	2.96	0.05	1.46	0.28	1.42	**1.00**	0.50	0.19	0.93	0.23	0.10	2.38	0.11	0.92
LCD	6.15	0.10	3.04	0.57	2.95	2.08	**1.00**	0.37	1.86	0.45	0.21	4.77	0.22	1.84
CFL	16.72	0.28	8.26	1.56	8.02	5.66	2.72	**1.00**	5.00	1.22	0.56	12.80	0.60	4.93
FUR	5.37	0.09	2.65	0.50	2.57	1.82	0.87	0.32	**1.00**	0.24	0.11	2.56	0.12	0.99
EBL	12.55	0.21	6.20	1.17	6.02	4.25	2.04	0.75	2.34	**1.00**	0.46	10.53	0.49	4.06
MBL	720.64	11.85	355.87	67.35	345.50	243.80	117.19	43.10	134.28	57.43	**1.00**	22.78	1.06	8.78
ASD DR	0.94	0.02	0.46	0.09	0.45	0.32	0.15	0.06	0.17	0.07	0.00	**1.00**	0.05	0.39
R FR	6.29	0.10	3.11	0.59	3.02	2.13	1.02	0.38	1.17	0.50	0.01	6.71	**1.00**	8.26
CRT TV	2.47	0.04	1.22	0.23	1.18	0.84	0.40	0.15	0.46	0.20	0.00	2.64	0.39	**1.00**

Table 2.5. Equivalent-CFL Index Results for 7th and 9th harmonic

h = 7 (columns) / h = 9 (rows)	MW	ASD FR	WSH	LCD TV	PC	LAP	LCD	CFL	FUR	EBL	MBL	ASD DR	R FR	CRT TV
MW	**1.00**	0.30	0.65	0.10	0.60	0.61	0.19	0.11	0.11	0.16	0.01	2.21	0.17	0.77
ASD FR	5.86	**1.00**	2.16	0.32	2.00	2.03	0.63	0.37	0.36	0.53	0.04	7.36	0.57	2.56
WSH	0.66	0.11	**1.00**	0.15	0.93	0.94	0.29	0.17	0.17	0.24	0.02	3.42	0.26	1.19
LCD TV	8.13	1.39	12.25	**1.00**	6.23	6.35	1.95	1.14	1.13	1.64	0.12	22.98	1.77	8.00
PC	2.96	0.51	4.47	0.36	**1.00**	1.02	0.31	0.18	0.18	0.26	0.02	3.69	0.28	1.28
LAP	0.90	0.15	1.36	0.11	0.30	**1.00**	0.31	0.18	0.18	0.26	0.02	3.62	0.28	1.26
LCD	5.73	0.98	8.63	0.70	1.93	6.34	**1.00**	0.58	0.58	0.84	0.06	11.76	0.91	4.09
CFL	7.20	1.23	10.85	0.89	2.43	7.97	1.26	**1.00**	0.99	1.44	0.11	20.16	1.56	7.02
FUR	9.50	1.62	14.30	1.17	3.20	10.51	1.66	1.32	**1.00**	1.46	0.11	20.37	1.57	7.09
EBL	3.75	0.64	5.65	0.46	1.27	4.15	0.66	0.52	0.40	**1.00**	0.07	13.98	1.08	4.87
MBL	88.00	15.03	132.57	10.83	29.68	97.43	15.37	12.22	9.27	23.45	**1.00**	186.41	14.38	64.90
ASD DR	0.32	0.05	0.48	0.04	0.11	0.35	0.06	0.04	0.03	0.08	0.00	**1.00**	0.08	0.35
R FR	33.65	5.75	50.69	4.14	11.35	37.26	5.88	4.67	3.54	8.97	0.38	106.26	**1.00**	4.51
CRT TV	0.98	0.17	1.47	0.12	0.33	1.08	0.17	0.14	0.10	0.26	0.01	3.08	0.03	**1.00**

Table 2.6. Equivalent-CFL Index Results for 11th and 13th harmonic

h = 11 (columns) / h = 13 (rows)	MW	ASD FR	WSH	LCD TV	PC	LAP	LCD	CFL	FUR	EBL	MBL	ASD DR	R FR	CRT TV
MW	**1.00**	0.14	0.80	0.10	0.42	1.86	0.27	0.16	0.13	0.34	0.02	4.01	0.23	1.17
ASD FR	6.85	**1.00**	5.52	0.66	2.91	12.81	1.88	1.13	0.92	2.34	0.14	27.68	1.61	8.05
WSH	0.48	0.07	**1.00**	0.12	0.53	2.32	0.34	0.20	0.17	0.42	0.03	5.01	0.29	1.46
LCD TV	4.35	0.63	8.98	**1.00**	4.43	19.50	2.86	1.71	1.40	3.56	0.21	42.12	2.46	12.26
PC	0.90	0.13	1.85	0.21	**1.00**	4.40	0.65	0.39	0.32	0.80	0.05	9.51	0.55	2.77
LAP	0.38	0.05	0.77	0.09	0.42	**1.00**	0.15	0.09	0.07	0.18	0.01	2.16	0.13	0.63
LCD	2.35	0.34	4.85	0.54	2.62	6.27	**1.00**	0.60	0.49	1.25	0.07	14.74	0.86	4.29
CFL	4.14	0.60	8.55	0.95	4.62	11.05	1.76	**1.00**	0.82	2.08	0.12	24.57	1.43	7.15
FUR	13.68	2.00	28.22	3.14	15.25	36.48	5.82	3.30	**1.00**	2.55	0.15	30.13	1.76	8.77
EBL	2.68	0.39	5.53	0.62	2.99	7.15	1.14	0.65	0.20	**1.00**	0.06	11.83	0.69	3.44
MBL	73.42	10.72	151.49	16.88	81.86	195.80	31.23	17.72	5.37	27.37	**1.00**	200.04	11.67	58.21
ASD DR	0.21	0.03	0.43	0.05	0.23	0.56	0.09	0.05	0.02	0.08	0.00	**1.00**	0.06	0.29
R FR	3.92	0.57	8.08	0.90	4.37	10.44	1.67	0.95	0.29	1.46	0.05	18.67	**1.00**	4.99
CRT TV	0.94	0.14	1.93	0.22	1.04	2.50	0.40	0.23	0.07	0.35	0.01	4.47	0.24	**1.00**

2.3.1.3 Comparison of All Appliance Types

The Equivalent-CFL index compares the harmonic impact of the appliances on the basis of individual units. The fact that each household may have multiple appliances of the same type is recognized is this study. The implication is that the total harmonic currents generated by each type of appliance (that can be 1 or more units) in a typical house must also be compared. For this purpose, the number of appliances that could be installed in a North American household is estimated from statistical surveys [33], [46]. The average number of TVs is indicated to be 2, and the average number of refrigerators, laundry washers and dryers is indicated to be about 1. As mentioned earlier for the lighting loads, an average North American house has a total number of between 27 and 30 installed lamps, and the IEA (International Energy Agency) estimate is 25 lamps [33]. At present, about 25% of all lamps are CFLs [36] so it is assumed that 6 CFLs are installed in a typical house. The average number of magnetic-ballasted fluorescent lamps is estimated to be 2 [33]. Based on these data, the total harmonic impact of each appliance type in a household is determined and quantified as the "Total Equivalent-CFL" index. The values of this index and the associated assumptions are shown in Table 2.7.

The Total Equivalent-CFL index compares the harmonic impact of each type of appliance installed in a typical household. Several comparisons can be made by using Table 2.7. For example, the harmonic impact of CFLs is comparable with that of the home-office equipment such as desktop PCs. The washer (ASD-based) and the microwave oven are identified as more significant harmonic sources. The LCD TV injects little harmonic content, whereas the CRT TV injects an amount comparable to that of the CFLs. The regular laundry dryer (not presented in the table) is not a significant harmonic source, whereas its upgraded ASD-based counterpart injects a considerable amount of harmonics. The collective load of CFLs in a typical household is a harmonic contributor comparable to the other harmonic sources.

Table 2.7. Comparing the harmonic impact of collective home appliances

Appliance type	Operating Power [W/unit]	Number of units	Total Power [W]	Power Ratio	Total Equivalent CFL
MBL	30	2	60	0.67	0.15
LCD TV	300	1	300	3.33	0.20
ASD FR	170	1	170	1.89	0.21
R FR	150	1	150	1.67	0.28
FUR	500	1	500	5.56	0.58
LCD	40	2	80	0.89	0.78
CFL	15	6	90	1.00	1.00
CRT TV	70	1	70	0.78	1.00
LAP	75	1	75	0.83	1.05
PC	100	2	200	2.22	2.18
ASD DRY	1000	1	1000	11.11	2.76
WSH	180	1	180	2.00	2.87
MW	1200	1	1200	13.33	4.05

2.3.2 Rate of Harmonic Decline

The magnitude of the harmonic currents from home appliances can be further understood from another perspective, which is based on the characterization of the decline rate of the current spectrum for these devices. Engineering mathematics books indicate that a square waveform such as that presented in Figure 2.6a has the spectrum presented in Figure 2.6b. The current spectrum is presented as a percentage of the fundamental frequency component. This spectrum is characterized by $I_h = I_1/h$, where h = *1, 3, 5, 7*... Other waveforms have the characteristics shown in Table 2.8.

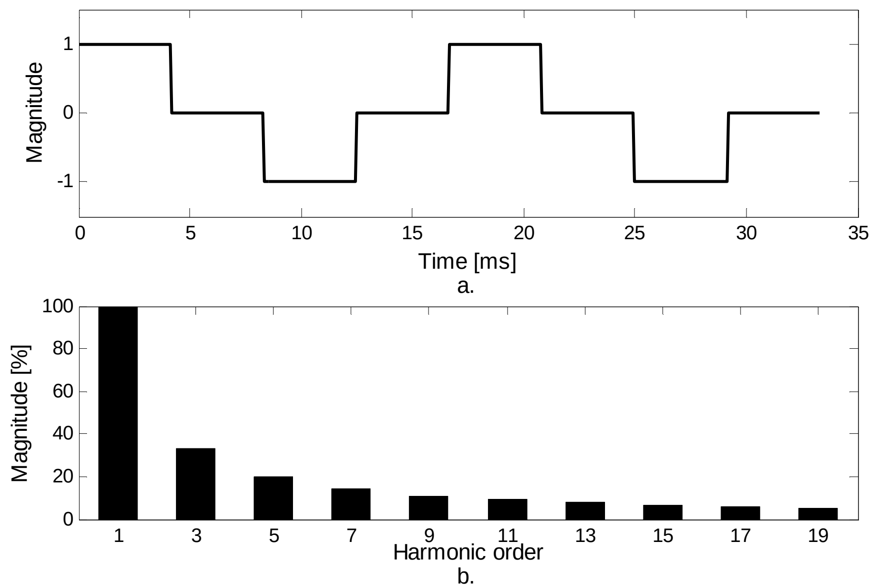

Figure 2.6. Square wave: (a) current waveform and (b) spectrum

Table 2.8. Harmonic decline for several pulse forms

Pulse form	**Decline function**
Square	$1/h$
Triangle	$1/h^2$
Trapezoid	$1/h^2$

Many studies have found that a first approximation to the harmonic characteristics of an ideal single-phase ASD is $I_h = I_1/h$ at all odd harmonics, because the waveform is approximated as a square wave [47]. For the home appliances, however, this type of characterization has not been established. The characterization of the harmonic current magnitudes for home appliances is proposed as

$$I_h = \frac{I_1}{h^{\alpha}}, \tag{2.4}$$

where α is a parameter that determines the decline rate of the current spectrum and is estimated by performing curve-fitting on the normalized (by the fundamental-frequency current) spectra of the home appliances. Such a relationship is proposed because the harmonic-generating home appliances, even those based on the single-phase rectifier topology, do not draw a square current waveform, and therefore cannot be approximated to the known relationship $I_h = I_1/h$. The characterization serves two purposes: (1) it can define patterns for the appliances' current spectra for each type of appliance, and (2) it can be used to compare the relative distortions of the home appliances' harmonic currents.

The individual spectra and fitted characteristics are shown in Figure 2.7, which shows that an acceptable fitting can be obtained for most of the appliances. Since the spectra are normalized, the fundamental-frequency component is equal to 1 and is omitted from the figures. The values for α for all appliances are shown in Table 2.9, which shows that the values for the parameter are diversified. The appliances are sorted according to the α values, which increase from left to right. Table 2.9 reveals that many of the appliances have $\alpha < 1$, which means that the currents drawn by those appliances contain an amount of harmonics that is higher than that contained in the ideal square-wave case. This finding can also be confirmed by comparing the total harmonic distortion of the square wave, which is 45.7%, to those of the appliances, which were presented in Table 2.2.

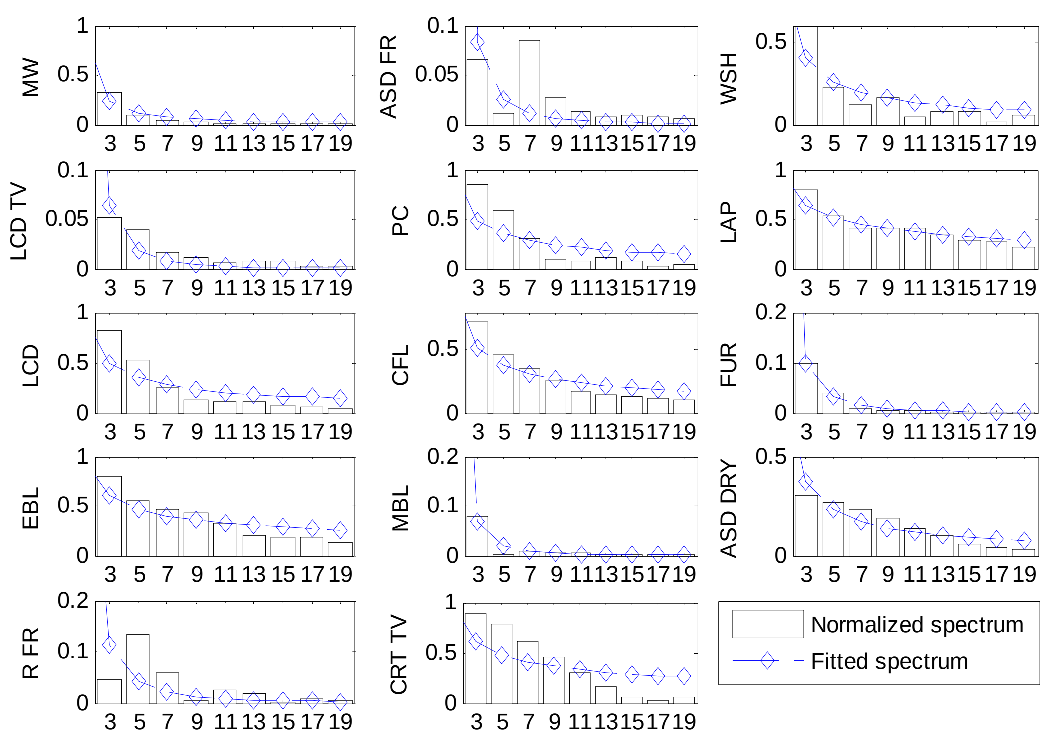

Figure 2.7. Current spectra and fitted $1/h^{\alpha}$

Table 2.9. Comparing α for all home appliances

	LAP	**CRT TV**	**EBL**	**CFL**	**PC**	**LCD**	**WSH**	**ASD DRY**	**MW**	**R FR**	**FUR**	**ASD FR**	**MBL**	**LCD TV**
$\boldsymbol{\alpha}$	0.41	0.46	0.47	0.60	0.65	0.66	0.83	0.90	1.32	1.99	2.12	2.27	2.43	2.49

The appliances' current data are shown in Figure 2.8, which reveals from a different perspective that most power electronic-based appliances have a spectrum with harmonics higher than those obtained from the I_1/h relationship. Figure 2.8 shows that the LCD TV, ASD-based fridge, furnace, magnetic-ballasted fluorescent lamp, and regular fridge are the appliances that have harmonics below the I_1/h curve. The appliances that have α close to 2 are the regular fridge and the furnace. As shown in Appendix A, these appliances draw current waveforms with triangular-like shapes. For these two appliances, the approximation to the ratio I_1/h^2 agrees well.

The curve fitting results are also shown in Figure 2.8. The curve named "All Appliances" shows the results for fitting all the appliances' currents. In this case, α was obtained as $\alpha = 0.8629$. The current spectra of the home appliances are very scattered at all harmonic orders, implying that a single value is not able to represent all devices and that determining the values of α for groups of similar appliances is more useful. Therefore, appliances of similar spectra were also grouped, and data fitting was performed for them: CRT TV, Laptop, PC, LCD monitor, CFL and electronic-ballasted fluorescent lamp were grouped, and one value for α was obtained for this group of appliances as $\alpha = 0.53$. These loads are similar because all are based on the single-phase capacitor-filtered diode bridge rectifier, and, as a result, they have comparable current spectra. These appliances have spectra with harmonic content significantly higher than that provided by the relationship I_1/h.

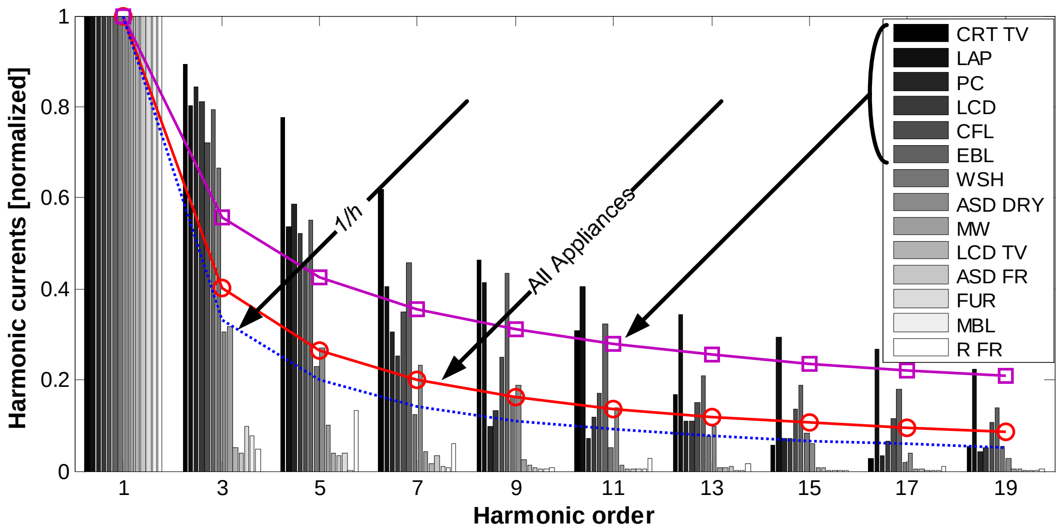

Figure 2.8. Current spectra of the home appliances and curve fitting to obtain α

By using these results, the harmonic magnitude characteristics of home appliances can be obtained by using as a first approximation the frequency-dependent relationship $I_h = I_1/h^{\alpha}$. Using the estimated values for the parameter α is one way to estimate the magnitudes of the current spectra of all appliances if the rated fundamental-frequency current is known. This information is useful as a first approximation to perform harmonic studies when the harmonic current spectra of the appliances are unavailable.

2.4 The Harmonic Phase Angle Study

The Equivalent-CFL index is useful for comparing the harmonic current magnitudes of the home appliances, but it does not provide information on the harmonic phase angle diversification. The harmonic current phase angles are important because they indicate how the harmonics from various home appliances will either add to or cancel out each other. The harmonic compatibility index (CI_h) is introduced in this section to account for the current harmonic phase angles of the appliances as these are operated together.

2.4.1 Index Definition

The adopted definition for the compatibility index is as follows:

1. Like the method used for the Equivalent-CFL index, for each type of appliance measured, the representative harmonic current of each appliance is used for the

harmonic compatibility index. The representative harmonic currents are presented in Appendix A.

2. For each harmonic order h, the phasor relationship of the appliance's current to that of the representative CFL current is determined by using the following equation:

$$CI_{h\_Appliance} = \frac{\left|\dot{I}_{h\_Appliance} + \dot{I}_{h\_CFL\_eq}\right|}{\left|\dot{I}_{h\_Appliance}\right| + \left|\dot{I}_{h\_CFL\_eq}\right|} = \frac{\sqrt{I^2 + I^2 + 2I^2\cos(\theta)}}{2I} = \left|\cos\left(\frac{\theta_h}{2}\right)\right|, \quad (2.5)$$

where

$$\theta_h = \operatorname{ang}\left(\dot{I}_{h\_Appliance}\right) - \operatorname{ang}\left(\dot{I}_{h\_CFL}\right), \quad (2.6)$$

$$\dot{I}_{h\_CFL\_eq} = \dot{I}_{h\_CFL} \times Ratio_{h\_Appliance}. \quad (2.7)$$

The meaning of this equation is that, since the magnitude of $\dot{I}_{h\_CFL\_eq}$ is scaled to be of the same magnitude as the magnitude of $\dot{I}_{h\_Appliance}$, only the phase angles of the appliance and the CFL are taken into consideration in the phasor operation. As θ_h varies between 0 and π radians, $CI_{h\_Appliance}$ varies between 0 and 1. Therefore, as $CI_{h\_Appliance}$ increases, the compatibility of the appliance and the CFL increases, and vice versa. Figure 2.9 is used to explain the index at each harmonic order h, as this figure shows some representative values for the index. Assume the CFL is being compared with Appliance1, Appliance2, Appliance3 and Appliance4. As Figure 2.9 reveals, the index calculated for Appliance1 (Figure 2.9a) means solely harmonic addition, resulting in $CI_{h\_Appliance1} = 1$ because both components are in phase; i.e., $\theta = 0^o$. Conversely, the index calculated for Appliance2 (Figure 2.9b) is $CI_{h\_Appliance2} = 1/\sqrt{2}$ because $\theta = 90^o$. The index calculated for Appliance3 (Figure 2.9c) is found to be $CI_{h\_Appliance3} = 1/2$ because the value of CI_h is of the same magnitudes of each of the individual phasors; i.e., $\theta = 120^o$. Finally, the index calculated for Appliance4 (Figure 2.9d) is $CI_{h\_Appliance4} = 0$ because both components are in opposite phase angles; i.e., $\theta = 180^o$.

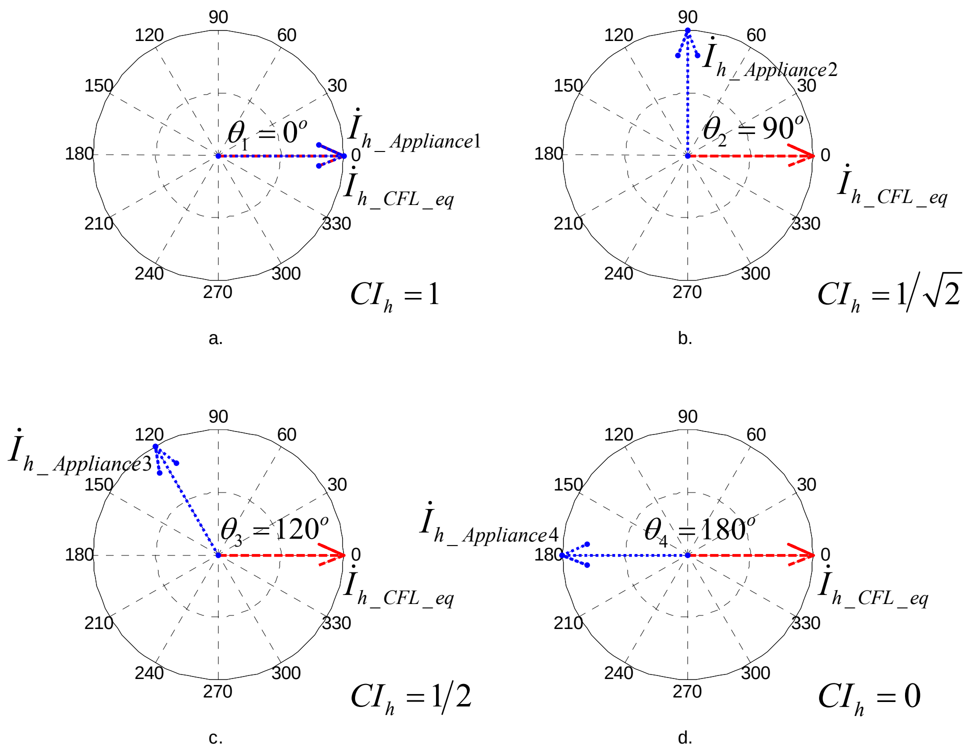

Figure 2.9. Phasor diagram to illustrate the compatibility index

3. An aggregation similar to that proposed for the magnitude-based Equivalent-CFL index is introduced for the harmonic compatibility indices, also by using the weighting factor $w_h = I_{h\_CFL} \Big/ \sqrt{\sum I_{h\_CFL}^2}$, which results in the following aggregated index:

$$CI_{Appliance} = \sqrt{\sum \left(w_h \times CI_{h\_Appliance} \right)^2}. \tag{2.8}$$

The resulting aggregation of the individual $CI_{h\_Appliance}$ carries the information about the combined harmonic compatibility into a single index. The calculation of the compatibility between the PC and CFL is used as an example. The individual current phasors are shown in Figure 2.10. The indices CI_{h_PC} and CI_{PC} are shown in the figure, where they have all been normalized by the CFL's third harmonic, to show the relative impact of each individual CI_{h_PC} on the total CI_{PC}.

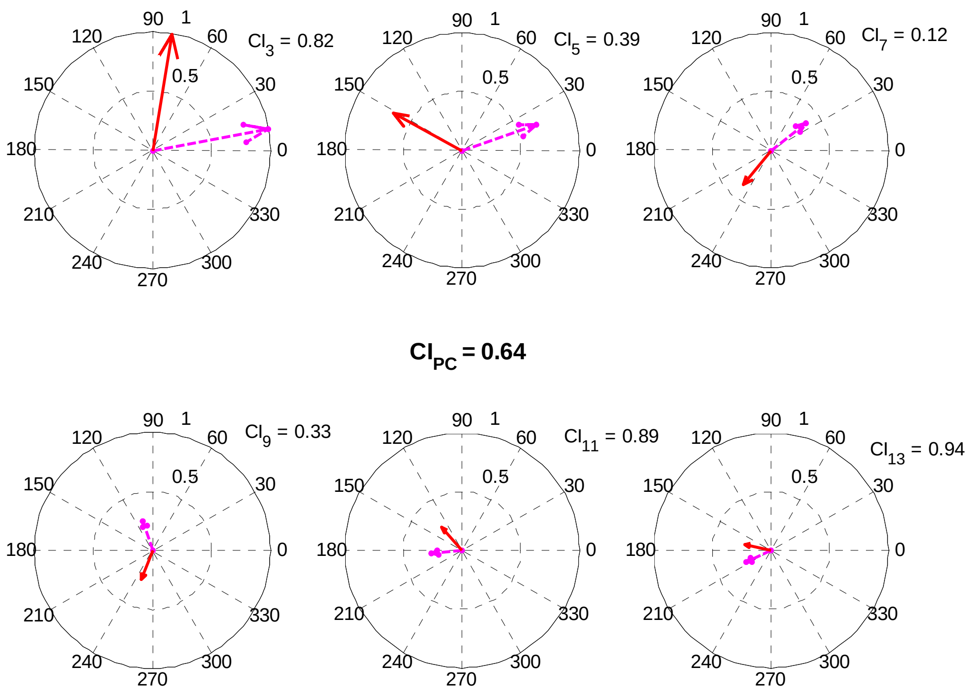

Figure 2.10. Normalized current phasors along with CI_h for PC and CFL

The phase angle-based Harmonic Compatibility index can reflect the measure of the harmonic cancellation between two appliances should there be no difference in magnitude. Therefore, if both appliances' current harmonics were of the same magnitude, the index $CI_{h\_Appliance}$ would reflect the amount of harmonic cancellation. Figure 2.11 is used to explain this statement. In the first case, θ_h = 0 and $CI_{h\_Appliance}$ = 100%. This result means zero harmonic cancellation. In the second case, $\theta_h = \pi/2$ and $CI_{h\_Appliance}$ = 71%. This result means 29% harmonic cancellation as compared to the first case. Therefore, the harmonic compatibility index reflects the amount of harmonic cancellation by considering the harmonic phase angles, but not the magnitude differences. For example, CI_{3_PC} = 0.82. This result means that if 7 CFLs are connected with 1 desktop PC ($Ratio_{3\_PC}$ = 7), there will be 18% 3rd harmonic cancellation as compared to that obtained by using the simple arithmetical summation.

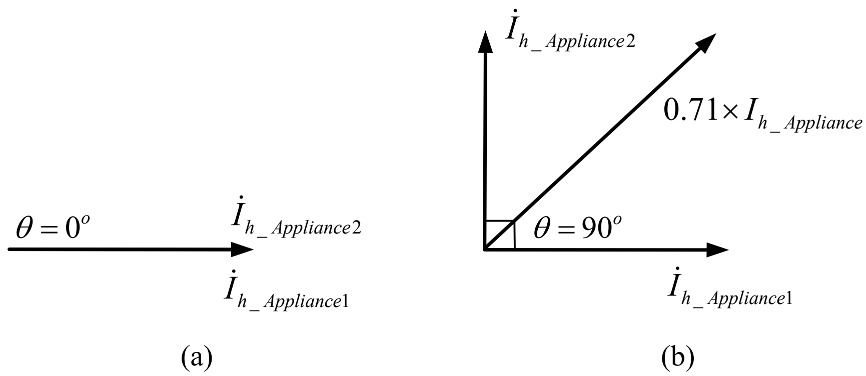

Figure 2.11. How $CI_{h\_Appliance}$ explains the amount of harmonic cancellation: (a) Case 1 and (b) Case 2

2.4.2 Results Provided by the Phase Angle-Based Index

The results for the compatibility index for all appliances are calculated and presented in Table 2.10, in ascending order of $CI_{Appliance}$.

Table 2.10. Harmonic Compatibility Index Results using CFL as a Template

	$CI_{Appliance}$	CI_3	CI_5	CI_7	CI_9	CI_{11}	CI_{13}
ASD FR	0.27	0.03	0.31	0.23	0.07	0.99	0.79
ASD DRY	0.35	0.29	0.34	0.32	0.75	0.53	0.15
R FR	0.61	0.27	0.98	0.14	0.53	0.64	0.70
CRT TV	0.63	0.82	0.39	0.22	0.30	0.72	0.56
PC	0.64	0.82	0.39	0.12	0.33	0.89	0.94
WSH	0.64	0.74	0.40	0.61	0.70	0.93	0.53
FUR	0.65	0.50	0.80	0.71	0.76	0.66	0.54
MW	0.74	0.94	0.34	0.73	0.01	0.13	0.87
LCD	0.81	0.93	0.73	0.54	0.82	0.65	0.63
LCD TV	0.88	0.89	0.86	1.00	0.72	0.53	0.99
MBL	0.89	0.85	0.97	1.00	0.84	0.07	0.27
EBL	0.92	0.97	0.92	0.86	0.98	0.30	0.08
LAP	0.93	0.98	0.91	0.87	1.00	0.16	0.88
CFL	1.00	1.00	1.00	1.00	1.00	1.00	1.00

To further illustrate the general behavior of the appliances, Figure 2.12 shows the distribution of the $CI_{h\_Appliance}$ indices by using histograms. The following conclusions can be drawn from the results presented Table 2.10 and Figure 2.12:

1. More appliances show higher compatibility at the 3rd harmonic than at other orders. This finding agrees with expected harmonic cancellation that can occur in distribution systems [48], and indicates that the harmonic cancellation at such an order is smaller than that observed at higher orders. The appliances that show notably low compatibility at the 3rd harmonic are the fridges and the ASD-based dryer.
2. The harmonic compatibility is generally low for harmonics at the 5th and above orders. This finding implies that the harmonic cancellation at these orders is higher than that observed for the 3rd harmonic.

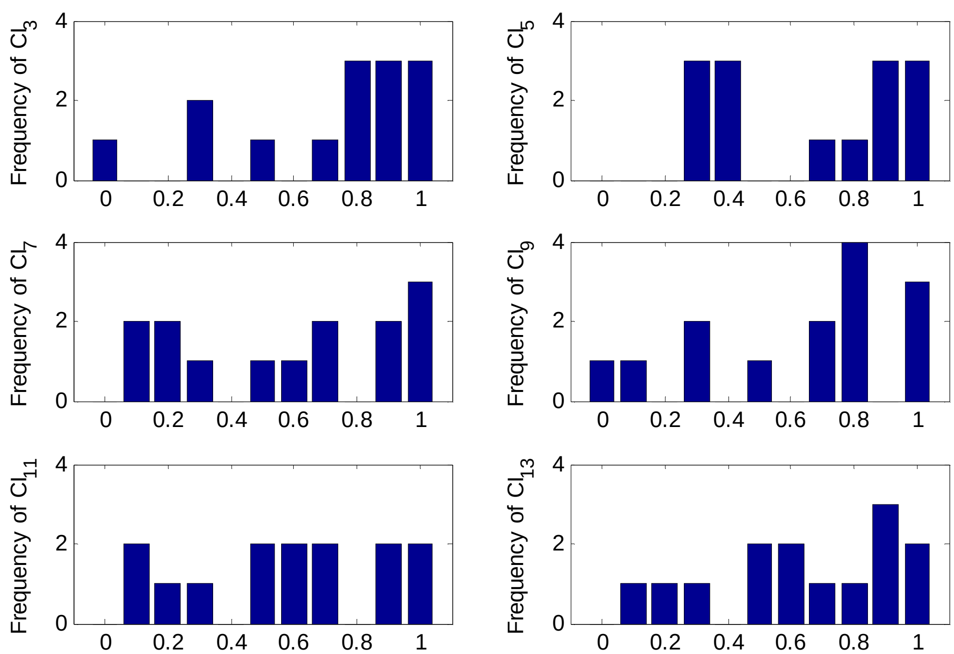

Figure 2.12. Distribution of the $CI_{h\_Appliance}$ indices

For the magnitude-based index, the Equivalent-CFL gives absolute results by using the CFL as a benchmark. These results are straightforward for assessing the relative harmonic severity among the appliances. For the phase angle assessment, the harmonic compatibility index using the CFL as a template does not provide directly the relative harmonic current angle difference between any two given appliances. In order to obtain such a relationship, the indices between any two appliances can be obtained by using the CFL-calculated $CI_{h\_Appliance}$ as follows:

$$CI_{h\_Appliance1-2} = \frac{\left|\dot{I}_{h\_Appliance1} + \dot{I}_{h\_Appliance2}\right|}{\left|\dot{I}_{h\_Appliance1}\right| + \left|\dot{I}_{h\_Appliance2}\right|} = \left|\cos\left(\frac{\theta_{h\_Appliance1}}{2} - \frac{\theta_{h\_Appliance2}}{2}\right)\right| =$$
$$CI_{h\_Appliance1} \times CI_{h\_Appliance2} + \sqrt{1-CI^2_{h\_Appliance1}} \times \sqrt{1-CI^2_{h\_Appliance2}}. \tag{2.9}$$

where the appliances currents are normalized to have the same magnitude. The results for the harmonic compatibility indices $CI_{h\_Appliance1-2}$ for each appliance in relation to all the other appliances at the 3rd-13th harmonic orders are shown in Table 2.11-Table 2.13. Therefore, these tables provide a direct measure of the harmonic compatibility between any two given appliances.

Table 2.11. Harmonic Compatibility Index Results for 3rd and 5th harmonic

h = 3 (columns) / h = 5 (rows)	MW	ASD FR	WSH	LCD TV	PC	LAP	LCD	CFL	FUR	EBL	MBL	ASD DR	R FR	CRT TV
MW	**1.00**	0.36	0.48	0.99	0.96	0.99	1.00	0.94	0.18	0.99	0.63	0.59	0.06	0.96
ASD FR	1.00	**1.00**	0.65	0.49	0.60	0.25	0.41	0.03	0.85	0.26	0.50	0.97	0.95	0.60
WSH	0.72	0.74	**1.00**	0.35	0.22	0.58	0.43	0.74	0.95	0.57	0.98	0.42	0.85	0.23
LCD TV	0.78	0.75	0.12	**1.00**	0.99	0.97	1.00	0.89	0.04	0.97	0.51	0.70	0.20	0.99
PC	0.73	0.75	1.00	0.13	**1.00**	0.93	0.97	0.82	0.09	0.93	0.39	0.79	0.33	1.00
LAP	0.07	0.10	0.74	0.58	0.73	**1.00**	0.99	0.98	0.29	1.00	0.71	0.50	0.06	0.93
LCD	0.39	0.42	0.92	0.28	0.91	0.95	**1.00**	0.93	0.13	0.99	0.59	0.63	0.11	0.98
CFL	0.34	0.31	0.40	0.86	0.39	0.91	0.73	**1.00**	0.50	0.97	0.85	0.29	0.27	0.82
FUR	0.28	0.32	0.87	0.38	0.87	0.98	0.99	0.80	**1.00**	0.29	0.88	0.68	0.97	0.09
EBL	0.05	0.09	0.73	0.59	0.73	1.00	0.94	0.92	0.97	**1.00**	0.71	0.50	0.05	0.93
MBL	0.55	0.52	0.18	0.95	0.17	0.80	0.56	0.97	0.64	0.80	**1.00**	0.26	0.74	0.40
ASD DR	0.77	0.79	1.00	0.19	1.00	0.69	0.89	0.34	0.83	0.68	0.11	**1.00**	0.84	0.79
R FR	0.51	0.48	0.22	0.94	0.22	0.82	0.59	0.98	0.68	0.83	1.00	0.15	**1.00**	0.32
CRT TV	0.73	0.75	1.00	0.13	1.00	0.73	0.91	0.39	0.87	0.72	0.17	1.00	0.22	**1.00**

Table 2.12. Harmonic Compatibility Index Results for 7th and 9th harmonic

h = 7 / h = 9	MW	ASD FR	WSH	LCD TV	PC	LAP	LCD	CFL	FUR	EBL	MBL	ASD DR	R FR	CRT TV
MW	**1.00**	0.83	0.99	0.67	0.60	0.97	0.97	0.73	1.00	0.98	0.74	0.88	0.57	0.51
ASD FR	1.00	**1.00**	0.91	0.15	0.94	0.67	0.94	0.23	0.85	0.69	0.25	1.00	0.93	0.90
WSH	0.72	0.76	**1.00**	0.54	0.72	0.92	1.00	0.61	0.99	0.93	0.63	0.95	0.70	0.64
LCD TV	0.69	0.64	0.01	**1.00**	0.20	0.83	0.47	1.00	0.65	0.81	0.99	0.24	0.22	0.30
PC	0.94	0.92	0.44	0.89	**1.00**	0.38	0.77	0.12	0.62	0.41	0.10	0.90	1.00	0.99
LAP	0.08	0.02	0.63	0.78	0.42	**1.00**	0.88	0.87	0.96	1.00	0.88	0.74	0.36	0.29
LCD	0.57	0.52	0.16	0.99	0.82	0.87	**1.00**	0.54	0.98	0.89	0.55	0.97	0.76	0.71
CFL	0.01	0.07	0.70	0.72	0.33	1.00	0.82	**1.00**	0.71	0.86	1.00	0.32	0.14	0.22
FUR	0.65	0.70	1.00	0.10	0.35	0.70	0.25	0.76	**1.00**	0.97	0.72	0.89	0.59	0.53
EBL	0.20	0.14	0.54	0.85	0.52	0.99	0.92	0.98	0.62	**1.00**	0.87	0.76	0.38	0.31
MBL	0.54	0.59	0.97	0.23	0.23	0.79	0.38	0.84	0.99	0.72	**1.00**	0.34	0.12	0.20
ASD DR	0.65	0.60	0.06	1.00	0.87	0.81	1.00	0.75	0.15	0.87	0.28	**1.00**	0.89	0.86
R FR	0.85	0.88	0.98	0.21	0.63	0.45	0.06	0.53	0.95	0.34	0.90	0.16	**1.00**	1.00
CRT TV	0.95	0.97	0.89	0.44	0.80	0.22	0.30	0.30	0.85	0.10	0.77	0.40	0.97	**1.00**

Table 2.13. Harmonic Compatibility Index Results for 11th and 13th harmonic

h = 11 / h = 13	MW	ASD FR	WSH	LCD TV	PC	LAP	LCD	CFL	FUR	EBL	MBL	ASD DR	R FR	CRT TV
MW	**1.00**	0.28	0.25	0.91	0.34	0.96	0.67	0.13	0.66	0.91	1.00	0.77	0.68	0.78
ASD FR	0.40	**1.00**	0.86	0.66	0.81	0.00	0.52	0.99	0.53	0.15	0.23	0.39	0.51	0.82
WSH	0.87	0.10	**1.00**	0.18	1.00	0.52	0.88	0.93	0.89	0.63	0.30	0.81	0.88	0.41
LCD TV	0.94	0.69	0.65	**1.00**	0.08	0.75	0.30	0.53	0.29	0.65	0.88	0.44	0.31	0.97
PC	0.99	0.55	0.78	0.98	**1.00**	0.60	0.92	0.89	0.93	0.70	0.39	0.86	0.92	0.32
LAP	1.00	0.40	0.87	0.94	0.99	**1.00**	0.86	0.16	0.85	0.99	0.97	0.92	0.86	0.57
LCD	0.93	0.02	0.99	0.74	0.85	0.92	**1.00**	0.65	1.00	0.92	0.71	0.99	1.00	0.06
CFL	0.87	0.79	0.53	0.99	0.94	0.88	0.63	**1.00**	0.66	0.30	0.07	0.53	0.64	0.72
FUR	0.88	0.08	1.00	0.66	0.79	0.88	0.99	0.54	**1.00**	0.92	0.70	0.99	1.00	0.04
EBL	0.55	0.55	0.89	0.23	0.40	0.55	0.83	0.08	0.88	**1.00**	0.93	0.97	0.92	0.44
MBL	0.23	0.80	0.67	0.12	0.06	0.22	0.58	0.27	0.66	0.94	**1.00**	0.81	0.72	0.74
ASD DR	0.61	0.49	0.92	0.30	0.47	0.61	0.86	0.15	0.91	1.00	0.91	**1.00**	0.99	0.20
R FR	0.27	0.99	0.24	0.58	0.43	0.27	0.12	0.70	0.22	0.66	0.88	0.60	**1.00**	0.07
CRT TV	0.09	0.95	0.41	0.43	0.26	0.10	0.29	0.56	0.39	0.78	0.95	0.73	0.98	**1.00**

2.4.3 Results for Aggregated CI_h

The indices $CI_{h\_Appliance1\text{-}2}$ presented in Table 2.11-Table 2.13 can be combined as a weight average. The aggregated indices can be obtained by using a weight-average similar to that of equation (2.10), and by using the same weighting factor $w_h = I_{h\_CFL} \Big/ \sqrt{\sum I_{h\_CFL}^2}$. The aggregated index is obtained as

$$CI_{Appliance1-2} = \sqrt{\sum \left(w_h \times CI_{h\_Appliance1-2} \right)^2}. \tag{2.10}$$

Table 2.14 shows the aggregate compatibility indices for each appliance in relation to all the other appliances. Table 2.14 also shows that the lowest compatibility levels are obtained when comparing the pulsed loads (PCs, Laptops, and LCD monitors) with the load from the fridge.

Table 2.14. Harmonic Compatibility Index Results for Aggregated harmonics

Total	**MW**	**ASD FR**	**WSH**	**LCD TV**	**PC**	**LAP**	**LCD**	**CFL**	**FUR**	**EBL**	**MBL**	**ASD DRY**	**R FR**	**CRT TV**
MW	**1.00**	0.72	0.66	0.87	0.84	0.80	0.83	0.74	0.47	0.79	0.62	0.70	0.41	0.83
ASD FR	0.72	**1.00**	0.72	0.57	0.72	0.31	0.52	0.27	0.70	0.33	0.49	0.89	0.82	0.73
WSH	0.66	0.72	**1.00**	0.34	0.67	0.69	0.72	0.64	0.93	0.69	0.75	0.74	0.69	0.66
LCD TV	0.87	0.57	0.34	**1.00**	0.72	0.83	0.76	0.88	0.34	0.82	0.75	0.54	0.56	0.71
PC	0.84	0.72	0.67	0.72	**1.00**	0.79	0.92	0.64	0.57	0.78	0.30	0.87	0.49	0.97
LAP	0.80	0.31	0.69	0.83	0.79	**1.00**	0.95	0.93	0.72	0.99	0.77	0.63	0.50	0.77
LCD	0.83	0.52	0.72	0.76	0.92	0.95	**1.00**	0.81	0.70	0.95	0.57	0.80	0.47	0.88
CFL	0.74	0.27	0.64	0.88	0.64	0.93	0.81	**1.00**	0.65	0.92	0.89	0.35	0.61	0.63
FUR	0.47	0.70	0.93	0.34	0.57	0.72	0.70	0.65	**1.00**	0.72	0.79	0.76	0.83	0.56
EBL	0.79	0.33	0.69	0.82	0.78	0.99	0.95	0.92	0.72	**1.00**	0.77	0.64	0.52	0.77
MBL	0.62	0.49	0.75	0.75	0.30	0.77	0.57	0.89	0.79	0.77	**1.00**	0.29	0.79	0.38
ASD DRY	0.70	0.89	0.74	0.54	0.87	0.63	0.80	0.35	0.76	0.64	0.29	**1.00**	0.69	0.85
R FR	0.41	0.82	0.69	0.56	0.49	0.50	0.47	0.61	0.83	0.52	0.79	0.69	**1.00**	0.51
CRT TV	0.83	0.73	0.66	0.71	0.97	0.77	0.88	0.63	0.56	0.77	0.38	0.85	0.51	**1.00**

As a further illustration, Figure 2.13 shows the distribution of the aggregated index for all appliances by using histograms. This figure is useful to identify the general compatibility trends of each individual appliance. For example, the figure shows that generally, the microwave oven is more compatible than the ASD-based fridge with all other appliances.

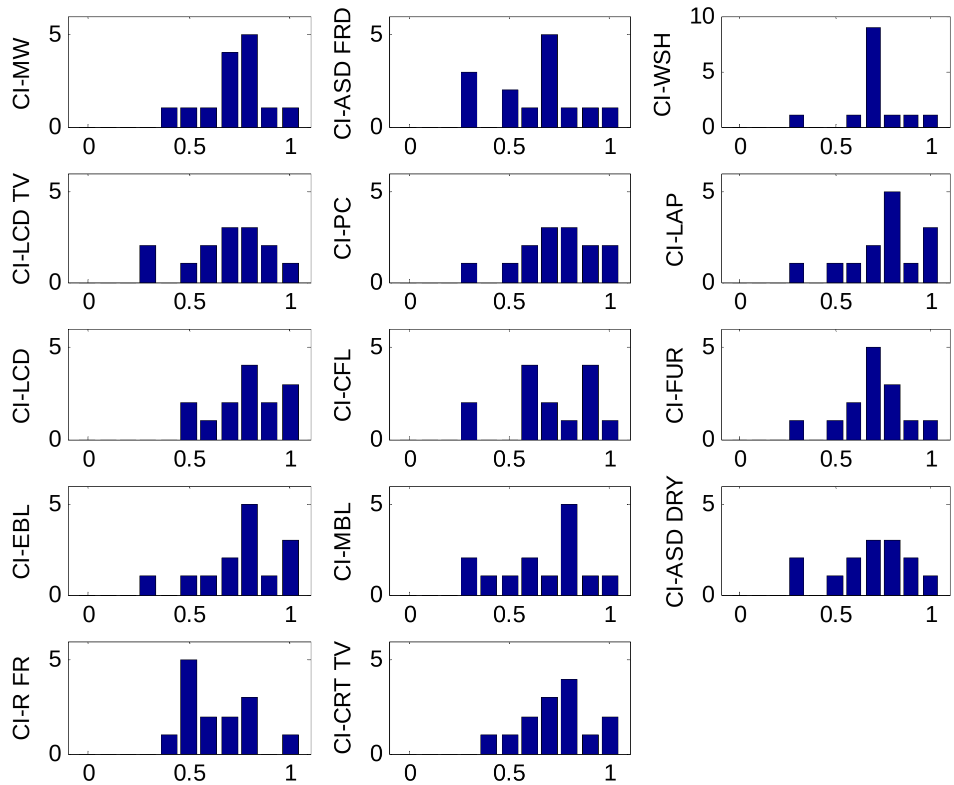

Figure 2.13. Distribution of the $CI_{Appliance\_1\text{-}2}$ indices for all appliances

2.4.4 Categorizing the Appliances by using the CI_h Index

Using the plots from Figure 2.2 and the results from Table 2.11-Table 2.14, the appliances can be further categorized into groups of high compatibility. A threshold is defined in order to state whether the compatibility level is low or high. For any angle smaller than 90^o between the phasors of two appliances, the projection of one phasor on the other results in addition. The respective $CI_{h\_Appliance}$ value is 0.71. The threshold 0.5 is also meaningful because it corresponds to the angle being equal to 120^o. Any harmonic with an angle larger than 120^o results in a cancellation such that the magnitude of the vector addition is smaller than the magnitude of any of the individual vectors.

The ranges shown in Table 2.15 and illustrated in Figure 2.14 are used as thresholds. This figure shows the regions and compatibilities by using Appliance1 as a reference.

Table 2.15. Harmonic Compatibility Index Categorization

Compatibility	**Angle**	$CI_{h\_Appliance}$ **value**
Low	$120^o < \lvert\Delta\theta\rvert$	$CI_{h\_Appliance} < 0.5$
Medium	$90^o \leq \lvert\Delta\theta\rvert \leq 120^o$	$0.5 \leq CI_{h\_Appliance} \leq 0.71$
High	$\lvert\Delta\theta\rvert < 90^o$	$CI_{h\_Appliance} > 0.71$

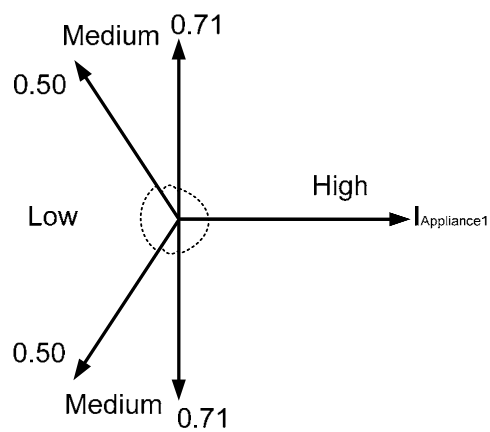

Figure 2.14. Locations for compatibility indices in coordinate space

Table 2.16 shows the appliances organized by similar characteristics. Appliances inside the same group, when connected together, have high harmonic compatibility.
The results provided by this table show that

1. The loads, such as CFLs, home entertainment and home-office computer loads, which use capacitor-filtered single-phase rectifiers, have high harmonic compatibility with each other. These loads have current waveforms that have either pulse or triangle shapes with high *FPF*.
2. ASD-based laundry washer, ASD-based laundry dryer, and the furnace, have high harmonic compatibility.
3. The 3rd harmonic currents dominate the total compatibility because for most of the home appliances, the 3rd harmonic is the highest.

Table 2.16. Compatibility among Appliances

H order	Group 1		Group 2		Group 3	
3rd	MW CFL LAP EBL	LCD TV PC LCD CRT TV	CFL MBL	WSH	WSH FUR	R FR
5th	LCD PC EBL LAP	ASD DRY FUR CRT TV WSH	CFL R FR	LCD TV MBL	MW	ASD FR
7th	PC R FR	CRT TV ASD DRY	LCD WSH FUR	MW EBL LAP	CFL LCD TV	MBL
9th	R FR CRT TV	MW ASD FR	R FR WSH	FUR MBL	LCD TV ASD DRY LCD	EBL LAP CFL
Total	MW CFL LAP EBL	LCD TV PC LCD CRT TV	CFL	MBL	WSH FUR	R FR

2.4.5 Impact of the Phase Angle on the Harmonic Current Cancellation

A case study is presented to illustrate the importance of the phase angles of the appliances' current harmonics. The harmonic currents of selected groups of appliances are analyzed. The combinations of appliances were determined by using survey results, as presented in Table 2.17. The harmonic injections of these groups are compared by both considering and ignoring the phase angle disparity. This study is useful to show the harmonic current cancellations that occur when appliances of different types are connected together. The indices proposed in this chapter are used to explain the results.

Table 2.17. Appliance Usage Patterns

Appliances Combinations			
Case 1	**Power: 663 W**	**Case 2**	**Power: 903 W**
• Furnace	• Fridge	• Furnace • PC + monitor • Fridge	• 2 CFLs • TV
Case 3	**Power: 1011 W**	**Case 4**	**Power: 2294 W**
• Furnace • PC + monitor • Laptop	• Fridge • 4 CFLs • TV	• Furnace • PC + monitor • Laptop • Microwave	• Fridge • 6 CFLs • TV
Case 5	**Power: 2632 W**	**Case 6**	**Power: 4049 W**
• Furnace • PC + monitor • Laptop • Microwave	• Fridge • 8 CFLs • 2 TVs	• Furnace • 2PCs + 2 monitors • Laptop • Microwave • 2 MBLs	• Fridge • 8 CFLs • 2 TVs • Washer + Dryer

The main results from these studies are presented in Figure 2.15. This figure shows the total power of the combination of appliances in the *x*-axis, and the current harmonics in the *y*-axis. A linear data fitting is also provided in order to show the rate of harmonic current increase as the total power increases. The upper line is the arithmetic sum, and the lower one is the phasor sum. This figure reveals the following:

- As the total power of the appliance combinations increases, the trends of harmonic currents increase accordingly, for both cases (arithmetic and phasor sum). Even though the trends increase, increasing the power does not necessarily increase the net current harmonics. As explained earlier, this result was expected due to large amount of harmonic cancellation, especially at harmonic orders above the 3^{rd}.
- The slopes of the linear data fitting show larger values difference as the harmonic orders increase. For the case presented in Figure 2.15, the angles of the slopes for the 3^{rd}, 5^{th}, 7^{th} and 9^{th} harmonics are 69^o, 54^o, 38^o and 27^o, respectively, for the case of the arithmetic sum. For the case of the phasor sum, the angles of the slopes are 60^o, 25^o, 14^o, and 5^o for 3^{rd}, 5^{th}, 7^{th} and 9^{th} harmonics, respectively. The results confirm that (1) the rate of increase of the harmonic currents is more

prominent at lower order harmonics, and that (2) the differences of the slope angle increase for higher-order harmonics.

- The observed behavior can be explained by using both indices. The Equivalent-CFL index is well suited for explaining the arithmetic sum. Between 900W and 2100W, for example, as the microwave oven is connected, an increase occurs in the 3rd harmonic current that is equivalent to that of $Ratio_3$ = 33 CFLs, whereas the increase in the 9th harmonic is equivalent to that of only $Ratio_9$ = 7 CFLs. On the other hand, the compatibility index is useful for explaining the phasor sum. For the same case, the microwave oven has high compatibility at the 3rd harmonic with the computing loads and CFL, but low compatibility with the furnace and fridge. For this reason, the increase in the 3rd harmonic current is not as high as that shown for the arithmetic sum, but is still high due to the relatively high harmonic compatibility. At the 9th harmonic, however, the microwave has low compatibility with all loads, except those from the PC and Furnace, resulting in significant harmonic cancellation. Therefore, there is barely any increase for that power demand step.

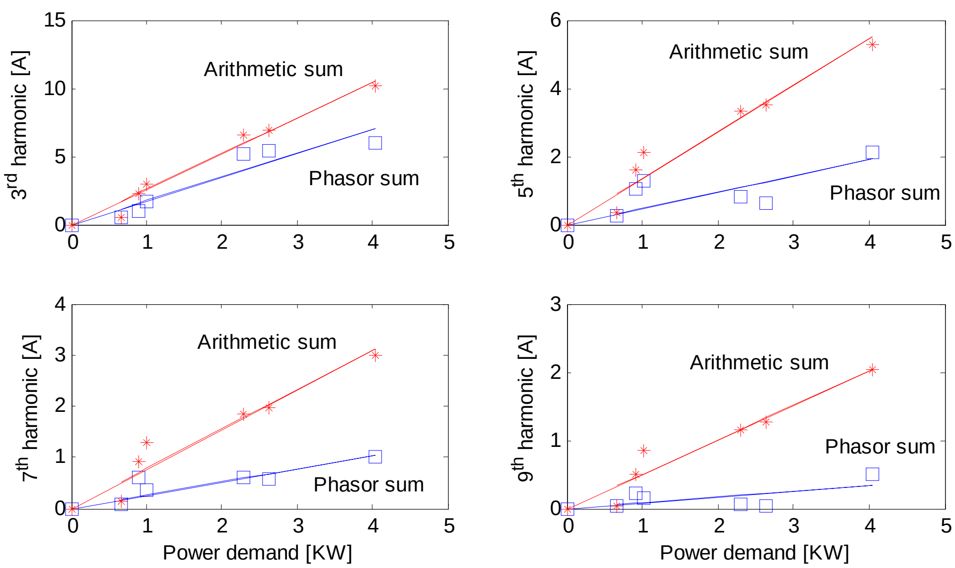

Figure 2.15. Impact of the harmonic current phase angles

Finally, the three groups in the first row of Table 2.16 will also be used for further illustration. The corresponding group of appliances was verified to be highly compatible at the 3rd harmonic, but not at higher-order harmonics. Figure 2.16 shows the results for the three cases, confirming that the difference among both summations is small at the 3rd harmonic but high at others.

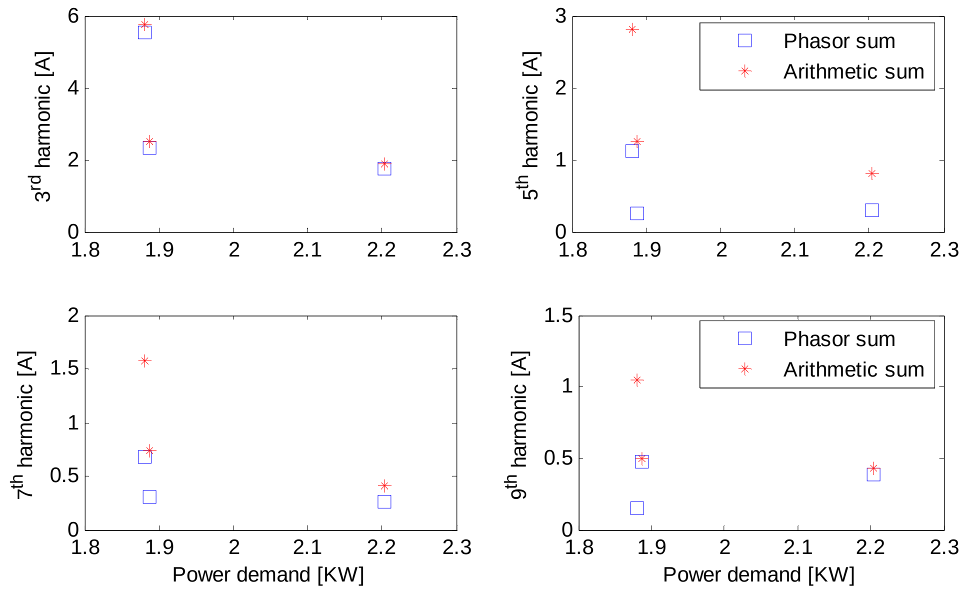

Figure 2.16. Impact of the harmonic current phase angles for combinations compatible at the 3rd harmonic

2.5 Summary and Conclusions

A comparison of the harmonic levels among harmonic-generating home appliances was carried out. The issues relating to the harmonic current magnitudes and phase angles were studied by using developed indices. The Equivalent-CFL index was introduced to quantify the relative severity of the magnitudes of the harmonic currents from home appliances. The harmonic compatibility index is an indication of how much current cancellation can occur between the harmonic currents of any two given appliances, and therefore deals with the phase angle cancellation issue. Both indices provide results that can be used as a benchmark for harmonic studies at a residential customer level.

The magnitude-based study was intended to provide a direct relationship between the severities of the current harmonics of two appliances, by considering their magnitudes only. The key conclusions are

- The Equivalent-CFL index compares the harmonic impact of appliances on the basis of individual units. Based on the index, the appliances can be ranked in the following ascending order on <u>an individual unit basis</u>, by taking into consideration their harmonic severities: MBL (0.42), CFL (1), ASD FR (1.14), EBL (1.15), LCD TV (1.32), R FR (1.35), LCD (2.35), FUR (2.53), CRT TV (5.81), LAP (6.15), PC (7.05), ASD DRY (12.58), WSH (16.09), and MW (26.42).
- The Total Equivalent-CFL index compares the harmonic impact of each type of appliances installed in a typical household. According to Table 2.7, the appliances can be ranked in the following ascending order on the basis of the <u>total number of units</u>, by taking into consideration their harmonic severities: MBL (0.15), ASD FR (0.19), LCD TV (0.2), R FR (0.28), FUR (0.58), LCD (0.78), CFL (1), CRT TV (1.00), LAP (1.05), PC (2.18), ASD DRY (2.76), WSH (2.87), and MW (4.05). As the number of CFLs increases in a house, their harmonic-producing role may become more prominent (if the use of other appliances does not increase).
- The Equivalent-Appliance index was used to compare the current harmonics of all appliances. The results were presented in tabular form, and the equivalencies among all devices were provided.
- The current spectrum decline rate study was performed in order to characterize the magnitudes of the current spectra of all appliances. The estimated parameter α is unique for each appliance or set of electrically similar appliances.

The phase angle-based Harmonic Compatibility index is a direct measure of the harmonic cancellation between two appliances should there be no difference in magnitude. It can be used to evaluate whether the appliances' harmonic currents will mainly add to or cancel out each other. It was found that the compatibility was highest at the 3^{rd} harmonic order, and low at the higher-order harmonics. Usually, the appliances had high compatibility to those of similar construction. For example, diode-bridge rectifier-based appliances had harmonic currents of high compatibility.

The next chapter studies the effect of the supply voltage harmonics on the appliances' current harmonics. This effect, traditionally referred to as the attenuation effect, is studied for some of the single-phase power electronic-based home appliances.

Chapter 3

The Harmonic Attenuation/Amplification Effect of Home Appliances

Harmonic currents produced by constant load harmonic sources are normally derived on the assumption of a perfectly sinusoidal supply voltage. This approach ignores the interaction between harmonic current injections and the supply voltage and, therefore, cannot consider the variation of the current spectrum due to the supply voltage distortion. The characterization of the impact of the supply voltage on the harmonic current injections of power electronic-based home appliances is the key to understanding the impact of the harmonic attenuation effect. In this chapter, the attenuation effect of home appliances employing a capacitor-filtered diode bridge rectifier is characterized. It is found that an unexpected harmonic amplification can occur under common supply conditions in residential areas. A corresponding analytical model is used to confirm the surprise findings from the analysis of the measurement results.

3.1 Introduction

In most harmonic studies dealing with power electronic-based equipment, the harmonic sources are represented by their typical current spectrum, which is obtained under the condition of undistorted voltage supply [4]. This model is obtained based on the premise that the harmonic current injection is fixed and independent of the supply voltage distortion. This model is reasonably accurate only if the voltage supply shows little distortion. However, the bus voltage supplying any harmonic source is usually distorted due to the large amount of harmonic sources dispersed throughout the power system. As a result, the harmonic source will inject harmonic currents that differ from its spectrum obtained from an undistorted supply. The traditional current-source modeling method cannot account for these effects or accurately estimate the harmonic injections.

The harmonic attenuation effect refers to the impact of supply voltage harmonics on the harmonic currents produced by a nonlinear load. A number of studies showed that a nonlinear load will inject less harmonic currents when supplied with distorted voltage than when supplied by an undistorted voltage. In [24], a time-domain analytical model of a single-phase diode bridge rectifier was developed in order to study the attenuation and diversity effects through simulations. Significant attenuation of harmonic currents above the 3rd order was found when a number of identical nonlinear loads shared a common system impedance. This reference was one of the first to acknowledge that the harmonics reduction due to attenuation depends on the system supply voltage. The work in [49] expanded the model presented in [24], using a more realistic system to understand the combined effect of attenuation and diversity on the net harmonic current produced by a large number of distributed single-phase power electronic loads.

The attenuation effect of many devices has been documented in several studies. Some of them have characterized this effect by using EMTP simulation or experimental tests. Reference [50] used EMTP simulation and found that increasing the distortion of the supply voltage reduced the harmonic current injection of CFLs, single-phase diode bridge rectifiers, and single-phase thyristor-bridge rectifiers. Reference [51] presented an empirical technique for solving an iterative harmonic power flow that accounted for the attenuation effect. The authors characterized the attenuation effect of personal computers through measurements. In [52], the importance of the attenuation effect of PCs was also studied by carrying out experiments. Reference [53] found that television sets tended to inject noticeably less harmonic currents when supplied by distorted voltage. In [54], the authors found that variations in the THD_V resulted in variations in the THD_I, power factor, and efficacy of magnetic-ballasted and electronic-ballasted tube fluorescent lamps. This finding was obtained from the authors' experiments. The harmonic attenuation effect of CFLs was documented in references [55]-[56], where this researcher used experimental results to characterize the harmonic attenuation effect of several types of CFLs. The authors concluded that this effect could account for up to 25% harmonic overestimation.

However, some studies have found that an increase in current distortion, rather than a decrease, occurred for some voltage conditions. Reference [57] extended the work presented in [24] to analyze in more detail the effect of supply voltage harmonics on the load input current waveshape. In this reference, the authors used thousands of random synthetic voltage waveforms in their simulation studies and observed that the input current *THD* increased for the single-phase diode bridge model. The use of random vectors, however, does not necessarily reflect the true performance of a system. In [58], the authors measured 13 types of lamps (two electronic-ballasted fluorescent lamps and 11 magnetic-ballasted lamps) under generated voltage supplies and monitored the harmonic current injections. The measurement results presented in this reference revealed that the THD_I increased when the THD_V was above 15%. Therefore, the measurements presented in this reference also have the limitation of using random supply conditions that do not necessarily provide a reliable approach to handle the problem.

The studies summarized in Section 3.1 are representative of most of the studies published on harmonic attenuation and amplification. Overall, these studies suggested that current harmonic reduction is always the consequence of increasing voltage distortion for power electronic loads. Few studies dealing with the analysis of the harmonic amplification have been published. Although references [57]-[58] acknowledged that it is theoretically possible that increased current distortion can occur, this possibility has been neither investigated nor observed under credible voltage conditions. No published study has dealt with harmonic amplification occurring under realistic voltage supply conditions. The objective of this chapter is to present a comprehensive study of the harmonic attenuation of single-phase power electronic-based home appliances. This chapter presents the measurement results of electronic appliances to analyze the harmonic attenuation effect. It was observed that harmonic amplification occurred more often than had been expected. In order to confirm this finding, an analytical model was used to conduct several studies of home appliances. The most common power electronic load, the basic construction of many home appliances, is explained in the next section.

3.2 Single-Phase Capacitor-Filtered Diode Bridge Rectifier

The single-phase power electronic load is the most common harmonic source in residential and commercial distribution systems. The switch-mode power supplies of personal computers and television sets are typical examples of such a load [24], [51]. The load uses a capacitor-filtered diode bridge rectifier as shown in Figure 3.1. The rectifier consists of a circuit that rectifies a sinusoidal voltage from a power line, a DC-link capacitor, and an equivalent resistor. The various circuit components are

V_{th}: Thevenin equivalent system voltage,

R_{th}, L_{th}: Thevenin equivalent system impedance parameters,

R_s, L_s: local supply impedance parameters,

C: DC-smoothing capacitor,

R_{eq}: equivalent load resistance representing the inverter, control, and equivalent load.

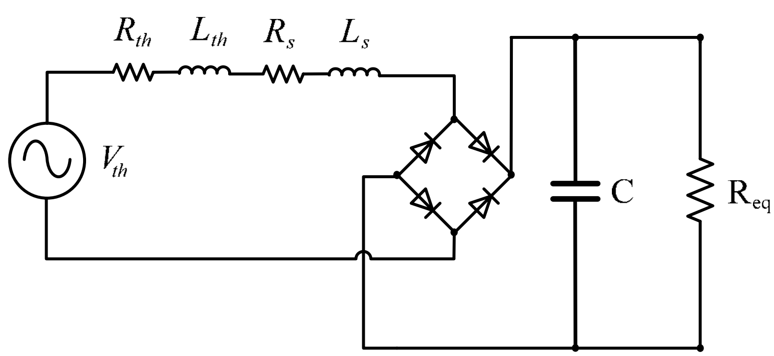

Figure 3.1. Capacitor-filtered diode bridge rectifier circuit

Figure 3.2 illustrates a typical measured PC input current waveform along with its corresponding spectrum magnitude, expressed as a percentage of the fundamental component. The waveform pulses occur when the AC source is at a higher voltage than the DC link of the rectifier and, therefore, the capacitor starts being charged. During this time, the diodes are forward-biased, and the current flows [51]. Since the drawn current is taken in short pulses, it is highly distorted, and its spectrum is rich in odd harmonics. The current *THD* is typically above 100%. The width of the current pulse depends on the rectifier circuit parameters. When the current pulse is wider, its *THD* becomes lower and vice versa.

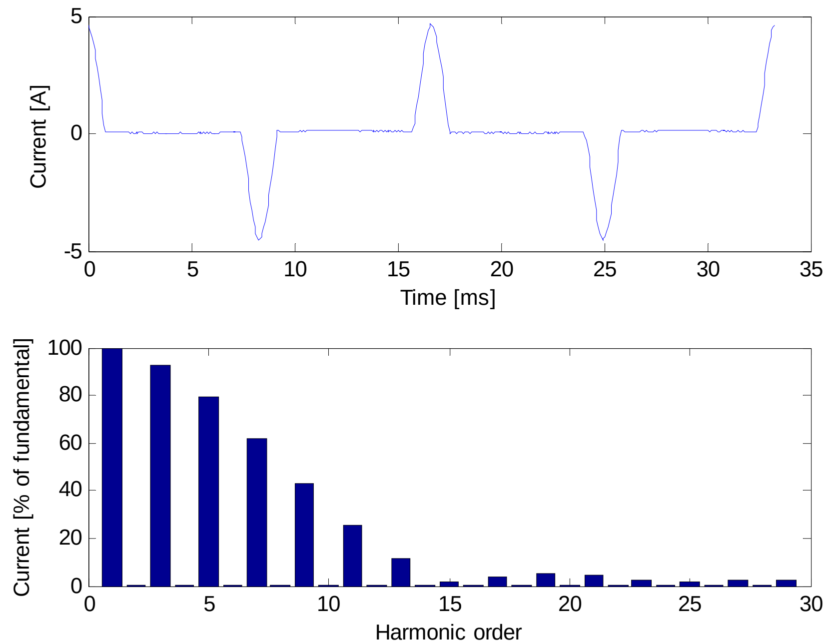

Figure 3.2. Typical measured input current waveform for a PC load and its harmonic spectrum magnitude.

3.3 Characterizing the Harmonic Attenuation Effect of Single-Phase Harmonic Sources

The attenuation effect can be explained by using Figure 3.3, which presents the measured 3rd harmonic current of a 27W CFL for different voltage conditions. This figure reveals that a reduction of the harmonic current occurs when the supply voltage becomes more distorted.

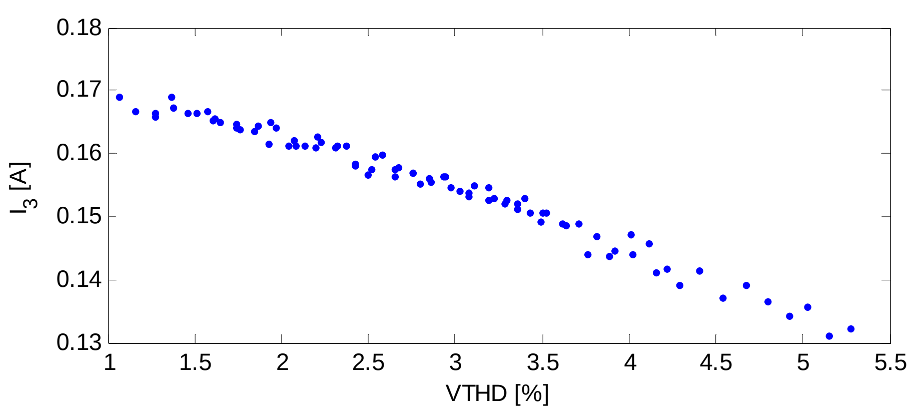

Figure 3.3. Third harmonic current for different supply conditions.

In the following section, the harmonic attenuation of several home appliances is characterized.

3.3.1 Causes of the Harmonic Attenuation Effect

The harmonic attenuation effect of power electronic-based appliances occurs when the supply voltage is distorted [24], [50]. The circuit presented in Figure 3.1 will be used to explain the effect. Controlled and uncontrolled single-phase rectifiers draw a pulse current to charge up their DC capacitor. This pulse is drawn when the applied AC voltage is higher than the capacitor voltage. As the pulse current is drawn, a voltage drop on the supply system impedance occurs, and, as a result, the peak voltage is reduced. This reduction causes the voltage distortion at the point of common coupling (PCC) and is the reason why almost all voltages in power distribution and utilization systems have a flat top. As the supply voltage becomes more flat-topped due to the increased use of nonlinear appliances, more time is required to charge up the DC capacitor of the appliances, and the current pulses drawn by them become wider. Consequently, most of the harmonics become smaller in magnitude. Figure 3.4 illustrates this effect on the measured current drawn by a CFL.

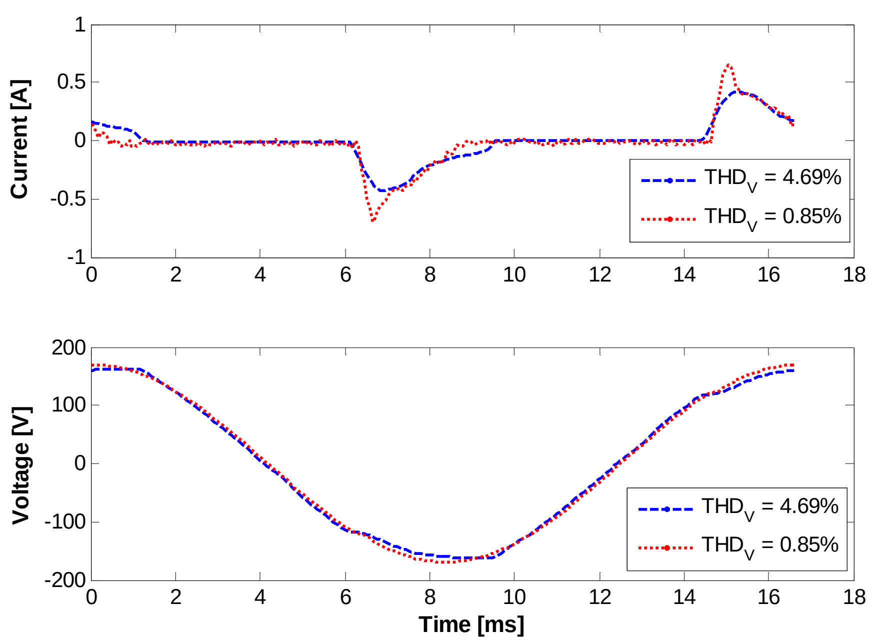

Figure 3.4. Illustrating the Attenuation Effect

3.3.2 Definition of the Attenuation Factor

The relationship between the supply voltage harmonics and the load current harmonics is the attenuation effect. The traditional index used to describe the attenuation effect was presented in [24] and is characterized as

$$AF_h = \frac{I_{h-N}}{N \times I_{h-1}}, \tag{3.1}$$

where
AF_h is the attenuation effect at the h-th harmonic,
I_{h-N} is the resultant current magnitude at h-th harmonic for N parallel units, and
I_{h-1} is the current magnitude at h-th harmonic when $N = 1$.

In this thesis, the index adopted to quantify the attenuation effect is based on the above understanding, and is a modification of that introduced in [24]:

$$AF_h = \frac{I_{h-distorted\_v}}{I_{h-ideal}}, \tag{3.2}$$

where
AF_h is the attenuation effect at the h-th harmonic,
$I_{h\text{-}distorted\_v}$ is the current magnitude at the h-th harmonic measured when the supply voltage is distorted, and
$I_{h,ideal}$ is the current at the h-th harmonic produced under non-distorted supply voltage conditions.

For example, if AF_h is equal to 0.6, then the CFL will output 40% less h-th harmonic current than when it is supplied by an ideal sinusoidal source.

By comparing the indices presented in (3.1) and (3.2), it is evident that

- For the traditional index (3.1), N units are operated in parallel, and the base I_{h-1} used for the denominator is the current from one unit measured in the measurement site. This denominator does not necessarily correspond to the current source model obtained under undistorted voltage supply.

- The proposed index (3.2) is easier to implement because the operating loads do not need to be identical. Therefore, a more flexible set-up can be used.
- It is possible to better understand the influence of the system background harmonics on the device harmonic currents when using the proposed index than when using the traditional index.

3.3.3 Characterizing the Harmonic Attenuation Effect of CFLs

3.3.3.1 Experimental Set-up

The experimental set-up is shown in Figure 3.5. The instruments used in this set-up are the same as those explained for the set-up described in Chapter 2. The main consideration in determining the attenuation effect is to mimic the supply system conditions and appliance-usage patterns in a typical North American residential house. According to the electric codes, the standard wires used in residences typically vary from AWG 14 to AWG 8 and are at most 40 meters long [59]. Most small appliances, such as televisions and microwaves, and lighting devices are fed by using wire AWG 14. Therefore, to reflect the actual scenario, a long supply wire of 40 meters was used. As Figure 3.5 shows, the wire length was varied by connecting the block of CFLs at 7, 14, 20, 27, 33 and 40 meters to determine the impact of supply system impedance (wire length) on the attenuation factor.

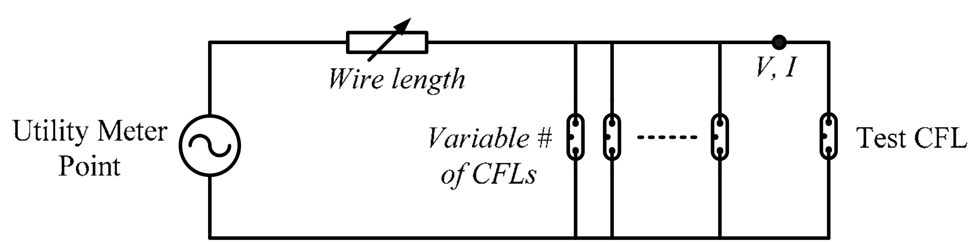

Figure 3.5. Measurement set-up

The sample CFL selected for evaluation is rated 27W. The number of CFLs connected in the background was varied to create different voltage distortions at the data recording point. This arrangement of using identical CFLs to create voltage distortion was intended to yield an aggressive estimate of the AF_h as all harmonic sources will draw pulse currents during the same period. As explained earlier, it is stated in [33] that an average North American house has a total number of 27-30 installed lamps and that the *IEA* estimate is 25 lamps per household. To consider this whole range, the harmonic voltages were created by using 1 to 30 CFLs.

It was noticed that due to widespread use of nonlinear appliances, the supply voltage used for conducting the test had been already distorted before any CFL was connected. The background voltage distortion was about 3.5% *THD* at the experimental site used for the measurements presented in this subsection.

3.3.3.2 Results

Extensive measurements were conducted to determine the attenuation effect. The main results are shown in this section. There are two types of results: the change of attenuation factors under different test conditions and the change of the total harmonic currents produced by the test CFL. Both types of result reveal the same phenomenon but present it from different perspectives.

Figure 3.6 shows the change in the *AF* as the number of background CFLs added to the interface point at different wire lengths increases. Figure 3.6 shows that the *AF* values are less than 1 for most harmonics, implying the existence of the attenuation effect. However, for the 7^{th} and 9^{th} harmonics, the *AF* values are initially greater than 1. This finding implies that the sample CFL outputs more 7^{th} and 9^{th} harmonics for the given voltage distortion condition. This finding is surprising, and further analysis confirms that the 7^{th} and 9^{th} harmonics increase under some plausible harmonic voltage conditions. If more CFLs are added, the *AF* values for all harmonics go below 1. Therefore, when N = 1, the attenuation effect is due to the background harmonics, which depend on the magnitudes and phase angles of each harmonic component; in this case, the attenuation factor can be less or more than 1. When N increases, in addition to the effect of the supply source *THD*, the self-attenuation due to the CFLs connected at the end of the wire is prominent; in this case, the *AF* decreases as the number of CFLs increases.

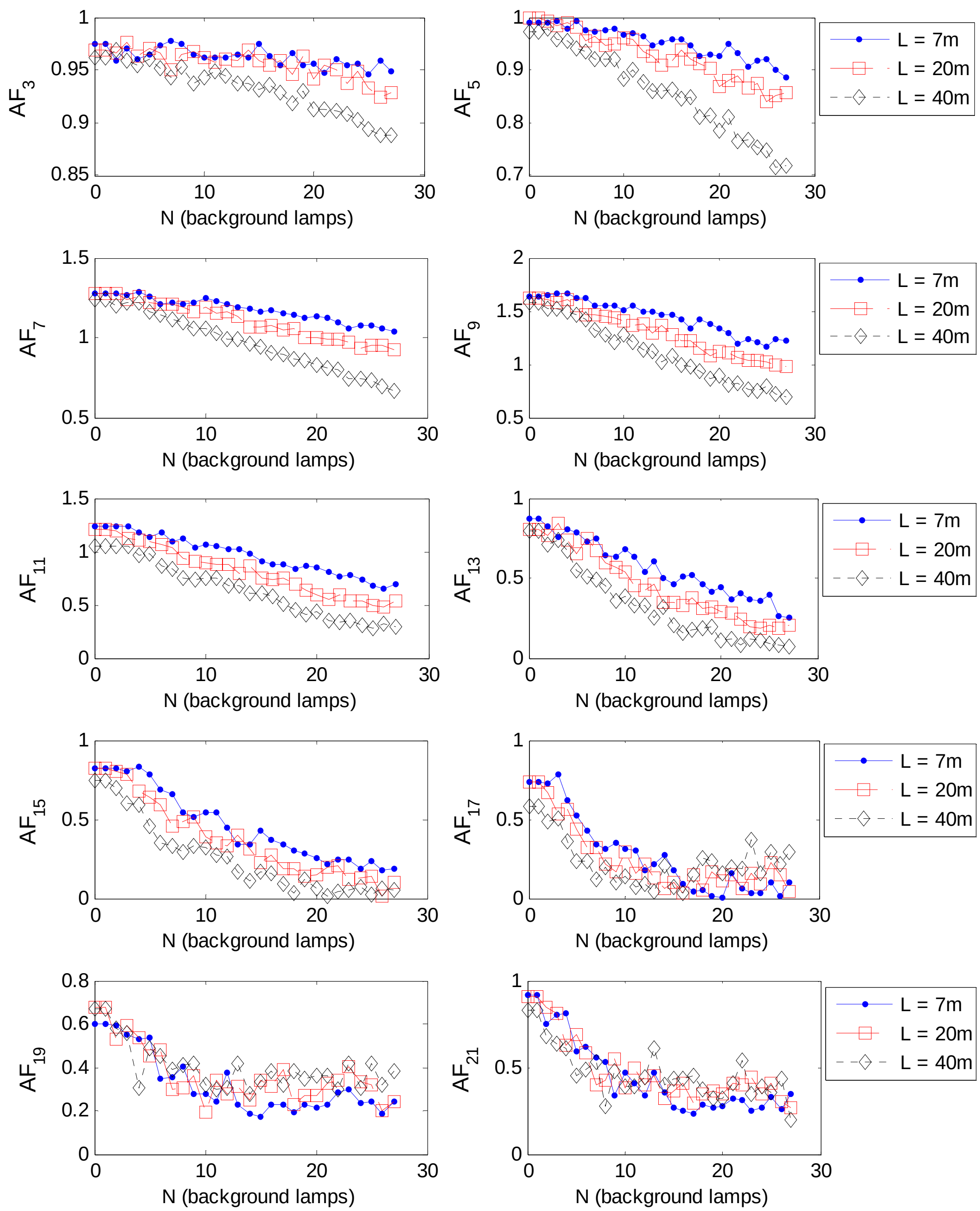

Figure 3.6. Attenuation Factor variation as background lamps increase

Therefore, the attenuation effect does exist but, in creditable supply voltage conditions, the CFL may output more harmonic currents than would be outputted in the ideal conditions. This situation can be seen more clearly in Figure 3.7, which shows the *AF* as a function of the supply voltage *THD*. The voltage *THD* index has included the effect of both the wire impedance and the background harmonic sources. The background voltage experienced during the *AF* measurement is summarized in Table 3.1.

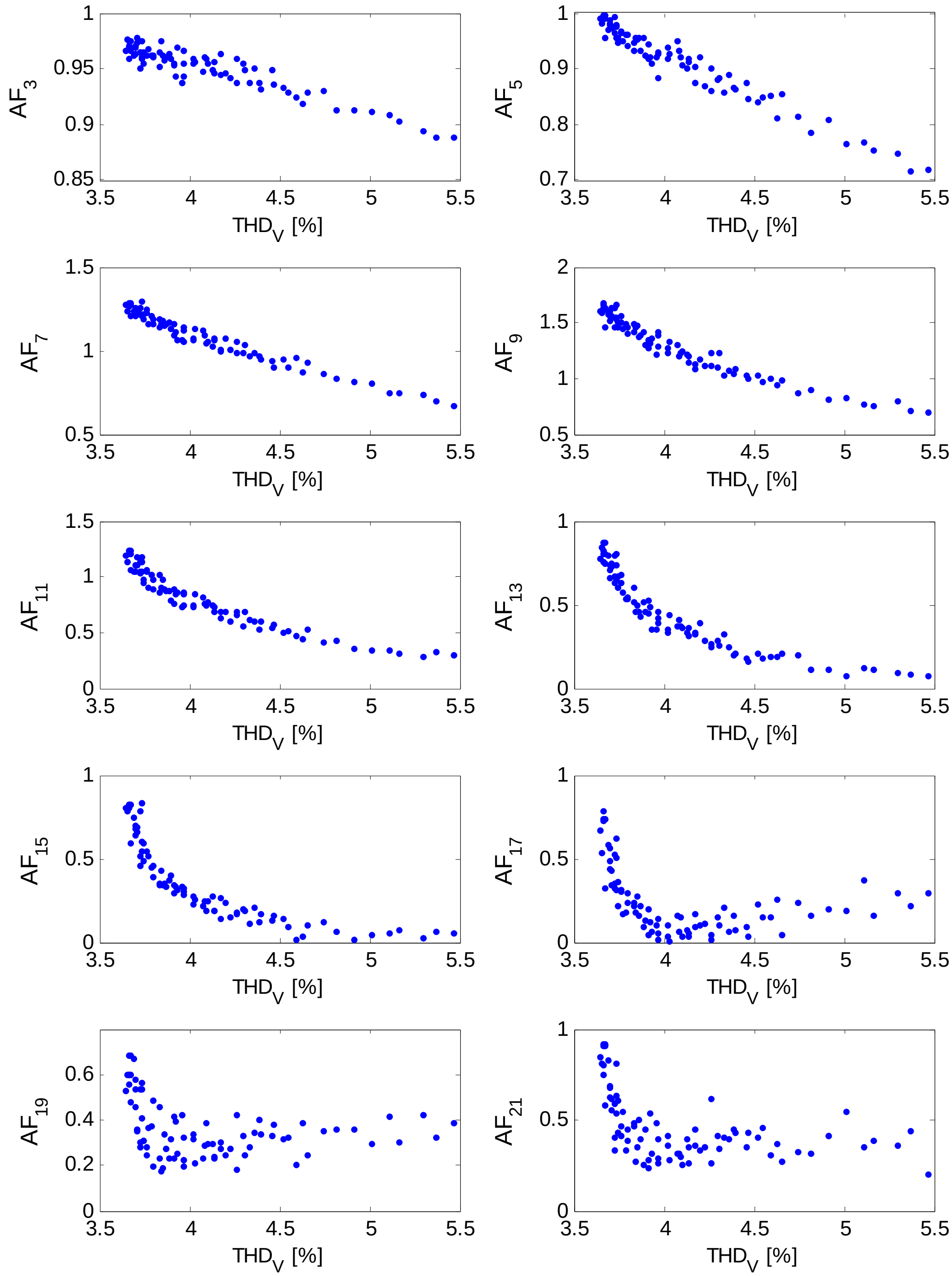

Figure 3.7. Attenuation Factor variation as THD_V increases

Figure 3.6 and Figure 3.7 reveal that the attenuation effect is quite significant for the high-order harmonics. A reduction of 50% harmonic currents is possible when the voltage *THD* is increased to 5.5%. The background lamps (i.e., the background harmonic sources) have a more significant impact than the wire length on the *AF* value.

Table 3.1. Background voltage supply

Harmonic order	Magnitude [V]	Angle [degrees]
1	119.97	-0.05
3	1.90	-115.76
5	2.25	-140.56
7	0.84	158.94
9	0.88	154.16
11	0.12	62.97
13	0.29	42.53
15	0.41	-35.43

The attenuation effect can also be assessed by examining the variation of the CFL harmonic current *TDD* as a function of the supply voltage harmonics. The results are shown in Figure 3.8, which shows that as the voltage *THD* increases from 3.5% to 5.5%, the total harmonic current output is reduced by about 30%. The figure on the right-hand side represents the *TDD* as a function of the voltage *THD*. The curves corresponding to different wire lengths show the same pattern in this case as their correspondent harmonic voltages are similar.

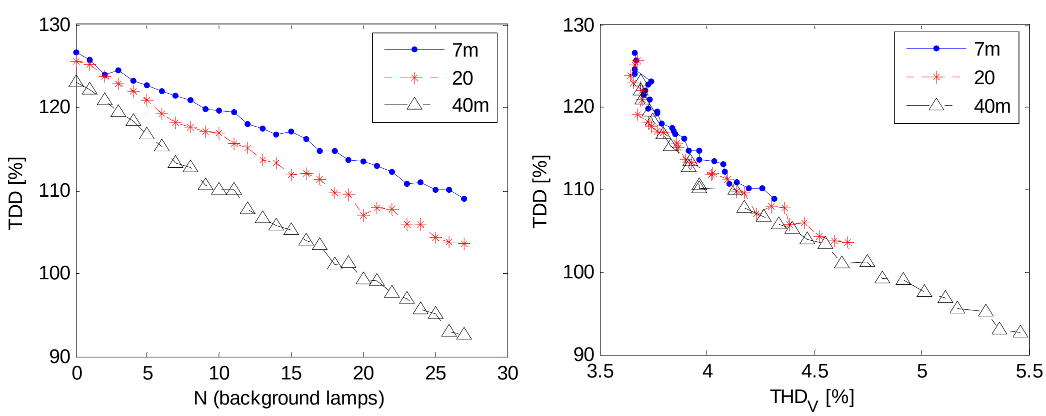

Figure 3.8. *TDD* variation as *N* and THD_V increase

3.3.4 Characterizing the Harmonic Attenuation Effect of a TV, PC, LCD monitor, Laptop, and Microwave Oven

The attenuation effect characterizations of the other home appliances are presented together in this subsection. The selected appliances are the CRT TV, the PC, the LCD monitor, the laptop, and the microwave oven. All those appliances are based on the single-phase diode-bridge rectifier, except the microwave oven, which is analyzed in this section for further illustration on the attenuation effect of home appliances.

3.3.4.1 Experimental Set-up

The experimental set-up is shown in Figure 3.9. To characterize the attenuation effect of the other home appliances, no background harmonic sources were intentionally connected, as the mimicked house scenario did not have multiple identical appliances. The average number of TVs, PCs, computer monitors, laptops and microwave ovens is at most 2 per household [33], [46]. Therefore, besides comparing the current waveform of the appliance measured at the site measurement to that measured under undistorted supply voltage condition, the wire length was varied between 0 and 40m.

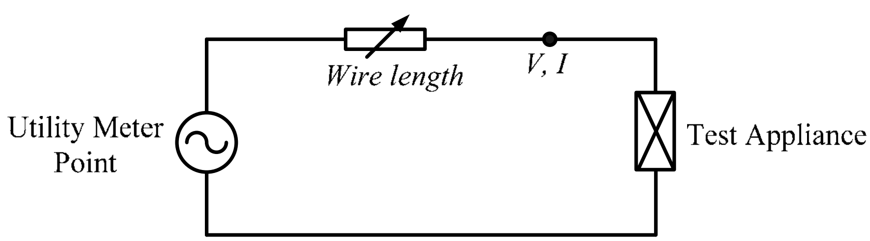

Figure 3.9. Experimental set-up for characterizing the *AF* of the home appliances

3.3.4.2 Results

Sample results are shown in Figure 3.10, which presents the harmonic attenuation effect for the five appliances. The denominator of (3.2) is the case with an undistorted voltage supply. As in the CFL case, the attenuation factor is below unity at most harmonic orders, but above unity at some harmonics. The appliances were measured at different voltage conditions because the measurements were taken on different days. The effect of varying the wire length is not shown in Figure 3.10 because of its small impact.

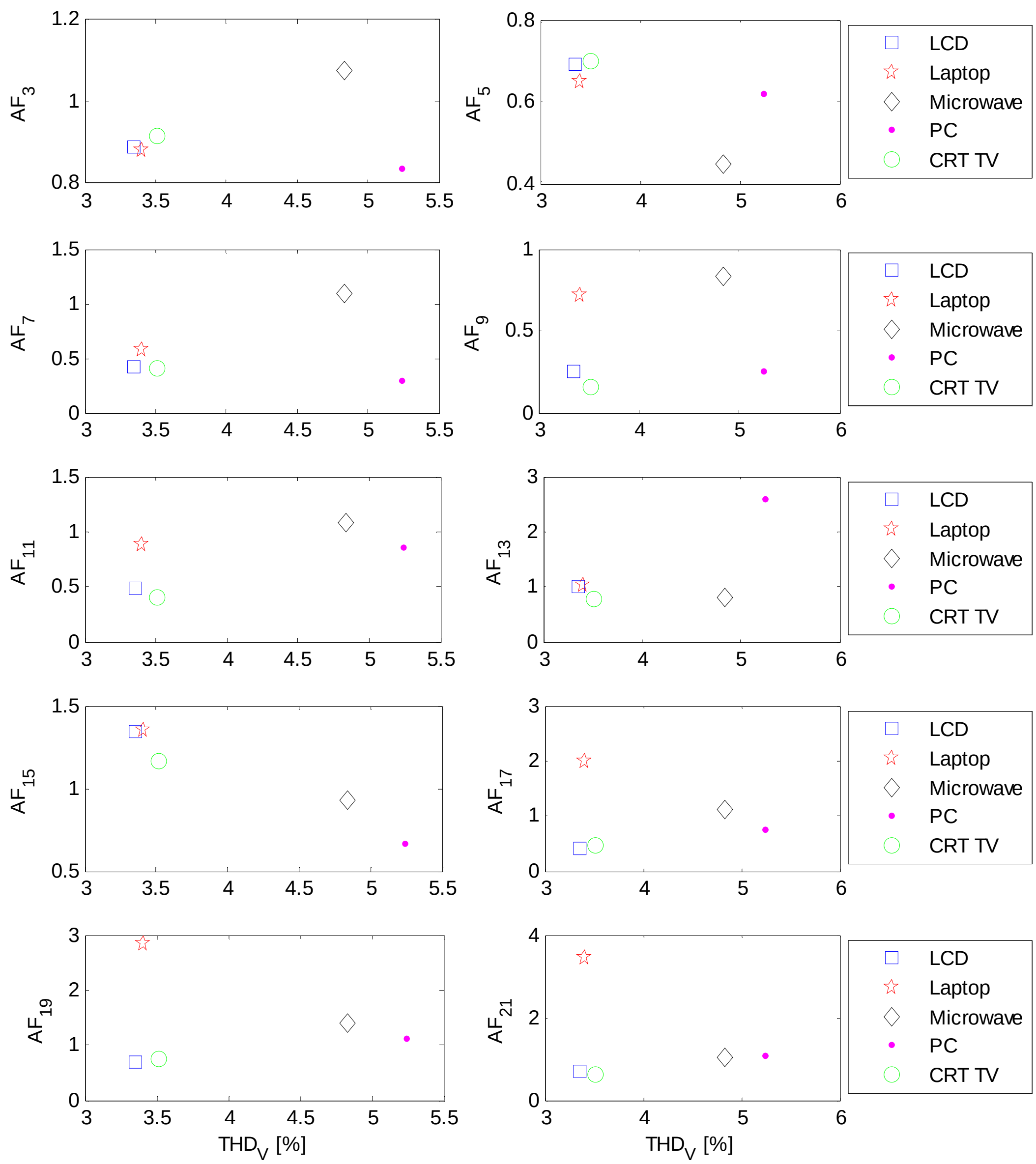

Figure 3.10. Attenuation Factor of five appliances

The attenuation effect was also assessed by using the appliances' harmonic current *TDD* as a function of the supply voltage harmonics (see Figure 3.11). Figure 3.10 and Figure 3.11 imply that the behavior of the home appliances, especially the LCD, Laptop and CRT TV, was similar to that of the CFLs, as the home appliances were measured at voltage conditions similar to those at which the CFLs were measured. Their behaviors, however, were not identical because of the differences in circuitry among the appliances and the CFLs.

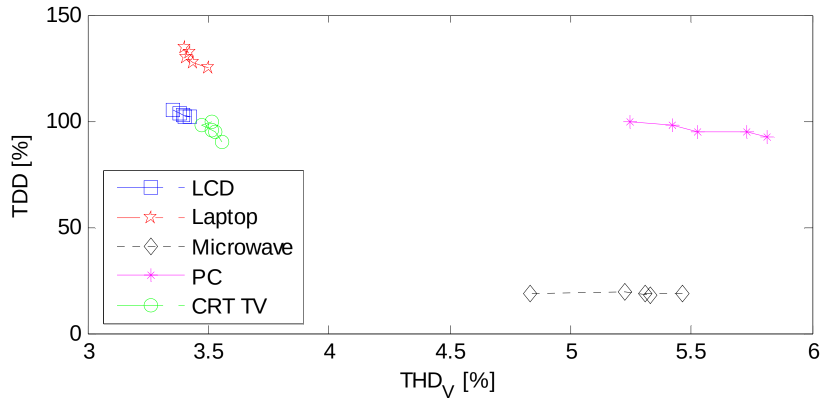

Figure 3.11. *TDD* variation as THD_V increases for the five appliances

In order to further illustrate the self-attenuation of some of the above devices, the results for the LCD monitor, Laptop, PC, and CRT TV supplied by a near-ideal supply and varying the conductor length are shown in Figure 3.12. In this figure, the attenuation factors always start at unity and then decrease due to the self-attenuation.

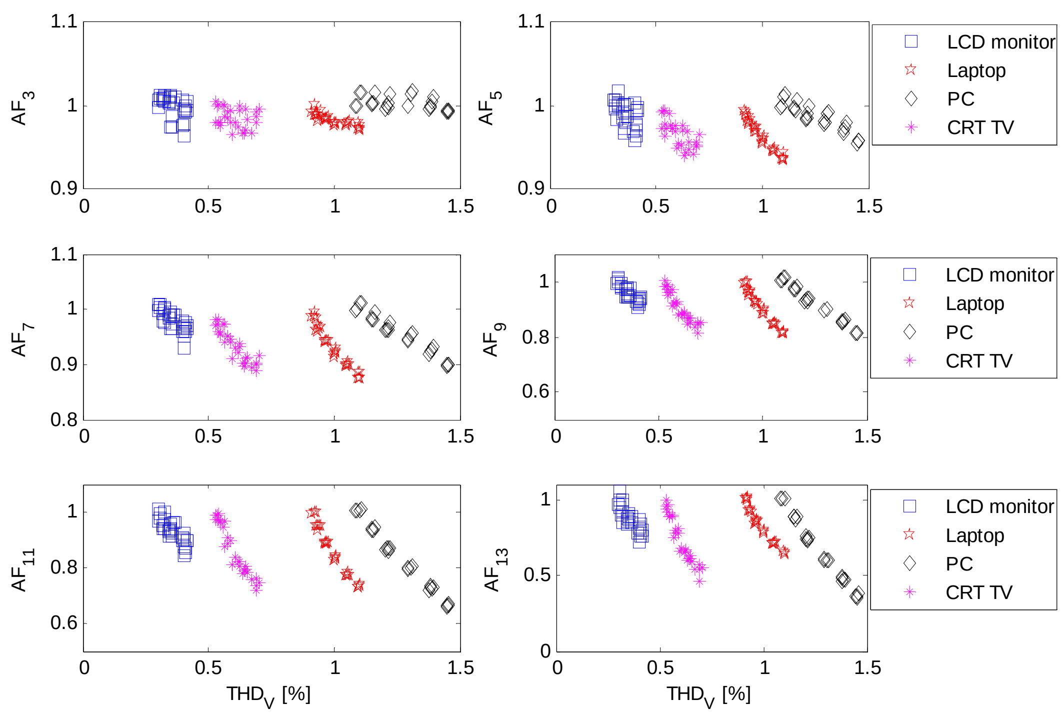

Figure 3.12. *AF* variation as THD_V varies for selected appliances

3.4 Current Harmonic Amplification

The sample experiments presented in the previous sections were selected from extensive experiments done in three urban areas in Edmonton. Based on the processed measurement results, it was found that harmonic amplification was frequently experienced, especially at the 7th and 9th harmonics. This surprise finding was further investigated by using an analytical model that represents the capacitor-filtered diode bridge rectifier. This model was derived at the University of Alberta and was presented in [61], which this researcher co-authored. The extensive measurements performed during this thesis work were used to verify and fit the analytical model. It is used in this section to understand how the voltage distortion affects the current harmonic attenuation (or amplification) effect.

According to [61], the analytical derived model is developed as

$$\begin{bmatrix} \dot{I}_1 \\ \dot{I}_3 \\ \dot{I}_5 \\ \vdots \\ \dot{I}_K \end{bmatrix} = \begin{bmatrix} Y^+_{1,1} & Y^+_{1,3} & Y^+_{1,5} & \cdots & Y^+_{1,H} \\ Y^+_{3,1} & Y^+_{3,5} & Y^+_{3,5} & \cdots & Y^+_{3,H} \\ Y^+_{5,1} & Y^+_{5,3} & Y^+_{5,5} & \cdots & Y^+_{5,H} \\ \vdots & \vdots & \vdots & \ddots & \vdots \\ Y^+_{K,1} & Y^+_{K,3} & Y^+_{K,5} & \cdots & Y^+_{K,H} \end{bmatrix} \begin{bmatrix} \dot{V}_1 \\ \dot{V}_3 \\ \dot{V}_5 \\ \vdots \\ \dot{V}_H \end{bmatrix} + \begin{bmatrix} Y^-_{1,1} & Y^-_{1,3} & Y^-_{1,5} & \cdots & Y^-_{1,H} \\ Y^-_{3,1} & Y^-_{3,5} & Y^-_{3,5} & \cdots & Y^-_{3,H} \\ Y^-_{5,1} & Y^-_{5,3} & Y^-_{5,5} & \cdots & Y^-_{5,H} \\ \vdots & \vdots & \vdots & \ddots & \vdots \\ Y^-_{K,1} & Y^-_{K,3} & Y^-_{K,5} & \cdots & Y^-_{K,H} \end{bmatrix} \begin{bmatrix} \hat{\dot{V}}_1 \\ \hat{\dot{V}}_3 \\ \hat{\dot{V}}_5 \\ \vdots \\ \hat{\dot{V}}_H \end{bmatrix}, \quad (3.3)$$

where

$$Y^+_{k,h} = \frac{\sqrt{1+(h\omega RC)^2}}{\pi R}(\delta-\alpha)e^{j\arctan(h\omega RC)} \quad (h=k), \quad (3.4)$$

$$Y^+_{k,h} = \frac{2\sqrt{1+(h\omega RC)^2}}{\pi R(h-k)}\sin\frac{(h-k)(\delta-\alpha)}{2}e^{j(\frac{(h-k)(\delta+\alpha)}{2}+\arctan(h\omega RC))} \quad (h \neq k), \quad (3.5)$$

$$Y^-_{k,1} = \frac{2\sqrt{1+(\omega RC)^2}}{\pi R(1+k)}\sin\frac{(1+k)(\delta-\alpha)}{2}e^{-j(\frac{(1+k)(\delta+\alpha)}{2}+\arctan(\omega RC))}, \quad (3.6)$$

where

α is the firing angle of the diode bridge,

δ is the extinction angle of the diode bridge,

$\dot{I}_k$ is the phasor of the k-th harmonic current,

$\dot{V}_h$ and $\hat{\dot{V}}_h$ are the phasor of the h-th harmonic voltage and its conjugated, respectively, and

k and h are the odd integers up to the highest concerned harmonic orders of current and voltage.

The details on how obtain this model are presented in [61]. The DC parameters (*R* and *C*) were adjusted in order to have the model fit a CFL response. Simulations using the analytical model are used here to confirm the results obtained from the CFL measurements, as they are qualitatively equivalent.

The same voltage waveforms recorded in the measurements used to obtain Figure 3.6-Figure 3.8 are used as input for the analytical model. Figure 3.13 shows the change of the *AF* as the number of background CFLs is increased. Only harmonics 3^{rd}-13^{th} are shown because they are dominant. Figure 3.13 reveals that harmonic amplification occurs at orders 7^{th}-11^{th} (when $N=1$). This finding verifies the measurement results obtained in the last section. Figure 3.14 shows the *AF* as a function of the supply voltage *THD*, which includes the effect of both the wire impedance and the background harmonic sources. Therefore, the previous findings that harmonic amplification occurs for the analyzed voltage conditions were confirmed by using the analytical model.

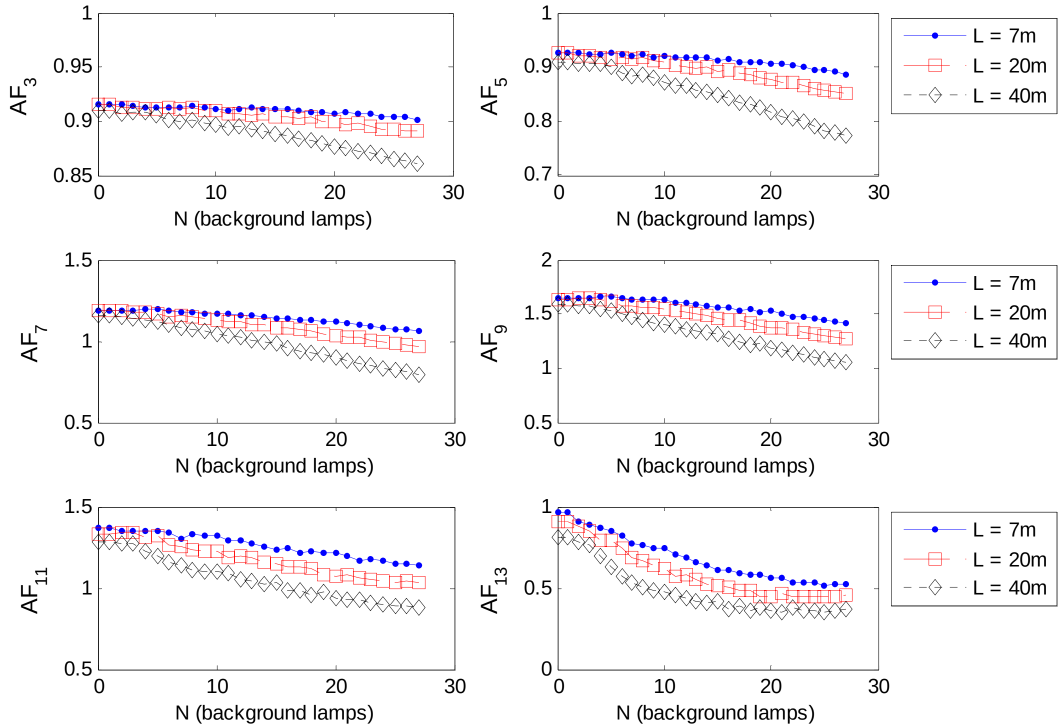

Figure 3.13. Attenuation Factor variation as background lamps increase

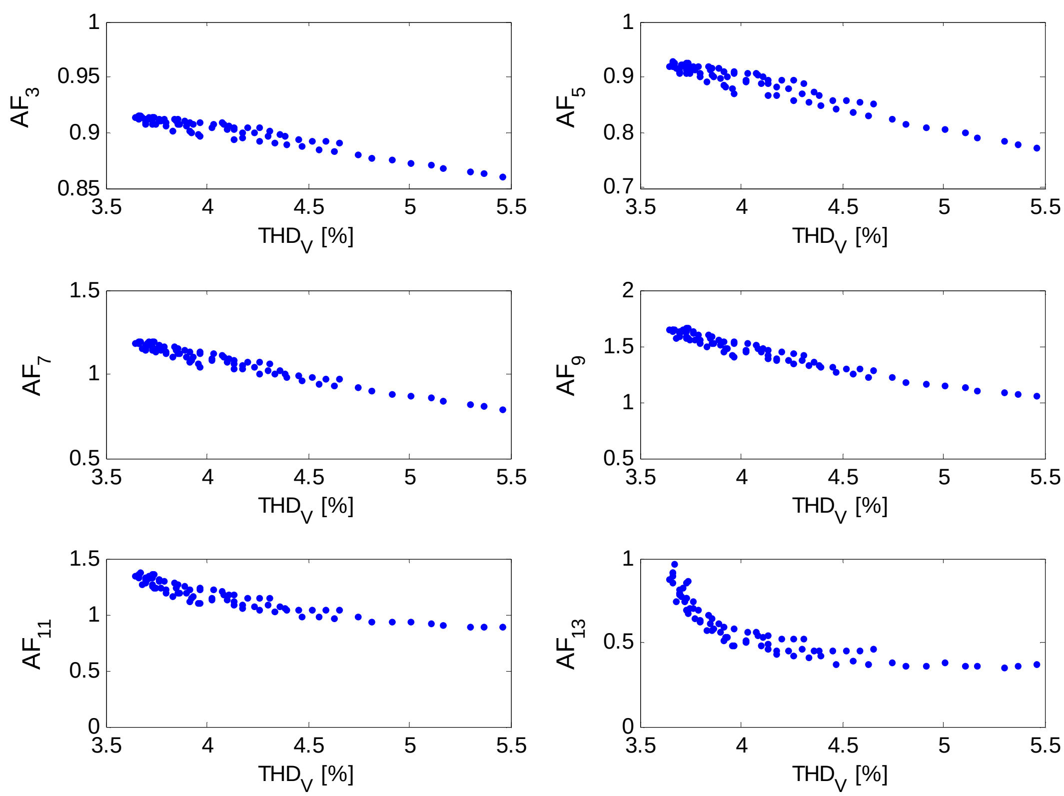

Figure 3.14. Attenuation Factor variation as THD_V increases

Figure 3.15 can be used to explain the observed phenomenon. When N = 1, the attenuation effect is due to background harmonics and is referred to here as mutual attenuation. Since it highly depends on the magnitudes and phase angles of each harmonic component, mutual attenuation can result in an attenuation factor that can be less or more than 1. If more identical loads are added in parallel, the amount of current harmonics increases. This current increase at all harmonic orders is caused by devices that have the same or very similar firing and extinction angles. As a result, the increasing distortion in the currents is a consequence of more peak-shape currents, which cause a voltage drop on the supply conductor and make the voltage at the connecting point become more flat-topped. As a result, AF_h decreases at all harmonic orders. Since this distortion happens due to an increase in the devices of the same type, it is referred to here as self-attenuation. If devices of different types are added in parallel to generate distortion, the situation would be different because their firing and extinction angles would differ. This situation would not necessarily result in harmonic attenuation, for the result could be either attenuation or amplification.

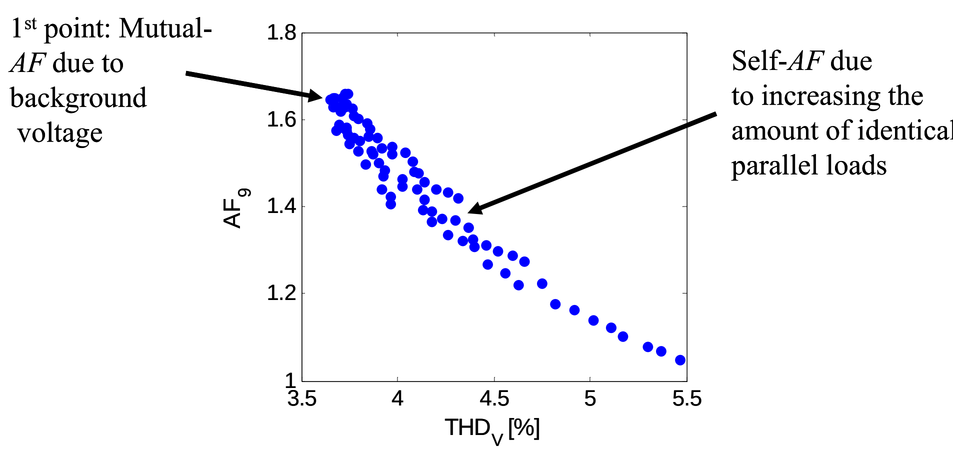

Figure 3.15. AF_9 as THD_V increases

A further investigation was conducted by using the same analytical model. Contour plots of AF_h were obtained under distorted voltage obtained by superimposing the harmonics onto an undistorted waveform. Figure 3.16 and Figure 3.17 show the cases in which the 3rd and 5th harmonic voltages, respectively, with varied magnitudes and phase angles, are superimposed onto the undistorted supply. In these figures, 'Atten.' means the harmonic attenuation range, and 'Ampli.' means the harmonic amplification range. The figures reveal that, taking into consideration all possibilities of the magnitudes and phase angles of voltage harmonics at the supply, the possibility of harmonic amplification occurring at any harmonic order is comparable to that of harmonic attenuation. In reality, however, not all ranges may be practical, as no 3rd harmonic amplification has been experienced in any measurement case. Figure 3.16 and Figure 3.17 also reveal that the amount of harmonic distortion contained in the voltage has a different impact on each AF_h. For example, 5% of the 3rd harmonic of the phase angle equal to 0 causes AF_3 = 1.07 and AF_5 = 1.16, which represent relatively small amplifications, but cause AF_7 = 1.33 and AF_9 = 1.39, which represent significantly larger amplifications. Conversely, if the same 3rd harmonic magnitude has a phase angle equal to $-3\pi/4$, the results are AF_3 = 0.9, AF_5 = 0.75, AF_7 = 0.60, and AF_9 = 0.77. Therefore, harmonics 7th and 9th are more susceptible to AF_h variation than harmonics 3rd and 5th, as the rate of change is higher for the former.

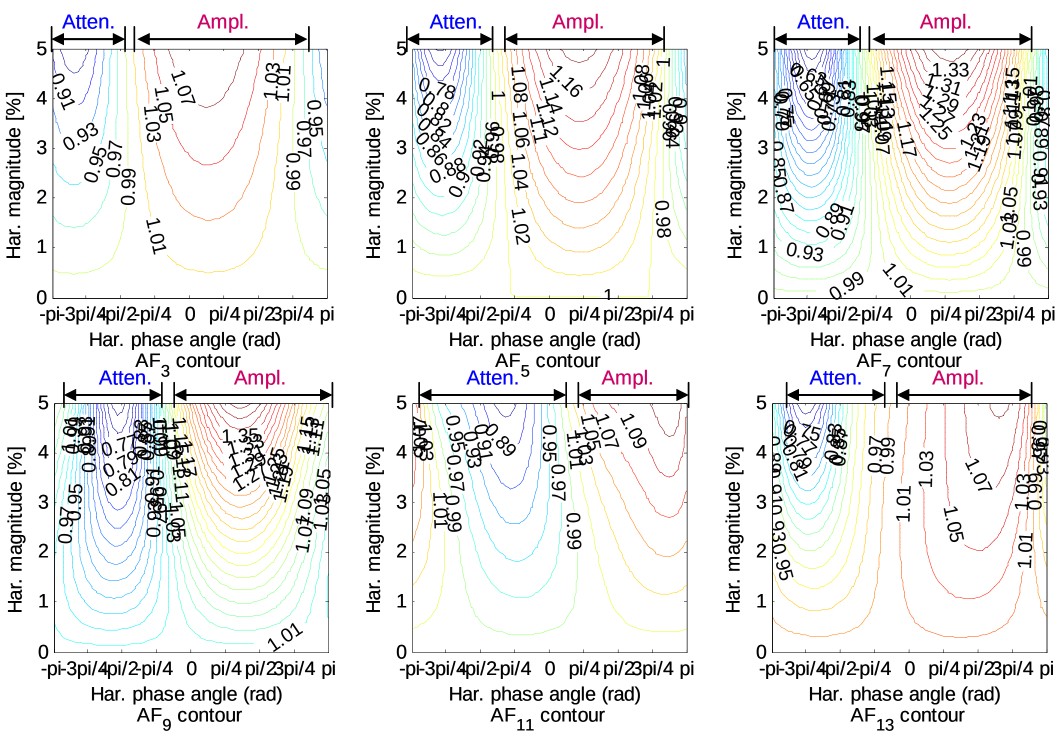

Figure 3.16. Harmonic attenuation and amplification ranges using 3rd harmonic voltage

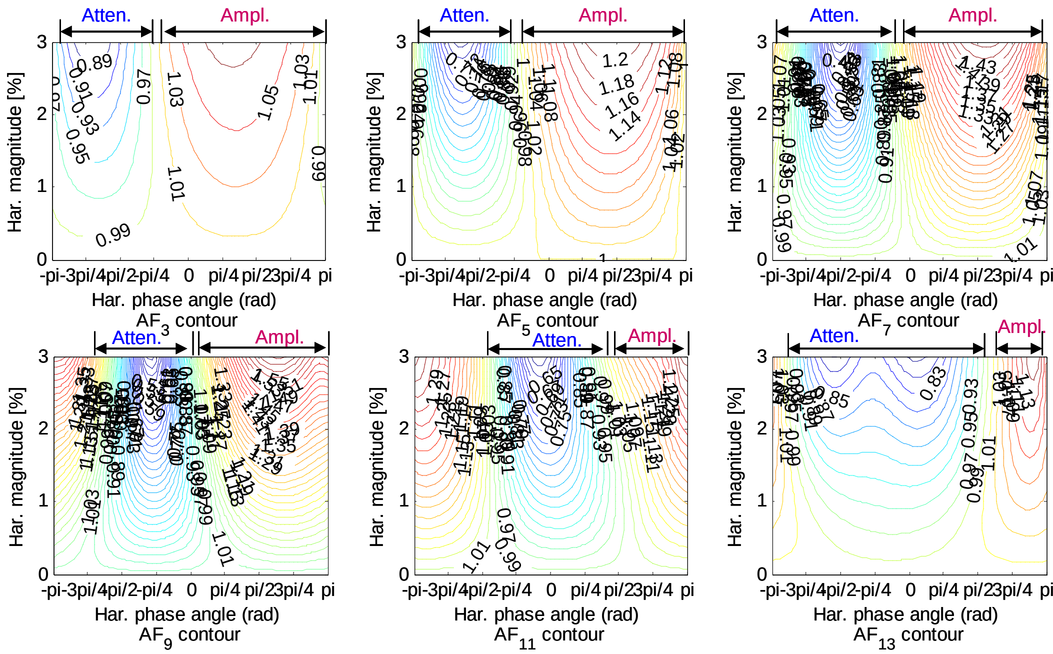

Figure 3.17. Harmonic attenuation and amplification ranges using 5th harmonic voltage

3.5 Conclusions

This chapter has shown that the harmonic attenuation/amplification effect can be significant for single-phase power electronic loads. The main findings are:

- Harmonic amplification can occur under credible voltage conditions. The CFL measurement results showed that harmonic amplification at the 7th and 9th harmonics occurred in most of the measurement sites.
- Harmonic amplification has not been studied or observed in other studies for two main reasons:
  - The traditional index used to describe the attenuation effect did not consider the appliance supplied by undistorted voltage as the base case.
  - The traditional analysis method for characterizing the attenuation effect was applied by considering only the self-attenuation of the devices. Doing so involved adding more identical loads in the background of a test load in order to cause distortion. In this condition, harmonic attenuation is most aggressive.
- Other appliances showed similar harmonic behaviors to those of the CFLs. Differences were observed because the circuits are slightly different. The

microwave oven showed a different behavior to those of the other appliances, due to the difference in the appliance circuitry.

This chapter presented some of the extensive measurements conducted during this thesis work. The measurements were also used to fit an analytical diode rectifier model. This model, conversely, was used to confirm the measurement findings presented in this chapter.

The significance of the attenuation effect has been characterized for common home appliances based on the capacitor-filtered diode-rectifier topology. One way to consider this effect when doing harmonic studies is to incorporate it into the model of a nonlinear load. The next chapter proposes a modeling technique that can be used for power electronic-based appliances and provides a harmonic model that considers the attenuation effect.

Chapter 4

A Measurement-Based Approach for Constructing Harmonic Models of Electronic Home Appliances[1]

The adequate modeling of residential appliances' harmonic producing characteristics is essential for assessing their collective harmonic impact on power distribution systems. One way to accurately account for the harmonic attenuation/amplification effect of harmonic-generating home appliances is to use a harmonic model that considers the effect of the voltage supply harmonics on the load harmonic current. This chapter presents a method to obtain harmonic models for power electronic-based home appliances. The method is developed based on the measurements of the appliances to be modeled. The recorded data of voltages and currents are used to estimate the parameters of the harmonic model. The accuracy of the proposed method is verified for compact fluorescent lights and computer loads.

4.1 Introduction

Harmonic distortions caused by the widespread use of single-phase power electronic-based home appliances have become a concern in distribution systems. Initially, related studies focused primarily on these harmonic characteristics and on the analysis of their anticipated effects on the medium-voltage distribution feeder [35], [37]-[38], [41]-[42], [62]-[63]. At that time, all harmonic-generating loads were commonly modeled as constant harmonic current injections.

[1] A version of this chapter has been submitted for publication: A. B. Nassif, J. Yong, W. Xu, "A Measurement-Based Approach for Constructing Harmonic Models of Electronic Home Appliances," *IET Generation, Transmission and Distribution.*

As show in Chapter 3, the supply voltage harmonics have an impact on the harmonic currents of the harmonic loads due to the attenuation/amplification effect. Originally, this effect was a concern only when studying large harmonic loads. However, as single-phase converter-based home appliances proliferated, distributed (or dispersed) harmonic sources became a concern in harmonic analysis [40]. Researchers began to understand the harmonic attenuation effect and realized that the modeling of these devices had to be improved.

Most of the current literature dealing with the modeling of home appliances is based on time-domain simulation [64]-[65]. Any time-domain simulation can accurately account for the effects of harmonic attenuation and amplification. For example, EMTP or similar programs can be used for this purpose. This approach includes the topologies of the harmonic loads in the model, and provides good modeling accuracy. However, this approach has two limitations. First, setting up a detailed model and conducting simulation studies for multiple cases is difficult. Second, this approach provides little understanding of the impact of modeling inaccuracy and the attenuation effect on the results. Because of these limitations, time-domain based harmonic analysis methods are used for special cases only.

Progress has been made in the analytical modeling of converter bridges for harmonic studies. Reference [66] developed a model for converter loads in the frequency domain. Reference [67] extended the work of [66] and proposed a coupled frequency domain admittance matrix model for both single-phase and three-phase controlled converters. However, although the analytical modeling of single-phase converters is elegant and accurate, it usually results in a model that is too complicated to be used in large-scale harmonic modeling.

Few studies have been published on modeling single-phase nonlinear home appliances by using measurements. In reference [68], the author developed a technique to obtain a frequency-domain harmonically-coupled admittance relationship between the harmonic voltages and currents with the following structure:

$$\begin{bmatrix} \dot{I}_1 \\ \dot{I}_2 \\ \dot{I}_3 \\ \vdots \\ \dot{I}_M \end{bmatrix} = \begin{bmatrix} Y_{1,1} & Y_{1,2} & Y_{1,3} & \cdots & Y_{1,M} \\ Y_{2,1} & Y_{2,2} & Y_{2,3} & \cdots & Y_{2,M} \\ Y_{3,1} & Y_{3,2} & Y_{3,3} & \cdots & Y_{3,M} \\ \vdots & \vdots & \vdots & \ddots & \vdots \\ Y_{M,1} & Y_{M,2} & Y_{M,3} & \cdots & Y_{M,M} \end{bmatrix} \begin{bmatrix} \dot{V}_1 \\ \dot{V}_2 \\ \dot{V}_3 \\ \vdots \\ \dot{V}_M \end{bmatrix}. \tag{4.1}$$

The terms $Y_{k,j}$ of the "crossed frequency" admittance matrix can be obtained through the following 2 steps: (1) Only fundamental-frequency voltage is applied to a device and the terms of the first column ($Y_{k,l}$) are calculated using (4.1). The non-linear load must be tested maintaining constant the fundamental voltage and superimposing one variable harmonic voltage at a time. The authors imposed voltages with up to 20% variation with arbitrary phase angle. Then, supposing the effects of the fundamental voltage are constant, the terms $Y_{k,j}$ (with $j \neq 1$) are calculated as:

$$\dot{Y}_{k,j} = \frac{\dot{I}_k - Y_{k,1}\dot{V}_1}{\dot{V}_j}. \tag{4.2}$$

The drawback of the author's approach is that it does not consider that the appliance model is not constant over an indefinite supply voltage condition. In reality, as shown in Chapter 3, the admittance model depends on the firing and extinction angles, which in turn depend on the voltage waveform. As a result, the estimated model may not suit voltage conditions other than those used for obtaining the model. In addition, it requires many synthetic voltage signals obtained by using a high-precision signal generator to supply the load to be modeled. These supply voltage signals are required in order to obtain all the components of the admittance relationship.

This chapter proposes the development of a frequency-domain model for power electronic-based home appliances using a measurement-based approach. The main advantages of this method are:

- The derived model is derived based on the appliances' real measurements.
- The measurements are obtained from a practical range of supply voltage conditions and do not require a voltage signal generator.
- The model admittance matrices are constant for the voltage range of interest.

- The approach provides a simple model that can be easily incorporated into a harmonic power flow program.

The model's performance in representing CFLs has been assessed and its accuracy has been thoroughly validated. The modeling technique was also used to represent personal computers and LCD monitors. The model, therefore, is designed to have good performance over a practical range of voltage conditions.

4.2 Topologies of the Measurement-Based Model

As explained above, the objective of this chapter is to obtain the frequency-domain relationship between the voltage and the current for electronic home appliances. Real measured data are used to fit the model by using a least-squares approach. This section explains how the model topology was chosen for this purpose.

The traditional way to represent an uncontrolled converter for capacitor-filtered DC-link is to use a relationship such as [66]

$$\dot{I}_{ac} = Y^{+}\dot{V}_{ac} + Y^{-}\hat{\dot{V}}_{ac}, \tag{4.3}$$

where

$\dot{I}_{ac}$ is the current drawn by the nonlinear load,

Y^{+} and Y^{-} are the admittance relationships,

$\dot{V}_{ac}$ and $\hat{\dot{V}}_{ac}$ are the harmonic voltage and its conjugated value, respectively.

The relationship between the voltage and the current developed in [67] is a harmonically-coupled matrix form. Based on this reasoning, the prime objective during the first stage of this work was to fit this model. This fitting would result in a model based on the same structure, but aimed at representing uncontrolled converters. This model is called the Full Model. This model was further simplified twice in order to overcome numerical issues (see Appendix B). Therefore, the importance and role of the simplifications are also explained in this chapter.

4.2.1 The Full Model

For investigating harmonics only, (4.3) can be expanded as shown in (4.4):

$$\begin{bmatrix} \dot{I}_3 \\ \dot{I}_5 \\ \vdots \\ \dot{I}_H \end{bmatrix} = \begin{bmatrix} \dot{I}_{s3} \\ \dot{I}_{s5} \\ \vdots \\ \dot{I}_{sH} \end{bmatrix} + \begin{bmatrix} Y^+_{3,3} & Y^+_{3,5} & \cdots & Y^+_{3,H} \\ Y^+_{5,3} & Y^+_{5,5} & \cdots & Y^+_{5,H} \\ \vdots & \vdots & \ddots & \vdots \\ Y^+_{H,3} & Y^+_{H,5} & \cdots & Y^+_{H,H} \end{bmatrix} \begin{bmatrix} \dot{V}_3 \\ \dot{V}_5 \\ \vdots \\ \dot{V}_H \end{bmatrix} + \begin{bmatrix} Y^-_{3,3} & Y^-_{3,5} & \cdots & Y^-_{3,H} \\ Y^-_{5,3} & Y^-_{5,5} & \cdots & Y^-_{5,H} \\ \vdots & \vdots & \ddots & \vdots \\ Y^-_{H,3} & Y^-_{H,5} & \cdots & Y^-_{H,H} \end{bmatrix} \begin{bmatrix} \hat{\dot{V}}_3 \\ \hat{\dot{V}}_5 \\ \vdots \\ \hat{\dot{V}}_H \end{bmatrix} \tag{4.4}$$

where

$\dot{I}_{sh}$ is the estimated current-source of the equivalent circuit,

$Y^+_{h,h}$ and $Y^-_{h,h}$ are the estimated components of the coupled admittance matrices,

$\dot{V}_h$ and $\hat{\dot{V}}_h$ are the harmonic voltage measurements and its conjugated values, respectively.

On the right-hand side of this relationship, the vector $\left[\dot{I}_{sh}\right]$ is a constant current source injection. It represents the relationship between the fundamental voltage and the harmonic currents. The relationship between the harmonic voltages and harmonic currents, $Y^+\dot{V}_{ac} + Y^-\hat{\dot{V}}_{ac}$, represents the harmonic current deviations from the current drawn when the load is supplied by an undistorted supply (attenuation or amplification). The circuit presented in Figure 4.1 is the representation of this model.

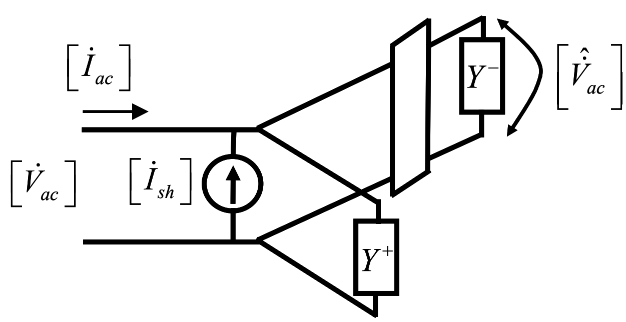

Figure 4.1. Equivalent circuit for the Full Model

In order estimate this model, the manipulations shown in (4.5)-(4.8) were carried out. The matrices and their dimensions below the equations are shown, with *H* being the highest desired harmonic order. Since only odd harmonics are used, the dimension of the Y matrices is $(H - 1)/2$. During all experimental tests performed on the home appliances, no harmonic voltages or currents with even harmonic orders were observed. Consequently, the admittance and current injections corresponding to the even order harmonics were assumed zero and are omitted from the formulations.

Equation (4.4) is re-arranged in the following form:

$$\underbrace{\dot{I}_h}_{(H-1)/2,1} = \underbrace{\dot{I}_{sh}}_{(H-1)/2,1} + \underbrace{Y^+\dot{V}}_{(H-1)/2,1} + \underbrace{Y^-\hat{\dot{V}}}_{(H-1)/2,1} \Rightarrow \underbrace{\dot{I}_h}_{(H-1)/2,1} = \underbrace{\begin{bmatrix} \dot{I}_{sh} & Y^+ & Y^- \end{bmatrix}}_{(H-1)/2,H} \underbrace{\begin{bmatrix} 1 \\ \dot{V} \\ \hat{\dot{V}} \end{bmatrix}}_{H,1}. \tag{4.5}$$

In order to carry out the least-squares estimation, m independent measurements were used. Therefore, the application of the least-squares solution gives:

$$\underbrace{\dot{I}_h}_{(H-1)/2,m} = \underbrace{\begin{bmatrix} \dot{I}_{sh} & Y^+ & Y^- \end{bmatrix}}_{(H-1)/2,h} \underbrace{\begin{bmatrix} \underbrace{1}_{1,m} \\ \dot{V} \\ \hat{\dot{V}} \end{bmatrix}}_{H,m} \Rightarrow \underbrace{\dot{I}_h}_{(H-1)/2,m} \underbrace{\begin{bmatrix} \underbrace{1}_{m,1} & \dot{V} & \hat{\dot{V}} \end{bmatrix}}_{m,H} = \underbrace{\begin{bmatrix} \dot{I}_{sh} & Y^+ & Y^- \end{bmatrix}}_{(H-1)/2,H} \underbrace{\begin{bmatrix} \underbrace{1}_{1,m} \\ \dot{V} \\ \hat{\dot{V}} \end{bmatrix}}_{H,m} \underbrace{\begin{bmatrix} \underbrace{1}_{m,1} & \dot{V} & \hat{\dot{V}} \end{bmatrix}}_{m,H}. \tag{4.6}$$

By isolating the matrices $\dot{I}_{sh}$, Y^+ and Y^-, the final solution is obtained as

$$\underbrace{\begin{bmatrix} \dot{I}_{sh} & Y^+ & Y^- \end{bmatrix}}_{(H-1)/2,H} = \underbrace{\dot{I}_h}_{(H-1)/2,m} \underbrace{\begin{bmatrix} 1 & \dot{V} & \hat{\dot{V}} \end{bmatrix}}_{m,H} \left(\underbrace{\begin{bmatrix} \underbrace{1}_{1,m} \\ \dot{V} \\ \hat{\dot{V}} \end{bmatrix}}_{H,m} \underbrace{\begin{bmatrix} 1 & \dot{V} & \hat{\dot{V}} \end{bmatrix}}_{m,H} \right)^{-1}. \tag{4.7}$$

This approach, however, is vulnerable to numerical difficulties that are inherent in the least squares solution (see Appendix B). The normal matrix was ill-conditioned for most of the data, and as a result, its inversion resulted in numerical instability. For the CFL case, for example, the condition numbers were in the order of 10^8. In an attempt to circumvent this problem, a model simplification was adopted, as shown in the next subsection.

4.2.2 The Coupled *Y* Model

In order to address the issue of numerical difficulties, the full model was simplified to the coupled *Y* model. The circuit topology to represent this model is similar to that presented in [68], and its mathematical structure is presented in (4.8):

$$\begin{bmatrix} \dot{I}_3 \\ \dot{I}_5 \\ \vdots \\ \dot{I}_H \end{bmatrix} = \begin{bmatrix} \dot{I}_{s3} \\ \dot{I}_{s5} \\ \vdots \\ \dot{I}_{sH} \end{bmatrix} + \begin{bmatrix} Y_{3,3} & Y_{3,5} & \cdots & Y_{3,H} \\ Y_{5,3} & Y_{5,5} & \cdots & Y_{5,H} \\ \vdots & \vdots & \ddots & \vdots \\ Y_{H,3} & Y_{H,5} & \cdots & Y_{H,H} \end{bmatrix} \begin{bmatrix} \dot{V}_3 \\ \dot{V}_5 \\ \vdots \\ \dot{V}_H \end{bmatrix}, \tag{4.8}$$

where

$\dot{I}_{sh}$ is the estimated current-source of the equivalent circuit,

$Y_{h,h}$ is the estimated components of the coupled admittance matrix,

$\dot{V}_h$ is the harmonic voltage measurements.

This model is clearly a simplification of the Full Model. As compared to (4.4), the coupled *Y* model does not have the conjugate counterpart of the voltage, and therefore the measurement approach can use $\dot{V}_{ac}$ to find $\dot{I}_{ac}$. As shown in the results and explained in Appendix B, the numerical noise of the least-squares estimation is smaller, resulting in improved conditioning of the normal matrix. Since the introduced approach is based on the use of least squares, it is able to provide a model that is functional over a wide range of voltage conditions. The equivalent circuit to represent this model is shown in Figure 4.2.

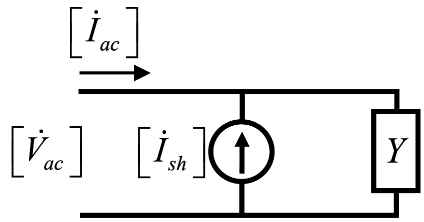

Figure 4.2. Equivalent circuit for the coupled *Y* model

In order to estimate the coupled *Y* model's parameters, a procedure similar to that used for the Full Model is adopted. As in the previous case, the estimate is done by using the measurements of the current and voltage waveforms:

$$\left[\dot{I}_h\right]=\left[\dot{I}_{sh}\right]+\left[Y\right]\left[\dot{V}\right]\Rightarrow\left[\dot{I}_h\right]=\left[\dot{I}_{sh}\quad Y\right]\begin{bmatrix}1\\ \dot{V}\end{bmatrix}. \tag{4.9}$$

As *m* independent measurements are used, this equation can be manipulated into the least-squares estimation form, as follows:

$$\left[\dot{I}_h\right]=\left[\dot{I}_{sh}\quad Y\right]\begin{bmatrix}\underbrace{1}_{1,m}\\ \dot{V}\end{bmatrix}\Rightarrow\left[\dot{I}_h\right]\begin{bmatrix}\underbrace{1}_{m,1} & \dot{V}\end{bmatrix}=\left[\dot{I}_{sh}\quad Y\right]\begin{bmatrix}\underbrace{1}_{m,1}\\ \dot{V}\end{bmatrix}\begin{bmatrix}\underbrace{1}_{m,1} & \dot{V}\end{bmatrix}. \tag{4.10}$$

Finally, the matrices $\dot{I}_{sh}$ and *Y* can be obtained from

$$\underbrace{\left[\dot{I}_{sh}\quad Y\right]}_{(H-1)/2,(H-1)/2+1}=\underbrace{\dot{I}_h}_{(H-1)/2,m}\underbrace{\begin{bmatrix}\underbrace{1}_{m,1} & \dot{V}\end{bmatrix}}_{m,(H-1)/2+1}\left(\underbrace{\begin{bmatrix}\underbrace{1}_{m,1}\\ \dot{V}\end{bmatrix}}_{(H-1)/2+1,m}\underbrace{\begin{bmatrix}\underbrace{1}_{m,1} & \dot{V}\end{bmatrix}}_{m,(H-1)/2+1}\right)^{-1}. \tag{4.11}$$

As the estimation process was being carried out, obtaining this model also resulted in numerical problems. The normal matrix was also observed to be ill-conditioned, resulting in unreliable solutions. However, it was observed that the conditioning of this solution was better than that of the previous one, as the condition numbers were of the order of 10^7. The model was further simplified, in an attempt to succeed in the data-fitting task. In this simplification, the *Y*-like matrix to be estimated was assumed to be diagonal, resulting in a decoupled harmonic relationship. The decoupled Y matrix is discussed in the following section.

4.2.3 Decoupled *Y* Matrix

The decoupled Y matrix is a further simplification of the previous model. The new estimated model is a current source plus a diagonal admittance matrix. Further simplifying this model was found to greatly improve the conditioning of the normal matrix.

Figure 4.3 portrays the circuit representation of the decoupled model. As Figure 4.3 shows, the topology is a Norton Equivalent circuit. This topology was the motivation for using this simplified model, as the Norton equivalent approach has been widely used to represent distribution networks for harmonic studies [69]. The selected data used to obtain the equivalent circuit play an important role by determining the supply range of applicability for the model. The use of the least-squares fitting provides the estimated model with a wider range of applicability than the traditional two-point estimation presented in [69].

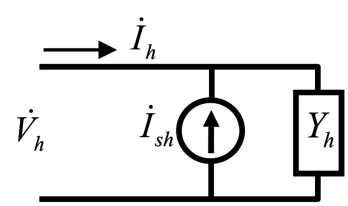

Figure 4.3. Equivalent circuit for the decoupled Y model

The equivalent circuit shown in Figure 4.3 is represented by equation (4.12):

$$\begin{bmatrix} \dot{I}_3 \\ \dot{I}_5 \\ \vdots \\ \dot{I}_H \end{bmatrix} = \begin{bmatrix} \dot{I}_{s3} \\ \dot{I}_{s5} \\ \vdots \\ \dot{I}_{sH} \end{bmatrix} + \begin{bmatrix} Y_{3,3} & 0 & \dots & 0 \\ 0 & Y_{5,5} & \dots & 0 \\ \vdots & \vdots & \ddots & \vdots \\ 0 & 0 & \dots & Y_{H,H} \end{bmatrix} \begin{bmatrix} \dot{V}_3 \\ \dot{V}_5 \\ \vdots \\ \dot{V}_H \end{bmatrix}, \tag{4.12}$$

where

$\dot{I}_{sh}$ is the estimated current-source of the equivalent circuit,

$Y_{h,h}$ is the estimated components of the decoupled admittance matrix,

$\dot{V}_h$ is the harmonic voltage measurements.

Equation (4.12) can be written as $(H - 1)/2$ equations with two unknowns. As a result, a solution can be obtained by using two independent measurements. The investigations carried out during this work revealed that the least-squares solution provides a better performance than other solutions over a wider range of voltage distortions. Therefore, the model presented in (4.12) can be re-arranged with m independent measurements as follows:

$$\dot{I}_h = \begin{bmatrix} \dot{I}_{sh} & Y_{h,h} \end{bmatrix} \begin{bmatrix} \underbrace{1}_{1,m} \\ \dot{V}_h \end{bmatrix} \Rightarrow \dot{I}_h \begin{bmatrix} 1 & \dot{V}_h \end{bmatrix} = \begin{bmatrix} \dot{I}_{sh} & Y_{h,h} \end{bmatrix} \begin{bmatrix} \underbrace{1}_{1,m} \\ \dot{V}_h \end{bmatrix} \begin{bmatrix} 1 & \dot{V}_h \end{bmatrix}. \tag{4.13}$$

For each harmonic order, the vector containing $\dot{I}_{sh}$ and $Y_{h,h}$ can be obtained by using:

$$\underbrace{\begin{bmatrix} \dot{I}_{sh} & Y_{h,h} \end{bmatrix}}_{1,2} = \underbrace{\underbrace{\dot{I}_h}_{1,m} \underbrace{\begin{bmatrix} 1 & \dot{V}_h \end{bmatrix}}_{m,2}}_{1,2} \underbrace{\left(\underbrace{\begin{bmatrix} 1 \\ \dot{V}_h \end{bmatrix}}_{2,m} \underbrace{\begin{bmatrix} 1 & \dot{V}_h \end{bmatrix}}_{m,2} \right)^{-1}}_{2,2} . \tag{4.14}$$

During the estimation process, this harmonic model was observed to be successful in representing electronic appliances. The condition numbers were of much lower value for this model, being of the order of 10^4. The estimation process is presented in the next section.

4.3 Strategy for the Model Derivation and Verification

A procedure is proposed to carry out the estimation and model verification, as shown in Figure 4.4. Figure 4.4 illustrates the procedure using a flowchart.

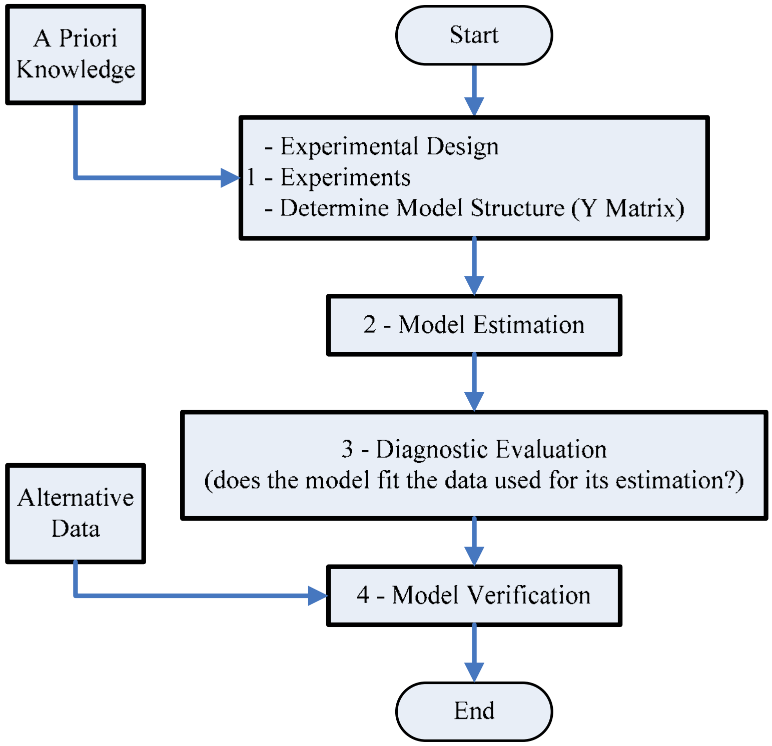

Figure 4.4. Procedure used to fit the recommended model

The procedure steps are presented as follows:

1. Each admittance model is estimated and evaluated. This procedure is performed for the three models (full model, coupled Y model and decoupled Y model) in (4.4), (4.8) and (4.12), respectively.
2. A random group of measurements is used to estimate the model. For the CFLs, 12 different types of bulbs were measured by using 24 random snapshots (2 snapshots from each of 12 measured CFLs). Measurements were taken at arbitrary (within a practical range) voltage supply conditions to perform the least-squares estimation. For the PCs and LCD monitors, 6 and 3 samples were measured, respectively.
3. The model diagnosis is performed; i.e., the estimated model is tested by using the data previously utilized for its derivation. The models were expected to fit this data very well and, in fact, did so.
4. Finally, the models accuracies are verified by evaluating the current response of the admittance model. In order to verify the models, a random set of data (that was not used in the models estimation) was used to evaluate how well the model could predict the current for a given voltage condition. These alternative data and

the data used for estimating the model were obtained from the same measurement site. To quantify this evaluation, the estimated current waveform is reconstructed from the predicted spectrum (up to the 11th harmonic) and evaluated through the time-domain correlation. The correlation coefficient is given by [70]:

$$r[\%] = 100 \times \frac{n\sum_{i=1}^{n} I_{actual}(i) I_{predicted}(i) - \sum_{i=1}^{n} I_{actual}(i) \sum_{i=1}^{n} I_{predicted}(i)}{\sqrt{\left[n\sum_{i=1}^{n} I_{actual}^{2}(i) - \left(\sum_{i=1}^{n} I_{actual}(i)\right)^{2}\right]\left[n\sum_{i=1}^{n} I_{predicted}^{2}(i) - \left(\sum_{i=1}^{n} I_{predicted}(i)\right)^{2}\right]}} \tag{4.15}$$

where

I_{actual} is the measured current waveform,

$I_{predicted}$ is the predicted current waveform using the admittance model.

In order to obtain a model that would be useful for a practical range of voltage conditions, an experiment set-up similar to that used in Chapter 3 was conducted for evaluating the attenuation effect. This test was carried out by connecting a 40m copper wire AWG #14 conductor at the utility meter point. A cluster of CFLs (varying from 1 to 30 lamps) was connected at several intermediate lengths of this conductor, in order to generate distortions. The conductor lengths and number of CFLs were based on estimates from electrical codes and the *IEA* [33], [59] and were chosen in order to obtain a practical and realistic range of voltage conditions. These conditions are suitable for estimating a model that will work for a practical and realistic range of voltage supply conditions.

Figure 4.5 presents the measurement set-up used to perform the model estimation and verification. As Figure 4.5 shows, it is the same set-up used in one of the studies presented in Chapter 3. For testing the PC and LCD monitor (Section 4.6), assorted devices (CFLs, PCs and monitors) were used in the background to cause the voltage distortion.

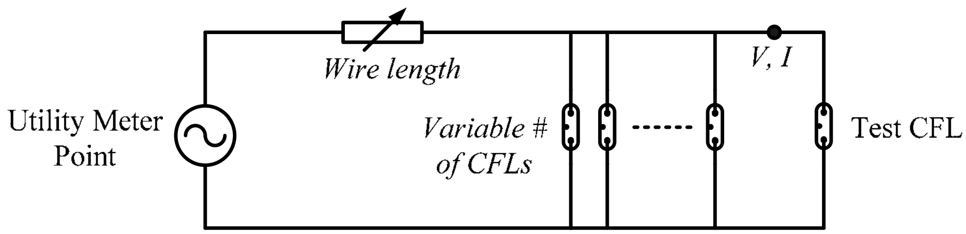

Figure 4.5. Measurement set-up to perform the model estimation and verification

4.4 Results and Verification for the CFL Model Estimation

The results provided in this section were obtained by using the model estimation strategy. The analysis was performed by using twelve CFLs of different brands and ratings in order to find a representative model for the CFLs. The detailed data for the measured CFLs are presented in Appendix A. As the twelve measured CFLs were not of the same rating, the currents and voltages were normalized by their rated values. The rated voltage is 120V, but the rated current depends on the lamp power consumption.

A group of 24 random snapshots, of which 2 were obtained from each sample of CFL, were used to fit the model. The estimated admittance matrix and current sources results are presented in Figure 4.6 and Figure 4.7, respectively. These figures show the results for the estimated decoupled *Y* model. Since they were obtained from the normalized values of voltages and currents, they are not in real units, which are indicated as "scaled." The current I_{sh} is also not in real units.

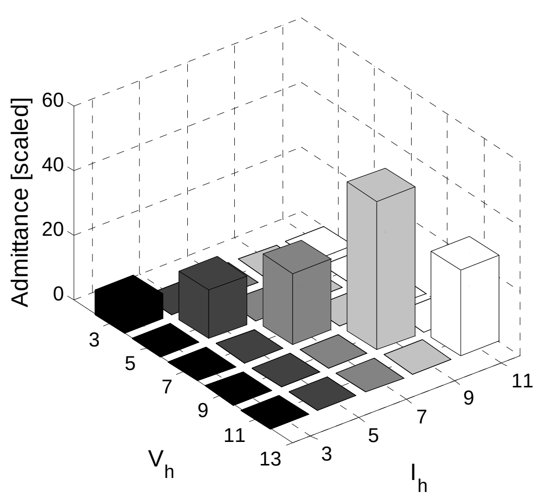

Figure 4.6. Estimated admittance for the CFLs decoupled *Y* model

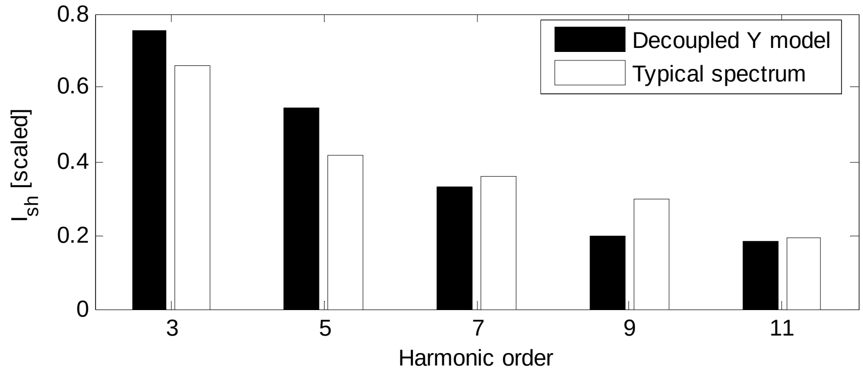

Figure 4.7. Current injections for the CFLs decoupled *Y* model

The model evaluation is assessed by using the model to predict the current waveforms of all 12 measured lamps. This assessment is performed by using the predictions of a random measurement snapshot, which was not used to estimate the model. This procedure is shown in Figure 4.8. Waveform comparison is more desirable than harmonic spectrum comparison because the former ensures that both the harmonic magnitudes and phase angles are verified.

Figure 4.8 shows the measured waveforms along with those obtained by using the decoupled *Y* model (dashed line – estimated current waveform, solid line – measured waveform). The other models' responses are omitted from the figure to improve visualization. The CFL names are omitted, and codes are assigned to them for the figure. The last two digits are the CFL rated power. The final results of the time-domain comparison (i.e., the correlation coefficients results) – obtained by using equation (4.15) – are presented in Table 4.1, which presents the results for the three models. It shows that the decoupled *Y* model can generally fit any kind of CFL. Notice that the estimated full-model and the coupled *Y* do not fit the alternative data with acceptable accuracy.

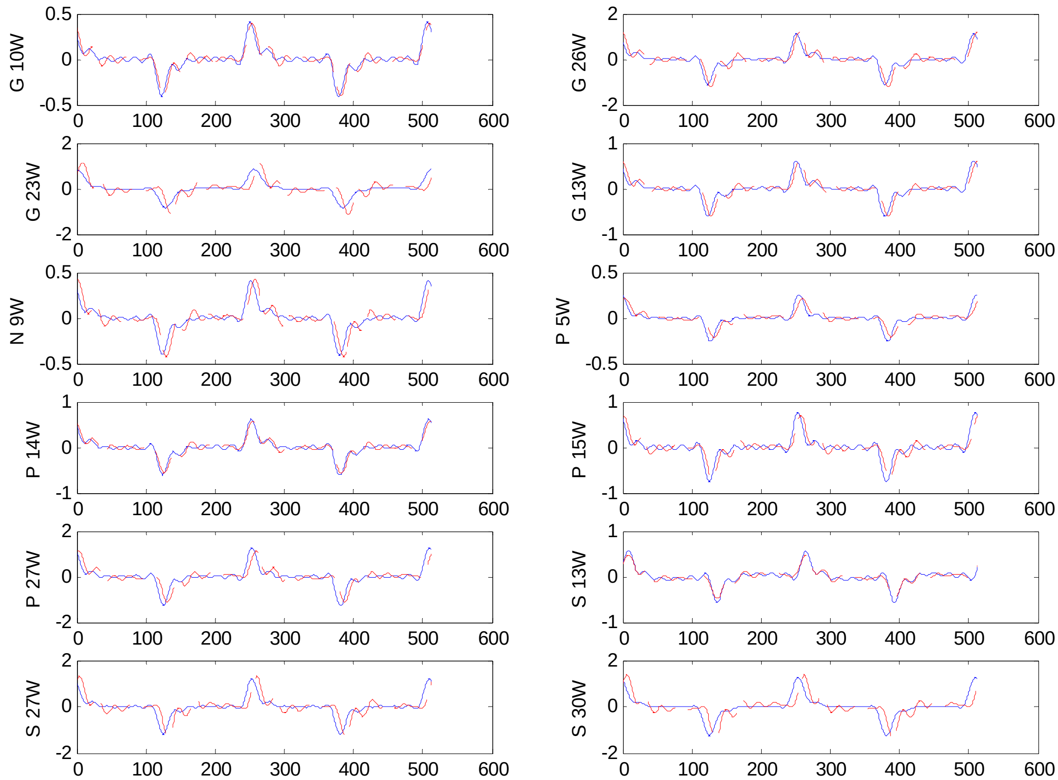

Figure 4.8. Time-domain measured and predicted current waveforms using decoupled *Y* model

Table 4.1. Average of the Correlation Coefficient Values for the Three Models

CFL Code	**Full model Y^+ & Y^-**	**Coupled *Y* model**	**Decoupled *Y* model**
G 10W	15.417	54.872	93.258
G 26W	2.7101	56.798	87.108
G 23W	-6.6554	34.156	73.946
G 13W	2.2773	57.35	87.562
N 09W	-6.4883	53.912	82.508
P 05W	-5.4301	56.303	82.465
P 14W	19.594	53.168	94.143
P 15W	2.1058	58.566	84.061
P 27W	-8.9367	55.304	77.885
S 13W	39.169	42.293	96.203
S 27W	-14.434	47.37	70.916
S 30W	-15.228	34.088	68.764

Based on the results presented, the decoupled *Y* model is recommended as the only model able to fit the CFL models well and to predict their harmonic currents injections. The coupled models, which in theory should provide a better prediction result, did not succeed in doing so because of their encountered numerical problems during the estimation processes. As a result, their obtained models were unreliable and provided poor prediction results.

4.5 Further Verification by using the Attenuation Effects

This section presents the CFL model verification by using the attenuation effect. In order to perform this verification, a concept called the Effective Lamp curves is introduced in this thesis. The verification in this section is not aimed at analyzing the attenuation effect of the CFL, but at verifying the derived model. This section briefly introduces the concept curves and presents the model validation results by using the concept.

4.5.1 The Effective-Lamp Index

The index called "Effective Lamp" was introduced in [56], which this researcher authored, to characterize the attenuation effect. Figure 4.9 shows sample results to explain the idea. According to this figure, the *x*-axis represents the actual number of CFL lamps connected to the supply system, and the *y*-axis represents the equivalent number of lamps that would generate approximately the same amount of harmonic currents if the CFL terminal were a supply clean of harmonics. Since the actual curves deviate from the current-source (ideal) case, an attenuation effect is present [24]. For example, if 20 lamps are connected to the system through a 40m wire, the amount of harmonic currents produced by these lamps is equivalent to that produced by 16 lamps under the undistorted voltage supply condition.

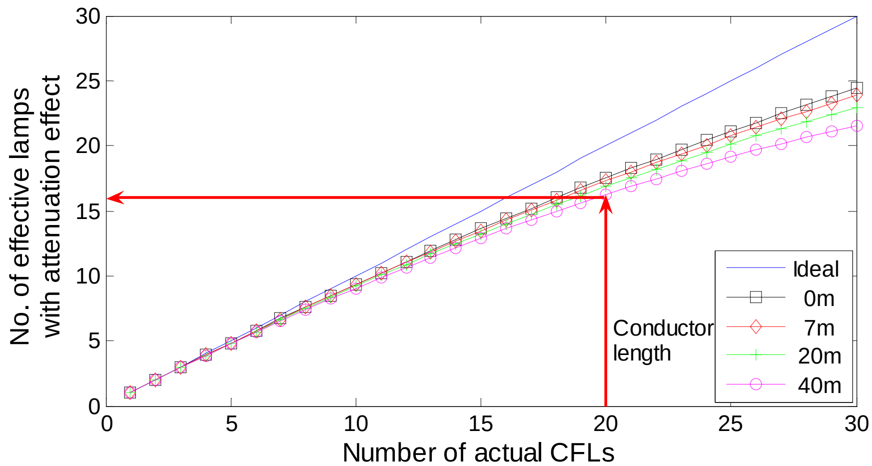

Figure 4.9. Attenuation Effect of the CFL lamps using the Effective-Lamp concept

The figure shows the effective lamp index for different conductor lengths. Here, the conductor refers to that connected between the CFLs and the undistorted supply system. For practical purposes, this conductor is the one supplying the CFL from the utility meter point.

4.5.2 Determination of the Effective-Lamp Curves

The Effective Lamp index is defined as follows:

$$N_{Effective-h} = \frac{I_h^N}{I_{h\_0}^1}, \tag{4.16}$$

where

I_h^N is the measured total h-th harmonic current for parallel N CFLs,

$I_{h\_0}^1$ is the h-th current harmonic produced by one CFL under undistorted voltage supply conditions.

This index is essentially the ratio of the h-th harmonic current produced by N lamps under the distorted supply voltage condition to the h-th harmonic current produced by one lamp under the undistorted supply voltage condition.

The above index is determined by using experimental results. The experiment set-up is shown in Figure 4.10.

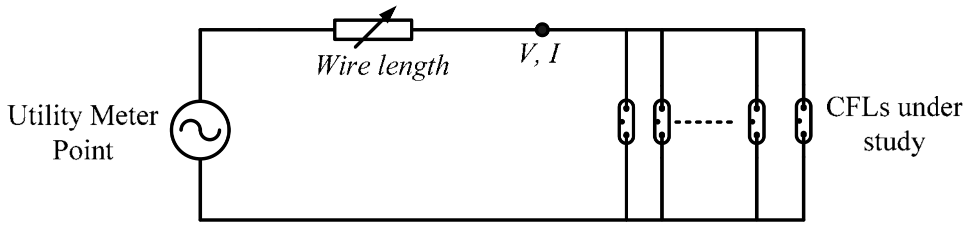

Figure 4.10. Measurement set-up to obtain the Effective-Lamp index

In the experiment, the number of lamps (*N*) is increased for different wire lengths. This procedure results in a family of $N_{Effective\text{-}h}$ curves, each representing the attenuation effect at a particular harmonic number. After obtaining the Effective Lamp index at each individual harmonic number, the indices are combined into one curve so that a single index is available to quantify the overall attenuation effect. The equation to combine the curves is shown below:

$$N_{Effective-total} = \sqrt{\sum \left(N^2_{Effective-h} \times \frac{\left(I^1_{h\_0}\right)^2}{\sum \left(I^1_{h\_0}\right)^2} \right)}. \tag{4.17}$$

The above operation is a weighted root-mean-square of the Effective-Lamp indices at different harmonic orders. The weighting factor is the magnitude $I^1_{h\_0}$ of the CFL harmonic currents under undistorted voltage supply. The sample results shown in Figure 4.9 were obtained by using this equation.

This experiment was designed to get the worst-case scenario, i.e., the one in which the harmonic attenuation is the most pronounced. In this case, $N_{Effective\text{-}total}$ is always less than *N* due to the attenuation effect. For example, if 20 CFLs are operating in parallel, $N_{Effective\text{-}total}$ could in the range of 15 to 19 depending on the harmonic number *h*. This finding implies that the actual harmonics produced by 20 CFLs are equivalent to 15 to 19 CFLs operated under the ideal voltage conditions for the presented case study.

4.5.3 Comparing the Effective-Lamp Curves from Measurements and from the Measurement-Based Model

The curves are compared to those obtained from the measurements. The Effective-Lamp curves can be predicted with acceptable degree of accuracy. Figure 4.11 compares the two curves (obtained from measurements and from the measurement-based model) in the same graph for each wire length. Figure 4.11 also shows the curve for the current-source model, which is a straight line. The figure not only validates the derived measurement-based model, but also shows the amount of harmonic overestimation caused by the adoption of the current-source model from a practical perspective.

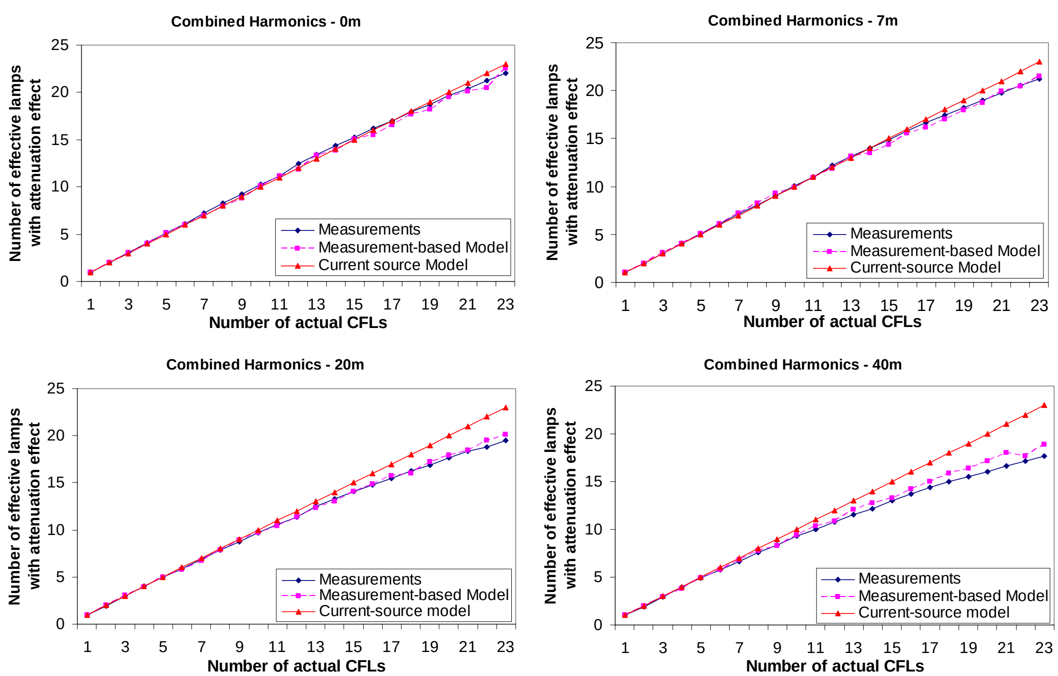

Figure 4.11. Comparison of the three approaches for 0m, 7m, 20m and 40m.

4.6 An Extension of the Least-Square Modeling to PCs and LCD Monitors

Personal Computers (PCs) and LCD monitors are the main single-phase harmonic contributors encountered in modern commercial buildings [62]. When performing harmonic analysis of PCs + monitors, one must account for the attenuation effect in order to obtain accurate values for their harmonic injections, particularly in office buildings, where these devices are among the main sources of harmonics. PCs typically run between 30W and 120W, and monitors between 30W-60W with a total harmonic distortion usually greater than 90%. The harmonic injections from large offices may cause unacceptable distortion levels in the phase voltages and neutral currents [60], [62]. This increase in voltage distortion can cause the current harmonic injections of these devices to deviate significantly from their typical spectra obtained under an undistorted voltage supply. An accurate model of PCs and monitors, including the attenuation effect, may be necessary to understand the true magnitude of the problems that may arise.

An accurate model can be obtained with either an analytical model or a measurement-based model. Like the results for the CFL case, the presented results for the PCs and LCD monitors were used to develop the frequency-domain models. Only the decoupled model is presented because, as in the CFL case, it was the only one that could satisfactorily represent the computers' behavior.

4.6.1 PC *Y* Model and Verification

As in the case of the CFLs, in order to obtain the model by using different PCs, their currents were normalized by their corresponding rated current, and the voltages were normalized by the rated voltage. Six PCs were tested and used for this purpose. The results are shown in Figure 4.12, which includes the current source and the *Y* matrix. The current-source and impedance parameters were obtained from normalized values and, therefore, are not to scale.

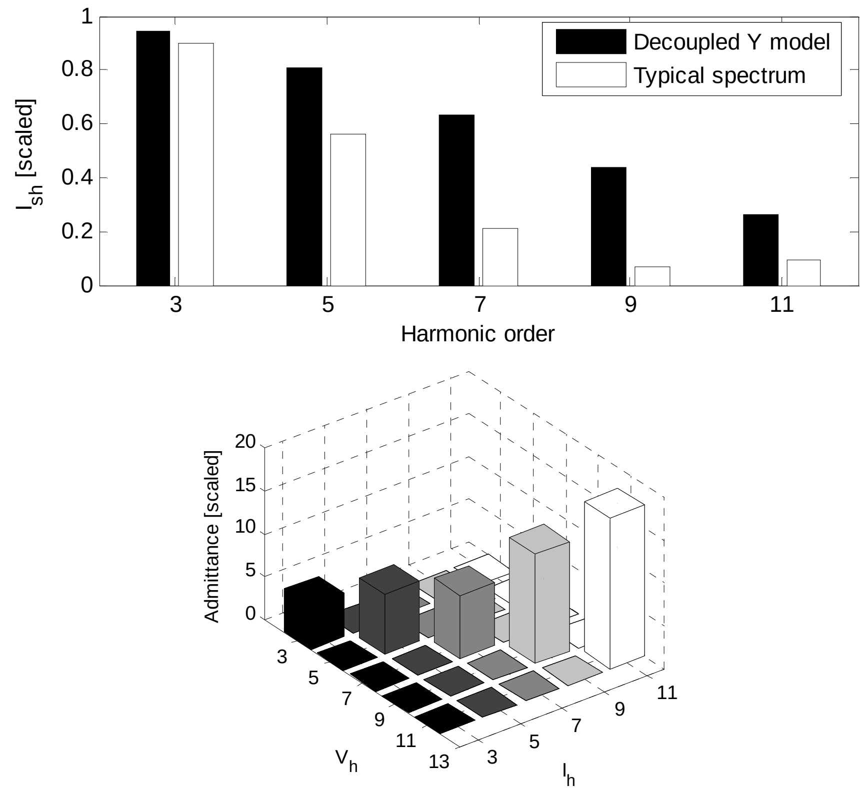

Figure 4.12. Scaled estimated current injections and decoupled *Y* model for the 6 PC case

The same strategy used for the CFL case in evaluating the estimated model was used for the PCs. All the available data were used to evaluate how well the model had predicted the current with a given voltage. The waveform was reconstructed from the obtained spectrum (up to the 11th harmonic) and compared to the actual waveform. The results for a random snapshot of the predicted and actual waveform are presented in Figure 4.13.

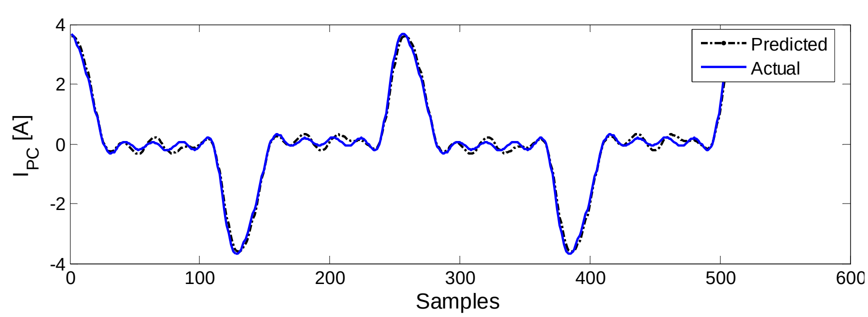

Figure 4.13. PC prediction results for a single snapshot

The obtained model was used to fit the current waveforms of 6 recorded PCs. In general, the decoupled *Y* model was able to fit all 6 PCs very well, with a correlation coefficient not smaller than 97.90% and averaging 99.3%.

4.6.2 LCD Monitor *Y* Model and Verification

As in the case of the CFLs and PCs, in order to obtain the model by using different LCD monitors, their currents were normalized by their corresponding ratings, and the voltages were normalized by their rated voltage. Three LCD monitors were used. The results for the decoupled *Y* matrix and the current source are shown in Figure 4.14. The current-source and impedance parameters were obtained from normalized values and are not to scale.

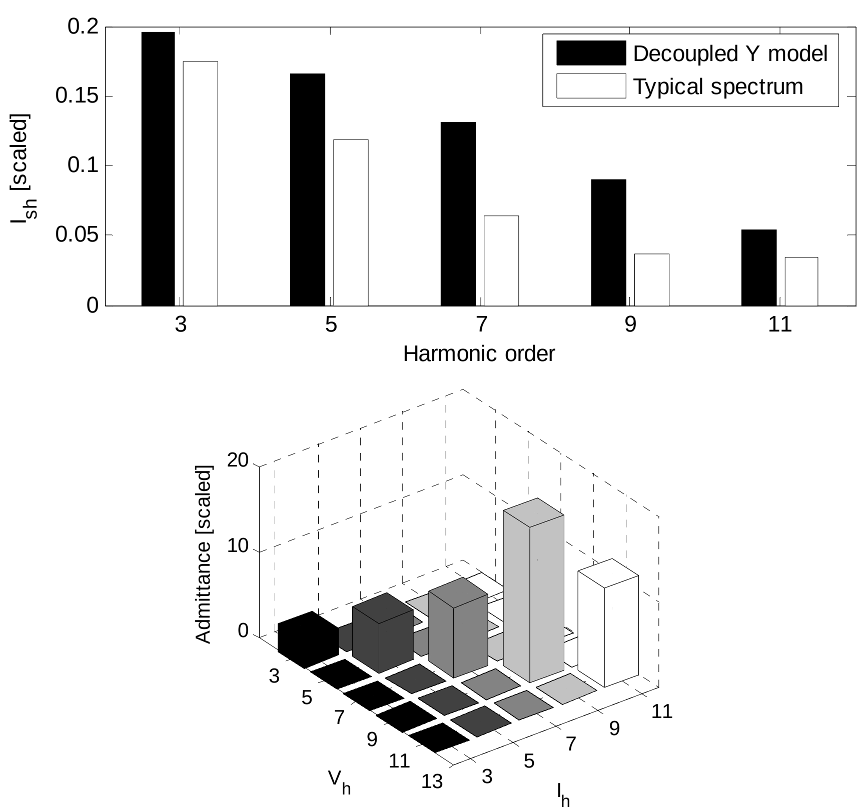

Figure 4.14. Scaled estimated current injections and decoupled *Y* model for the 3 LCD monitors case

The same strategy used for the CFL and PC cases in evaluating the estimated model was used for the LCD monitors. All the available data were used to evaluate how well the model had predicted the current with a given voltage. The waveform was reconstructed from the obtained spectrum (up to the 11th harmonic) and compared to the actual waveform. The results for a random snapshot of the predicted and actual waveform are presented in Figure 4.15.

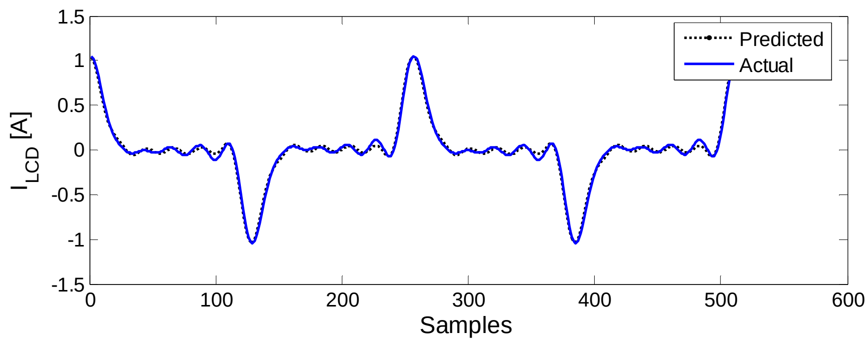

Figure 4.15. Prediction results for a single snapshot

The obtained model was used to fit the current waveforms of 3 recorded LCD monitors. In general, the decoupled *Y* model was able to fit these three samples very well, with a correlation coefficient not smaller than 98.50% and averaging 99%.

4.7 Conclusions

This chapter presented a new measurement-based admittance modeling technique for loads such as compact fluorescent lamps and computer loads. From the presented results, it can be concluded that

1. The Norton equivalent model for CFLs, PCs and LCD monitors can be obtained to perform the fitting under a practical range of voltage conditions.
2. The decoupled *Y* model can be obtained for a small random set of data among a large amount of recorded data. This model was able to fit the measured current waveforms of 12 types of CFL with high correlation coefficient, for the whole large set of recorded data.
3. The CFL results have been verified by using the Effective Lamp curves. Therefore, the model is able to consider the attenuation effect. This conclusion can be extended to PC and LCD monitor models.

The main contribution of this chapter is a technique able to provide satisfactory harmonic models for CFLs and home appliances. These models can be easily integrated into harmonic load flow programs and, as described in this chapter, can effectively account for the harmonic attenuation effect for a range of practical supply voltage conditions.

The measurement and characterization of harmonics have been the main concern in this thesis. The most common solution for mitigating these harmonics is the use of shunt passive harmonic filters. These filters can be of many topologies. An investigation on the topologies of such harmonic filters is presented in the next chapter.

Chapter 5

An Investigation on the Selection of Filter Topologies for Harmonic Mitigation[2]

Passive filters have been the most effective solution for power system harmonic mitigation. These filters have several topologies that give different frequency response characteristics. The current industry practice is to combine filters of different topologies to achieve certain harmonic filtering goal. However, there is a lack of information on how to select different filter topologies. This decision is based on the experience of the filter designers at present. The goal of this chapter is to investigate the filter topology selection issue. It presents a study on the effectiveness and costs of various filter topologies for harmonic mitigation. The research results show that the association of three single-tuned filters is a very appropriate solution for most typical harmonic problems.

5.1 Introduction

Harmonic distortions can have significant adverse effects on both power system components and customer devices. Various harmonic-mitigation techniques have been proposed and applied in recent years. Among those techniques, shunt passive harmonic filters are still considered as the most effective and viable solution to reduce harmonic distortions. Many industrial facilities install the filters to ensure that they comply with the harmonic limits specified by the supply utilities. It is expected that when harmonic mitigation in typical residential feeders becomes more commonly practiced, utilities will employ passive harmonic filters to mitigate harmonics in residential areas as well. Therefore, this research approach to the subject of harmonic filtering with shunt passive

[2] A version of this chapter has been published: A. B. Nassif, W. Xu, W. Freitas, "An Investigation on the Selection of Filter Topologies for Passive Filter Applications," *IEEE Transactions on Power Delivery*, vol. 24, no. 3, July 2009, pp. 1710-1718.

filters, intended to be a design strategy for industrial distribution systems in this chapter, can also be used to design mitigation schemes for harmonics in residential areas.

The passive filters have several topologies that give different frequency response characteristics. The common filters are the single-tuned filter and the high-pass filters. The single-tuned filter is aimed at filtering a single harmonic while high-pass filters are intended to reduce harmonics above certain frequencies. The high-pass filters have several variations, such as the first-order high-pass, second-order high-pass, and third-order high-pass. The current industry practice is to use the combination of several different topologies of filters to achieve desired harmonic filtering performance.

For example, [5], [10], [25] recommend that one or more single-tuned filters be used in combination with high-pass filters for a given facility. References [26]-[27] show an actual case study where two single-tuned filter branches were combined with a second-order high-pass filter to mitigate harmonics. In another case presented in [82], single-tuned filters are used in combination with a C-type high-pass filter to meet harmonic mitigation requirements.

The above situation naturally leads to the following question – what is the most appropriate combination of various filter topologies to achieve typical harmonic filtering requirements? Unfortunately, the answer is based on the experience of the filter designers, as we have not found publications researching this important problem. It is noted that many papers have been published in the subject of harmonic filter allocation and sizing for distribution feeders [82]-[87], but the question of filter topology selection remains to be answered.

This chapter is concerned about the filter topology selection issue. It presents our research results on the effectiveness and costs of various filter topologies for harmonic mitigation. The research uses a set of technical and economic criteria to evaluate the overall performance of different filter combinations. Further analysis is conducted on the quality factors of damped filters. The findings are also evaluated using sensitivity studies.

5.2 The Problem Description

Several filter topologies are available to a filter designer. These topologies are shown in Figure 5.1. Common frequency responses of the filters are shown in Figure 5.2.

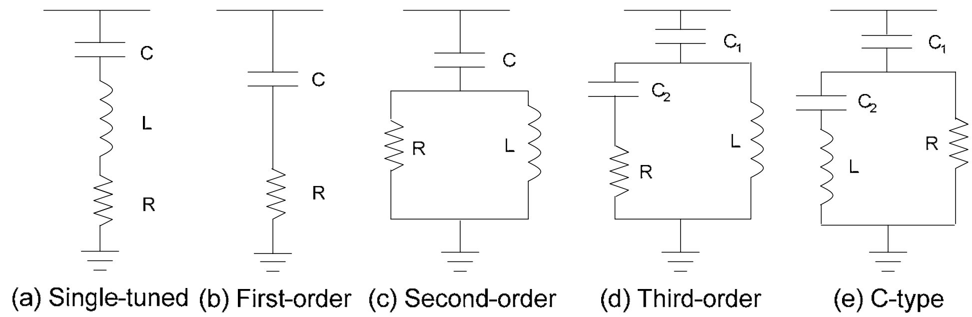

Figure 5.1. Topologies of shunt passive filters.

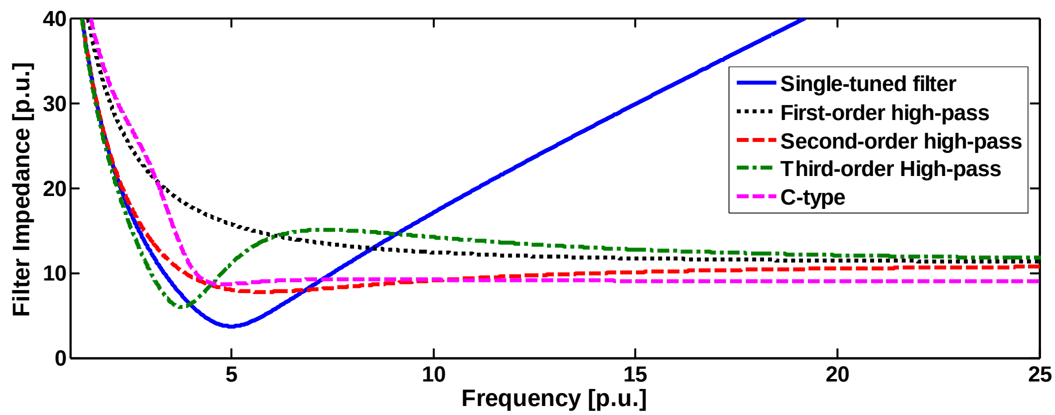

Figure 5.2. Shunt passive filters frequency responses.

The single-tuned filter (see Figure 5.1a) contains a capacitor in series with an inductor. The capacitor and inductor are sized such that the branch impedance is zero near a harmonic frequency, which bypasses that harmonic. The capacitor also provides reactive power compensation. A resistor can be used in order to adjust the tuning's sharpness and, as a consequence, the bandwidth [10]. In this case, the quality factor is given by:

$$Q = \frac{\sqrt{L/C}}{R}. \tag{5.1}$$

High-pass filters are able to trap a wide range of harmonics by providing a low impedance path at high frequencies. The resistor determines the sharpness of the tuning and the filter's frequency response behavior. In these cases, excepting the first-order filter, the quality factor is defined as follows:

$$Q = \frac{R}{\sqrt{L/C}} \cdot \tag{5.2}$$

Figure 5.1b presents the first-order high-pass filter, which provides small impedance at high frequencies because of the capacitor characteristics. Since this filter does not have an inductor, its resistance is chosen for limiting the current that flows through the capacitor. In order to have small impedances at high frequencies, the capacitor typically needs to be large. It increases the cost and could over-compensate the system. For the same reason, the performance at low frequencies is usually poor.

The second-order filter (see Figure 5.1c) consists of a capacitor in series with a parallel inductor and resistor. They are sized such that the filter behaves like the single-tuned filter below the tuning frequency and like the first-order high-pass filter at high frequencies. This is because the inductive reactance is small in low frequencies, bypassing the resistive branch, and large in high frequencies, diverting the current to the resistor branch. At the tuning frequency, a notch can be observed. In order to achieve this performance, the capacitor is tuned to the desired frequency with the inductor.

The third-order filter (see Figure 5.1d) exhibits high capacitive reactance at the fundamental frequency and low, predominantly resistive, impedance, over a band of higher frequencies. It behaves like the single-tuned filter below the tuning frequency, and like the first-order high-pass filter above it. This is because the inductive reactance is small at low frequencies, bypassing the RC branch, and large at high frequencies, and the current will flow through the branch composed by the capacitor and resistor. The capacitors C_1 and C_2 are both tuned with the inductor to the same desired frequency. As a consequence, the filter exhibits very low impedance at the tuning frequency, similarly to the single-tuned filter, and an anti-resonant peak at a near – but higher – frequency, as it can be seen in Fig. 2. This third-order filter exhibits less loss at the fundamental frequency than the second-order one due to the insertion of the capacitor C_2 in series with the resistor [88]. Due to this tuning scheme, the third-order filter shows a deeper notch valley at the tuning frequency than does the second-order filter.

The filtering performance of the C-type filter (see Figure 5.1e) lies in between that of the second- and third-order types. The series LC in parallel with the resistor is tuned to the power frequency. The resistor is, therefore, bypassed by the zero impedance branch formed by the tuned LC elements. The filter thus behaves as a capacitor at the fundamental frequency. There is little current flowing through the resistor and the loss is minimized. As frequency increases, the inductor becomes resonating with C_1+C_2, what makes the filter behave as a single-tuned filter with a damping resistor. At high frequencies, the inductor becomes large, and the current will flow through the resistive branch, resulting in a performance similar to that of the first order filter [89].

For all filters, the main capacitor is selected to compensate for the necessary reactive power at the installation bus. Given the voltage level and the power needed, the capacitance can be easily determined; the inductor is then selected in order to tune the filter branch to the desired frequency. In the case of high-pass filters that have more than one capacitor, the second capacitor is also tuned with the inductor in order to perform as described above. The resistor is determined by the desired value of the quality factor as will be discussed later.

When designing a harmonic filter, besides the reactive power compensation capability, the following factors are considered 1) filtering performance, 2) cost, 3) component stress level, and 4) electrical losses. Since a single high pass filter can be very expensive when applied to filtering all harmonics, a set of filters combining different filter topologies is typically used. According to common practice, single-tuned filters are used to filter low order harmonics while high pass filters are used to address high order harmonics. Even with this general guide, a filter designer still faces several filter topology combinations to consider. Taking into account the other design factors, the task of filter design could become a very complicated optimization problem.

The problem to be addressed by this thesis is to find what the most appropriate filter combinations for typical applications are. The result will eliminate the largest uncertainty in filter design. Without the topology factor, the filter design problem can be solved using a number of traditional optimization methods.

5.3 Strategy of Investigation

In this section, the proposed strategy of investigation is discussed. First, the main assumptions adopted to conduct the investigation are highlighted and justified. Then, the filter design requirements are revised. In the sequence, the proposed indices used to assess the filter effectiveness are introduced. Finally, the solution procedure is explained.

5.3.1 Assumptions

The basic strategy of this research is to compare the performances of all possible filter combinations based on several criteria. For this purpose, we assume that three filter branches are needed, as this is the most common situation encountered by industry. Each of the filters can be one of the types summarized in Table 5.1. As a result, there are a total of 125 combinations of topologies.

Table 5.1. Summary of Filter types

Filter type	Definition
1 ST	Single-tuned
1 HP	First-order high-pass
2 HP	Second-order high-pass
3 HP	Third-order high-pass
C	C-type

A typical general network configuration is selected for the evaluation, which is shown in Figure 5.3. The system represents an industrial facility where filters are added to prevent the PCC (Point of Common Coupling) harmonic indices from exceeding limits. As shown in Figure 5.3, the system is composed of a supply system connected to a 25kV bus via a transformer. This bus feeds a linear load Z_L (20% of the total load power) and a nonlinear harmonic generating load sized at 80% of the total load power. The nonlinear load is modeled as a harmonic current source whose magnitude follows *1/h* relationship, where *h* is the harmonic number. It is assumed that the higher order of the harmonic current injected by the non-linear load is 39th, as this range is generally wide enough to cover typical harmonic studies [4]. The power factor of the facility, before the installation of the filters, is about 0.9 lagging, and the total power is $S = 10 + j5$ MVA, which represents a large industrial customer in compliance with the typical requirements [84]. The transformer reactance is chosen 5% according to the recommendations standardized in [3]. The three filter branches are installed at the secondary side of the transformer, which are designed to filter 5th, 7th and 11th harmonics. As explained earlier, there are 125 filter topology combinations.

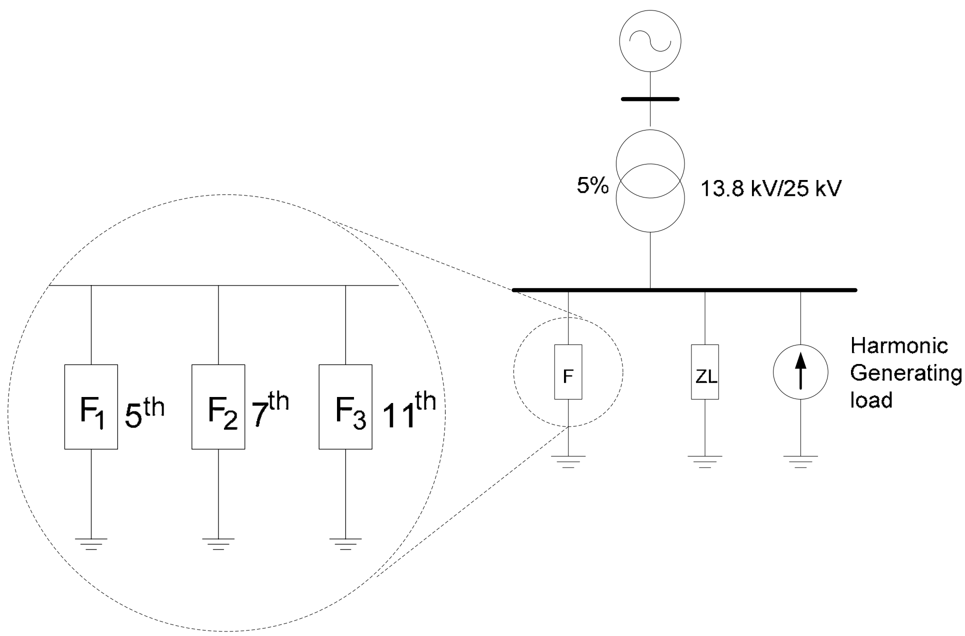

Figure 5.3. Three-branch filter

The three branches composing the filter are chosen to be of the same size. A decision of this type is necessary to maintain the problem feasible to be solved by exhaustive search. If such restriction is not imposed, one can verify that the number of size combinations might be so large that the problem would be impossible to be tackled. Moreover, this decision is not unrealistic since the filter design requirements (raised in the next subsection) are respected and will play a crucial role when determining the size of the branches. A common practice is to size high-pass filters larger than the single-tuned filters, which is aimed at avoiding overloading and keeping acceptable harmonic mitigation performance. However, to conduct our search, the minimum size of all filters is selected as to keep up with the loading and effectiveness requirements of high-pass filters. Therefore, all filters are of the same size and a fair decision can be made. This will be shown in more details in section 5.4.

5.3.2 Filter design requirements

For each filter combination, a set of filter design criteria must be respected. They include 1) harmonic mitigation performance, 2) power factor, 3) filter loading level, and 4) power losses.

5.3.2.1 Harmonic mitigation performance

The harmonic mitigation ability of the filter will result in the reduction of the harmonic distortion levels of a determined location. The performance can be measured via two approaches, which are based on the harmonic power flow and on the frequency scan, respectively. In the first approach, the analysis is intended to evaluate the filter capability of suppressing certain amount of harmonic currents in order to decrease the harmonic distortion below a stipulated threshold. The voltage total harmonic distortion (*THD*) is calculated via [3]

$$THD_V = \frac{\sqrt{\sum_{h=2}^{\infty} V_h^{\ 2}}}{V_1}, \tag{5.3}$$

where V_1 and V_h are the fundamental and harmonic magnitude voltages, respectively. The reduction in the voltage *THD* is calculated by subtracting this value before and after the installation of the filter. According to reference [3], the maximum permissible voltage *THD* for an industrial power system at a voltage level below 69 kV is 5%.

In the second approach, the analysis is intended to evaluate the filter capability of reducing the overall frequency response of the facility, calculated at the harmonic frequencies. As the general form of the frequency response is reduced in value, the harmonic currents are usually less prone to amplification [5].

5.3.2.2 Power factor

As previously described, the filters are composed of large capacitors and inductors. Due to these components relative sizes (determined by the tuning frequency), the capacitor impedance is much higher than the inductor impedance (or the impedance of the arrangement of inductor, capacitor and resistor – when applicable – in the case of high-pass filters). Since the main capacitor will withstand with the higher voltage, it provides considerable reactive power to the system. Therefore, it must be sized such that it will be able to provide a power factor with adequate value for the system [90]. The amount of injected reactive power is approximately proportional to the filter main capacitor size.

5.3.2.3 Filter loading level

Filter components are susceptible to failures and even breakdown if the voltage or current values through its components are exceeded by certain amount during certain period of time. According to IEEE Standard 1531 [91] and IEEE Standard 18-2002 [90], the utilized capacitors, which have to be capable of continuous operation under contingency system and bank conditions, must be able to withstand the following several factors:

a) 110% of rated rms voltage.
b) 120% of rated peak voltage including harmonics, but excluding transients.
c) 135% of nominal rms current based on rated kvar and rated voltage.
d) 135% of rated kvar.

Those conditions are verified after the filter is designed. They represent the extreme case of maximum allowed loading that the capacitor can withstand, and it is suitable to maintain these values as low as possible. This is also applicable to the lower voltage capacitors, in case of the high-pass filters that have more than one capacitor. At the same time, it is important to maintain the current through the inductor(s) as low as possible, while providing satisfactory harmonic mitigation performance.

The components' loading is closely associated with the components' stress, as long as the loading value is a concern. Therefore, the loading and stress terms are used in this work as meaning the same.

5.3.2.4 The power losses

The power losses are calculated by the power dissipated in the filter's resistor. The problem associated with this undesirable loss is straightforward, since waste of electrical power means financial inefficiency and possible excessive heating of the filter components.

5.3.3 Indices to Assess Filter Effectiveness

In order to compare the performance of the various filter combinations, we further establish a set of indices to quantify the performance of the different filters.

5.3.3.1 Voltage total harmonic distortion index (THD_V)

This index is to measure the harmonic reduction performance of the filter, and it is defined as the voltage *THD* at the PCC point, calculated using (5.3).

5.3.3.2 Frequency response index (*FS*)

This index measures the filter performance according to the overall frequency responses of the facility. It is calculated from the system frequency response with the filters installed and is obtained from the values of the frequency scan at the 5th, 7th, 11th, 13th, 17th, 19th harmonic, etc. harmonic (see Figure 5.4). Note that the filter tuning frequency is set to a value slightly below the harmonic frequency to avoid possible harmonic amplification due to resonance effects [25]. The impedance magnitudes are then weighted by a factor of $1/h$ because the harmonic currents injected by nonlinear loads typically have a $1/h$ magnitude relationship, and therefore the impedances calculated at each harmonic h are treated with the same significance. Finally, the obtained weighted factors are summed and grouped as the single index *FS*, given by

$$FS = \sum_{h=1}^{N} \frac{Z_h}{h}, \tag{5.4}$$

where Z_h is the harmonic impedances.

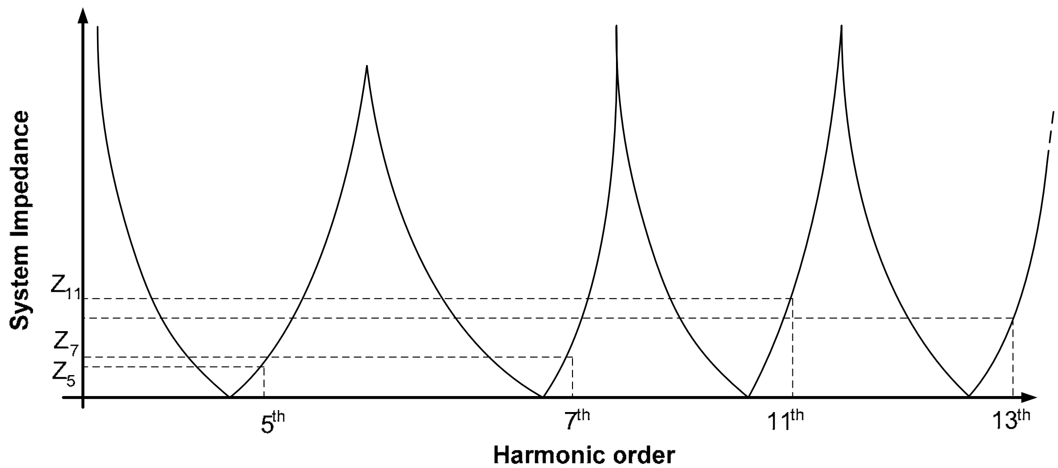

Figure 5.4. Illustration of the *FS* calculation

5.3.3.3 Filter component stress indices

These indices are introduced to measure the loading level of the filter structure. As discussed earlier, component stress is an important consideration in filter sizing [90]-[91]. The stress is defined as the rms value of the voltage/current normalized by the value of the fundamental component. For the voltage, the fundamental component is the bus fundamental voltage, and for the current, it is the value at the full-load fundamental frequency current of the filter branches. The filter capacitor is mainly concerned with the voltage stress and the inductor is concerned with the current stress [91]. The total filter stress level is defined as:

$$Stress = \frac{Stress_V + Stress_I}{2}, \tag{5.5}$$

where $Stress_V = \frac{V_{rms}}{V_1}$ and $Stress_I = \frac{I_{rms}}{I_1}$.

In case the filter has more than one capacitor, the average of their $Stress_V$ is taken.

5.3.3.4 The cost index

The cost index is to quantify the filter price. This index is calculated by summing the costs of the capacitors and inductors for each filter. In references [26]-[27], a survey on power capacitors and inductors for filter applications was presented. The capacitor cost is calculated by a simple relationship price/kVAr. This was obtained as $30/kVAr (per phase). For the inductors, there is no simple relationship as this component is custom designed. However, the inductor price depends fundamentally on the inductance value, on the rms current and on the power level. Based on references [26]-[27], where the inductors were sized for the same voltage (25kV) and power levels, the price is estimated as $12 per *mH* per phase.

5.3.3.5 The losses index

As explained earlier, the losses index is the total active power dissipated in the filter's resistor. This index is closely associated with the quality factor of the filters, because the resistance value is indeed determined by the filter quality factor. Therefore, this index plays a special role when evaluating the impact of the quality factor variation on the filter performance.

5.3.4 The Solution Procedure

The idea adopted by this research is to compare all possible 125 filter configurations based on the set of performance indices described earlier. It involves calculating the performance indices for each of the filter configurations. Note that an optimization procedure to identify the best filter configuration is not adopted, due to three considerations. Firstly, the number of configurations to be evaluated is manageable for exhaustive search. Secondly, exhaustive search will provide performance results for all filter configurations. They will help us to understand the advantages and disadvantages of the different filter combinations. Thirdly, solving the problem with an optimization procedure can be very complicated because of the combinatorial nature of the problem.

Before the exhaustive search can take place, the filter size and component parameters must be determined. There is a range of filter sizes that are considered in this work, i.e.

the ones that provide the PCC with the power factor between 0.95 lagging and 1. This means that we take into account all 125 combinations for several different filter sizes. Thus, the following guideline is presented:

a. The smallest capacitor size is obtained as to have a minimum-size filter that satisfies the requirements to avoid overloading [90] at the same time it supplies the necessary reactive power;
b. The largest capacitor value is obtained to provide a maximum-size filter that does not overcompensate the system, i.e., that does not result in a leading value of power factor;
c. The inductor(s), resistor(s) and secondary capacitor(s), when applicable, are sized according to the filters description presented in section 5.2 for each size value of the main capacitor.

Initially, the filters' voltage distortion and loading are analyzed, and if the combination does not satisfy these requirements, the capacitor size is increased. The voltage distortions and loading are analyzed for the new capacitor size, and the combinations that do not comply will have their capacitor size increased again. The process is repeated until the maximum filter size is reached. The increment in the capacitor size is done according to typical values of industrial capacitors.

The idea of the filter selection is to evaluate the introduced indices for all filter combinations for different power compensation levels. By working with those indices, the whole set of filter combinations will be gradually refined. After scrutiny, the resulting combinations will be, ultimately, a small group of filters. This group will be further investigated, and the most suitable filter combination will be ultimately selected. The following procedure presents the whole process proposed in this work and the algorithm flowchart is shown in Figure 5.5:

1. Define the minimum and maximum capacitor sizes to be used in the investigation based on the power factor compensation requirement.
2. Select one topology to be investigated.
3. Select the minimum capacitor rating.
4. Calculate the filter inductor(s), resistor and secondary capacitor (if applicable), *i.e.*, design the filter for the present capacitor.

5. Carry out a complete harmonic analysis and index calculation for this filter topology-size combination.
6. Check the loading limits and rule out the filter combinations that show overloading.
7. Check the voltage distortion in the bus of interest and verify if $THD_V < 5\%$. Rule out the filter combinations that do not comply with this limit.
8. Check if the largest capacitor size was already investigated for this topology combination. If not, increase the capacitor size and return to step 4. If yes, go to step 9.
9. Check if there is other topology combination to be tested. If yes, return to step 2. If not, go to step 10.
10. Sort the selected filters by price.
11. Verify Stress, THD_V and FS indices for the selected filters.
12. Select from the more expensive filters the ones with THD_V, FS and Stress as low as those of the less expensive filters to verify whether they will perform significantly better than the less expensive ones. Eliminate the filters with high FS, Stress and Price indices.
13. Perform the quality factor analysis to be able to draw further conclusions about the topology. Include the Losses index. The quality factor investigation is conducted by systematically varying Q of the selected filters and monitoring the indices variations. An optimal value of Q will then be chosen. This procedure is described and performed in subsection 5.4.2.

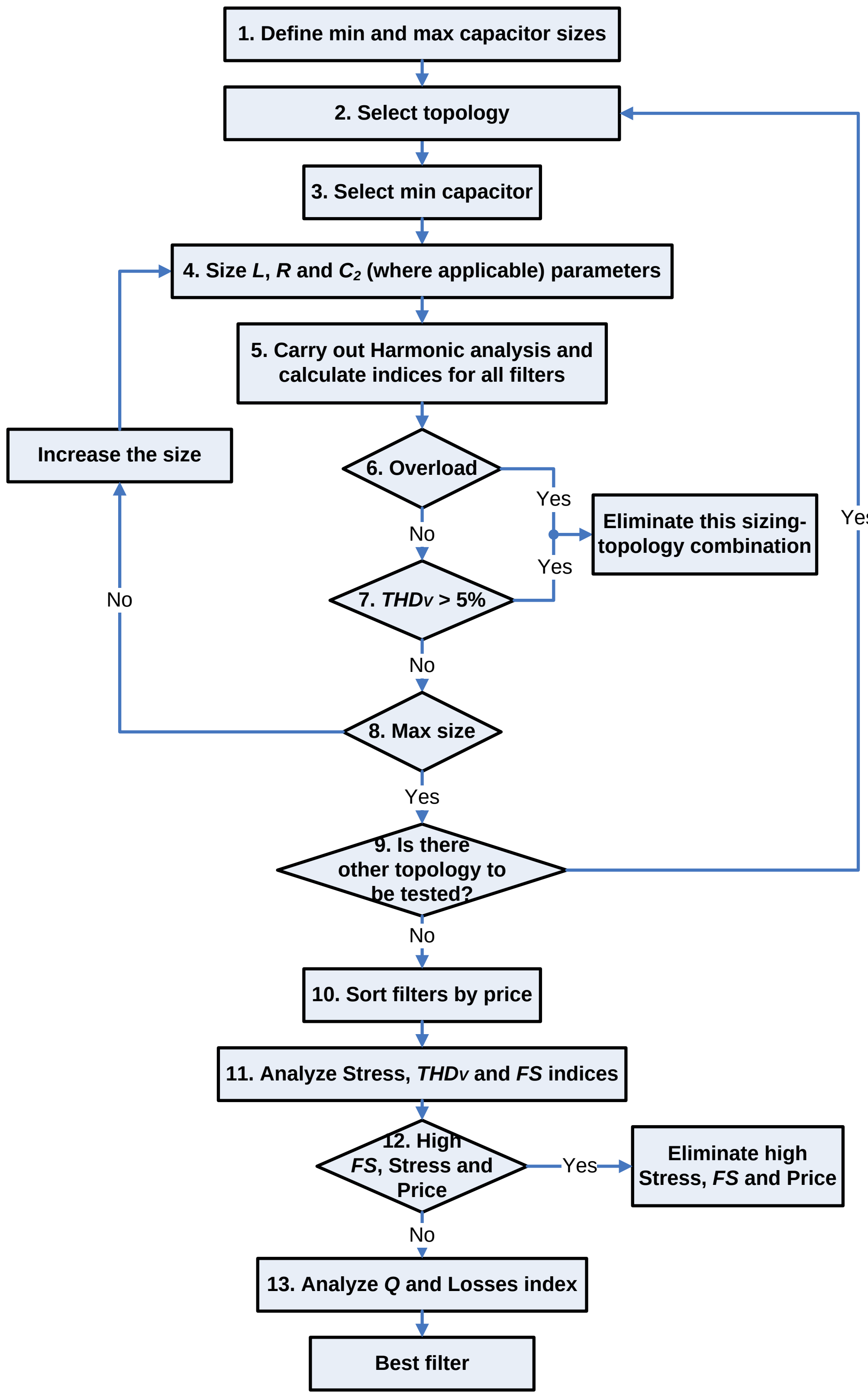

Figure 5.5. Algorithm for filter selection

5.4 Topology Selection Results

5.4.1 Filter Elimination Procedure (steps 1-12)

The system shown in Figure 5.3 was used to conduct the investigation. For this system, according to the reactive power compensation level requirement, the smallest capacitor was found to be equal to 3.6 MVAr (1.2 MVAr for each branch), and the largest one was found to be 5.1 MVAr (1.7 MVAr for each branch). This component was increased in steps of 300 kVAr (100 kVAr for each branch). Thus, for the final analysis, we have 750 cases to be investigated (125 topology combinations times 6 capacitor sizes). Table 5.2 shows the results of the procedure 1 to 6. In order to save space, not all the results are shown, but only some of them, which are selected as a sample. The shaded cells show cases that comply with THD_V and loading levels. In addition, the symbol "*" indicates the cases with overloading. Notice that some cases comply with THD_V but not with the loading conditions, and vice-versa.

Some generic conclusions can be drawn from this exhaustive search:

1. The first-order high-pass filter, when associated in the combination, always provides high stress and high THD_V. This can be explained by the fact that this filter will likely be more susceptible to resonance with the system [10]. In order to be effective, its size should be largely increased, which, for our system, would result in overcompensation of reactive power, leading to capacitive low power factor.
2. The C-type filter, most of the times, is efficient in keeping low THD_V, but not as desirable when loading is at stake. Similarly to the conclusion drawn for the first-order high-pass, this may be explained by the fact the C-type filter is more effective when large amount of reactive power is needed, which means larger capacity of the component. When large, the filter will provide a better high-frequency response. This is not the case for this general industrial system configuration.

Figure 5.6 presents the resulting filters after steps 1-7, showing the cost, stress and *FS* indices plotted in a single graph. They are sorted by price, which was normalized in order to facilitate the comparison. Thus, one can see that only 48 out of 750 filter combinations meet the requirements of THD_V and loading simultaneously.

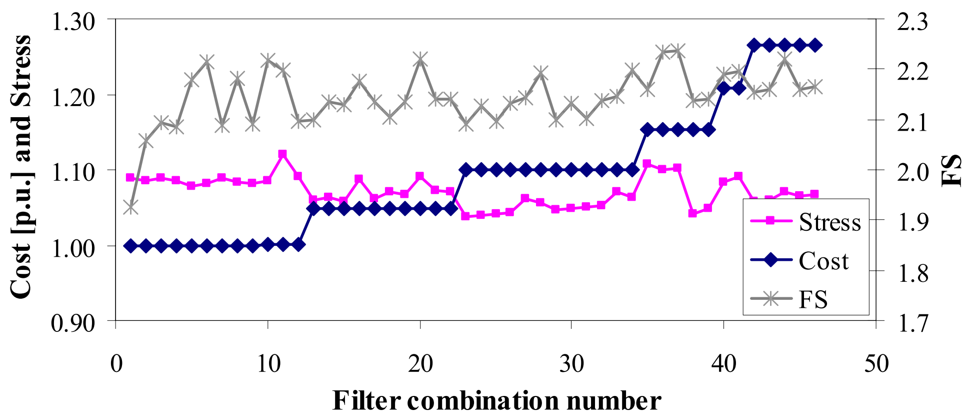

Figure 5.6. Cost, Stress and FS indices according to step 7

Table 5.2. Sample results of the steps 1-9 of the search strategy

Filter branches			THD_V [%]					
5^{th}	7^{th}	11^{th}	3.6 MVAr	3.9 MVAr	4.2 MVAr	4.5 MVAr	4.8 MVAr	5.1 MVAr
1ST	1ST	1ST	4.36	4.15	3.96	3.79	3.63	3.48
1ST	1ST	2HP	4.55	4.33	4.12	3.93	3.76	3.60
1ST	1ST	3HP	4.64	4.41	4.20	4.02	3.84	3.69
1ST	1ST	C	5.47	5.24	5.02	4.83	4.64	4.47
1ST	1ST	1HP	23.80*	17.50*	14.61*	13.21*	12.59*	12.46*
1ST	2HP	1ST	4.71	4.48	4.26	4.07	3.89	3.73
1ST	2HP	2HP	4.81	4.56	4.33	4.13	3.94	3.76
1ST	2HP	C	5.63	5.37	5.14	4.93	4.73	4.54
1ST	C	C	6.01	5.76	5.53	5.31	5.11	4.92
1ST	C	1HP	15.97*	15.08*	15.01*	15.45*	16.16*	16.89*
1ST	1HP	1ST	27.27*	36.96*	40.16*	31.18*	24.37*	21.33*
1ST	1HP	3HP	12.43*	12.34*	12.43*	12.72*	13.22*	13.94*
1ST	1HP	C	12.17*	11.34*	10.64*	10.09*	9.66	9.34
2HP	1ST	3HP	5.17	4.92	4.68	4.47	4.27	4.09
2HP	1ST	1HP	20.80*	16.53*	14.22*	13.00*	12.41*	12.23*
2HP	2HP	2HP	5.29	5.01	4.76	4.53	4.32	4.13
2HP	2HP	3HP	5.36	5.09	4.83	4.60	4.39	4.20
2HP	2HP	C	6.00	5.72	5.46	5.22	5.01	4.81

2HP	2HP	1HP	15.81*	13.92*	12.62*	11.77*	11.22*	10.87*
2HP	3HP	1ST	5.23	4.97	4.73	4.52	4.32	4.13
2HP	3HP	3HP	5.37	5.09	4.84	4.61	4.40	4.21
2HP	3HP	C	6.00	5.73	5.47	5.24	5.02	4.82
2HP	C	1ST	5.44	5.18	4.94	4.73	4.53	4.34
2HP	C	2HP	5.49	5.21	4.96	4.73	4.52	4.33
2HP	C	3HP	5.58	5.30	5.05	4.82	4.61	4.41
2HP	C	C	6.32	6.04	5.79	5.55	5.34	5.13
2HP	C	1HP	15.32*	14.49*	14.24*	14.30*	14.49*	14.64*
2HP	1HP	2HP	11.68*	11.54*	11.51*	11.60	11.78	12.04
2HP	1HP	3HP	12.05*	11.90*	11.87*	11.97*	12.17	12.44
2HP	1HP	1HP	18.67*	14.73*	12.45	11.09	10.24	9.72
3HP	1ST	1ST	4.98	4.74	4.52	4.33	4.14	3.97
3HP	1ST	C	5.89	5.64	5.40	5.18	4.98	4.79
3HP	2HP	1ST	5.24	4.98	4.75	4.53	4.33	4.15
3HP	2HP	2HP	5.31	5.03	4.78	4.56	4.35	4.16
3HP	2HP	1HP	15.80*	13.92*	12.63*	11.78*	11.24*	10.89*
3HP	3HP	1ST	5.25	4.99	4.76	4.54	4.34	4.16
3HP	3HP	3HP	5.39	5.12	4.87	4.64	4.43	4.24
3HP	3HP	C	6.02	5.74	5.49	5.25	5.04	4.84
3HP	C	3HP	5.59	5.31	5.06	4.84	4.63	4.43
3HP	C	C	6.33	6.05	5.80	5.57	5.35	5.15
3HP	1HP	1ST	22.98*	26.06*	26.14*	23.40*	20.69*	19.09*
3HP	1HP	2HP	11.73*	11.60*	11.59*	11.70	11.91	12.19
3HP	1HP	3HP	12.10*	11.96*	11.96*	12.08*	12.30	12.60
3HP	1HP	1HP	18.60*	14.69*	12.45	11.10	10.28	9.77
C	1ST	1ST	5.22*	5.00*	4.78*	4.59*	4.41*	4.24*
C	1ST	1HP	18.16*	15.42*	14.18*	13.77*	13.91*	14.46*
C	2HP	1ST	5.50*	5.24*	5.01*	4.79*	4.59*	4.41*
C	2HP	2HP	5.55*	5.28*	5.03*	4.80*	4.59*	4.40*
C	C	2HP	5.73*	5.46*	5.21*	4.98*	4.77*	4.58*
C	C	3HP	5.82*	5.55*	5.30*	5.07*	4.86*	4.67*
C	C	C	6.60*	6.32*	6.07*	5.84*	5.62*	5.42
C	1HP	1HP	16.12*	13.66*	12.40*	11.83*	11.70*	11.87*
1HP	1ST	1ST	18.80*	21.45*	25.39*	30.90*	37.23*	41.17*
1HP	2HP	1HP	20.19*	19.88*	19.27*	19.03*	19.52*	20.72*
1HP	3HP	1ST	17.24*	18.60*	20.23*	22.00*	23.84*	25.54*

1HP	1HP	C	21.21*	26.81*	34.24*	37.32*	31.43*	24.62*
1HP	1HP	1HP	24.56*	32.25*	38.28*	33.71*	26.05*	21.16

* indicates situation with overloading

For the following analysis, Filters #34 and up were eliminated because their prices are very high and no improvement on the stress and *FS* indices is observed when comparing to those of the less expensive filters. In addition, all filters with significant high stress and very close price to others were also eliminated (i.e., Filter # 11, 16 and 20). Figure 5.7 presents the resulting selection.

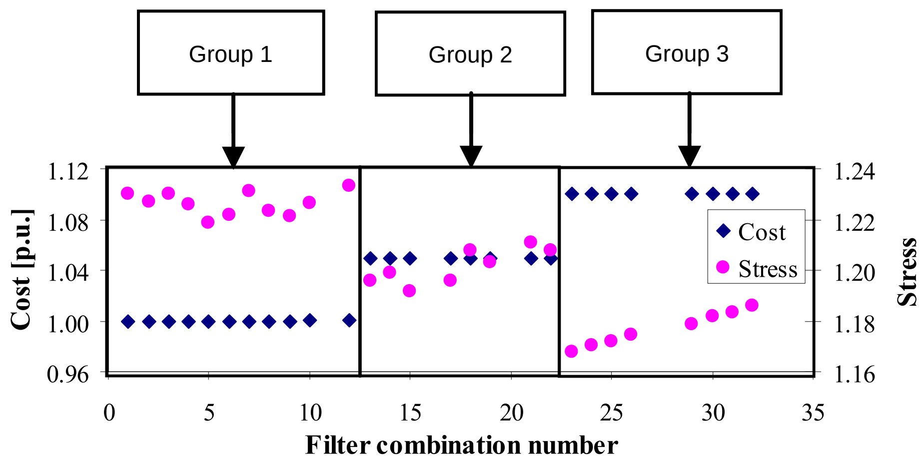

Figure 5.7. Cost and stress for selected filters according to step 8

Three dominant groups are obtained, as Figure 5.7 shows. All filters of group 1, which contains all potential selectable filters, as they are the most economical and have acceptable stress levels, were further investigated using the *FS* index. Figure 5.8 shows the *FS* and Stress indices of the group 1 filters. This figure shows that many of the filters are satisfactory according to the compromise Stress-*FS*. All the 11 filters in this group are taken for further consideration (as will be shown in the quality factor analysis section). In order to verify whether more expensive filters could lead to a significantly better performance, the best filter combination from each of the second and third groups were also chosen. Within groups 2 and 3, the filter with the lowest stress level was selected.

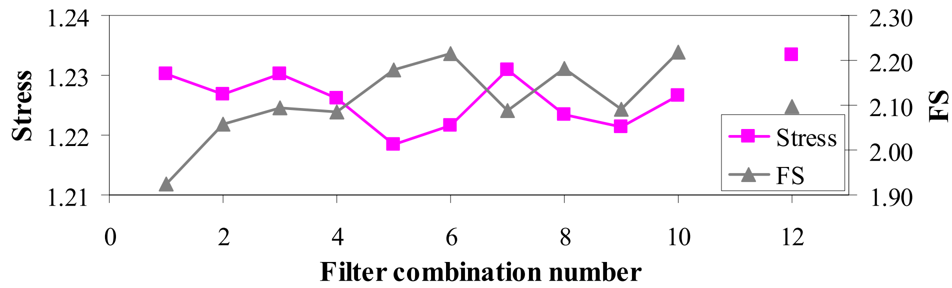

Figure 5.8. Cost and *FS* index for selected filters

Table 5.3 shows the 13 filters combinations selected after step 11 (eleven filters from the first group, one filter from the second, and one filter from the third). In Table 5.3, they are renumbered to facilitate reference to them. Table 5.3 shows that this selection of filters contains essentially only single-tuned, second-order and third-order branches. The quality factor analysis allowed further conclusions to be drawn, as will be shown in the next subsection.

Table 5.3. Resulting filters

Filter #	5^{th}	7^{th}	11^{th}
1	1 ST	1 ST	1 ST
2	1 ST	1 ST	2 HP
3	1 ST	1 HP	3 HP
4	1 ST	2 HP	1 HP
5	1 ST	2 HP	2 HP
6	1 ST	2 HP	3 HP
7	1 ST	3 HP	1 ST
8	1 ST	3 HP	2 HP
9	2 HP	1 ST	1 ST
10	1 ST	3 HP	3 HP
11	3 HP	1 ST	1 ST
12	2 HP	1 ST	2 HP
13	2 HP	1 ST	3 HP

5.4.2 Quality Factor Refining (step 13)

In high-pass filters, the sharpness of tuning may have significant impact on the performance and should be investigated. The index Losses (see section 5.3) was included in this analysis. All the filter configurations mentioned in subsection 5.4.1 were investigated. The first example presented here is filter #2. A variation of Q was done from Q = 1 until Q = 500, as this range is comprehensive enough to consider usual quality factors at this voltage level [10]. Figure 5.9a shows the THD_V, FS, Stress and Losses as Q varies. The Losses index was scaled by a factor of 10^{-4} to improve visualization. One can see that the larger Q is, the better the filter will perform. However, in the second-order high-pass filter configuration, an increase in Q represents an increase in the resistor branch, which resulting effect will be of the filter behaving like a series LC branch, so that the filter behaves very similarly to the single-tuned (filter #1 from Table 5.3). Another example is filter #7. The quality factor of both branches could be varied concurrently or individually in order to get the value of Q for each branch. Figure 5.9b shows the variation for the two branches simultaneously. They were also varied in a one-by-one basis, but these results are not shown here, because they are very similar to the ones in Figure 5.9.

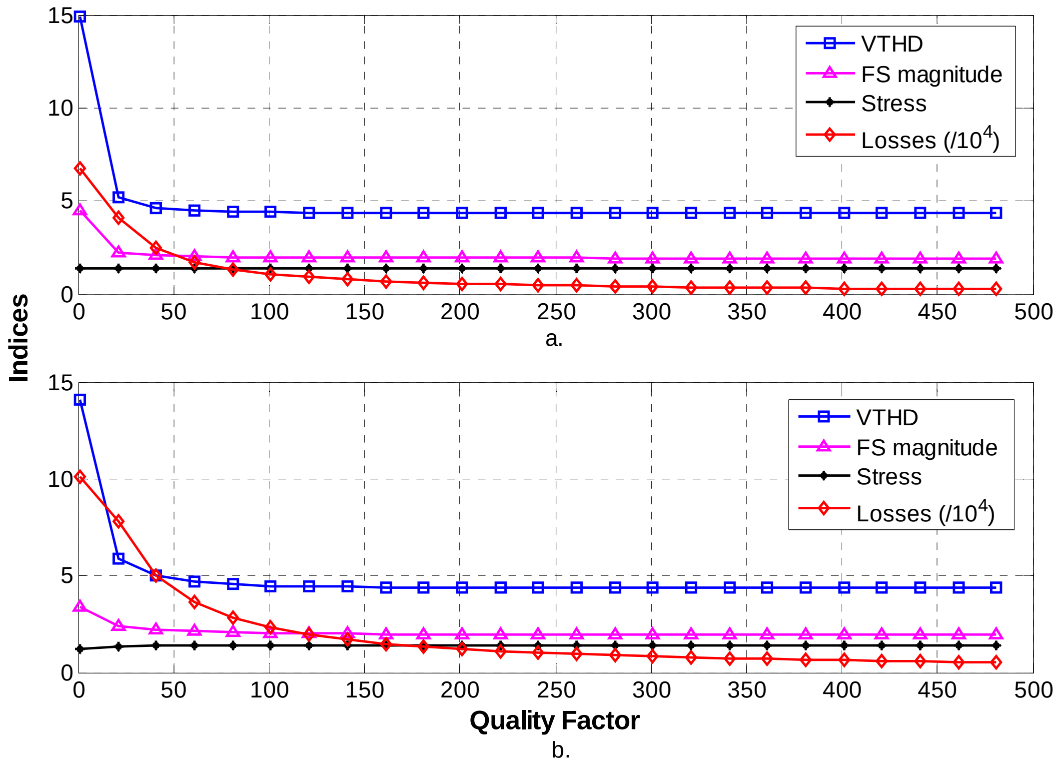

Figure 5.9. Indices behavior as the Quality Factor varies: (a) filter #2, and (b) filter #7.

All the filters shown in Figure 5.7, *i.e.*, 27 different filters, were tested and their quality factor analysis exhibits a similar behavior. The conclusion is that all filters show better indices levels as Q is increased, and therefore, they behave very similarly to the combination of three single-tuned filters. In conclusion, when the capacitive MVAr is split equally into three filter branches, a very appropriate combination for the filters is to use three first-order single-tuned filters for the 5th, 7th and 11th harmonic tuning frequencies.

5.5 Sensitivity Studies for the Selected Filter

Two sensitivity studies are conducted in this section. The first one deals with the impact of the number of filter branches on the bank performance, whereas the second one deals with different ways to allocate reactive power among the filter branches.

5.5.1 On the number of filter branches

The cost, performance and stress levels are the main concern in this analysis. In addition to the component-related cost, which was previously considered, there are additional costs inherent to packaging. A balance between the cost and benefits of adding or removing filter branches is to be sought. This section introduces sensitivity studies concerned with the number of single-tuned branches. The combination of three single-tuned filters is chosen as per the conclusions drawn in the last section.

For the system configuration analyzed in the last sections, a capacitor of size 4.8 MVAr can be split in one, two, three or four branches. Having a branch smaller than 1.2 MVAr potentially causes capacitor overloading; with this choice, it is possible to have up to 4 filter branches. They are tuned to 5^{th}, $5^{th}+7^{th}$, $5^{th}+7^{th}+11^{th}$, and $5^{th}+7^{th}+11^{th}+13^{th}$, respectively. The estimated filter branches construction costs were also obtained from [26]-[27]. Labor cost varies significantly depending on if retrofit is needed and on other factors, and are excluded from the total cost calculation due to large variation.

Table 5.4 shows the THD_V, *FS*, Stress and price (without and with the packaging and design costs) for each filter set. The price is given in thousand of dollars (x U$1000). The column “Price 1” does not include installation costs, whereas “Price 2” does include. THD_V is given in percentage values.

Table 5.4. Comparison on Number of Filter Branches

Tuned Orders	THD_V	***FS***	**Stress**	**Price 1 (x$1000)**	**Price 2 (x$1000)**
5^{th}	7.16	3.2	1.06	148.32	205.32
$5^{th}+7^{th}$	5.77	2.5	1.1	156.98	213.98
$5^{th}+7^{th}+11^{th}$	3.63	1.6	1.15	166.09	223.09
$5^{th}+7^{th}+11^{th}+13^{th}$	3.26	1.5	1.17	175.95	232.95

According to the results shown in Table 5.4, we can see that only the filters containing 3 and 4 branches comply with the harmonic distortion limits (below 5% [3]). Between these two solutions, the set with three filters provides higher loading margin, while keeping the harmonic distortion limits below 5%; in addition, it is more economical. Therefore, despite a slight decrease in performance (as pointed out by *FS* and THD_V), the safety margin is increased and the solution is satisfactory.

Figure 5.10 shows the frequency scan response for the four scenarios. This figure shows that the driving-point impedance is, in general, significantly lower as the number of branches is increased. This is also verified from the *FS* column of Table 5.4.

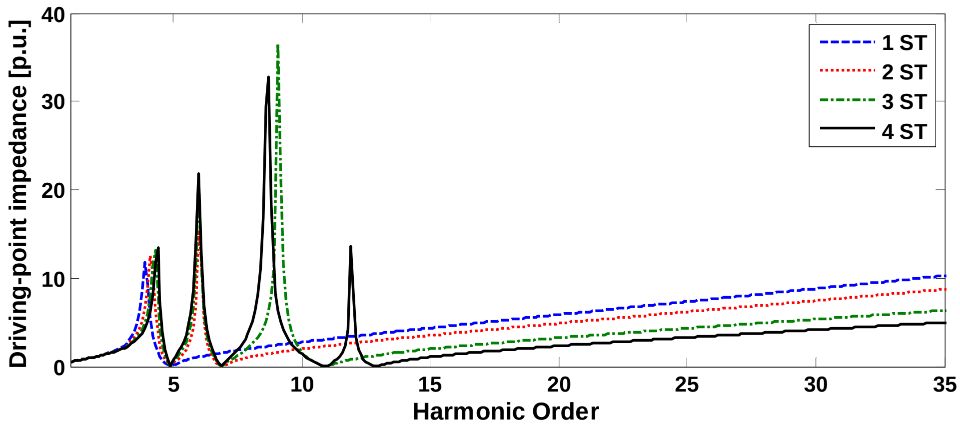

Figure 5.10. Frequency scan for several configurations

5.5.2 On the size of the filter branches

This study is concerned with allocating the necessary reactive power into the filter branches, which is done by sizing the three capacitors differently among each other. The idea is to verify if the filter performance is much superior when the three braches are differently sized. The three-filter-branch case is analyzed. An exhaustive search was performed, and all combinations of reactive power allocation among the three branches were analyzed. In this study, a total of 5.1 MVAr were distributed in the three branches; the reactive power increments were in steps of 100kVAr.

After the search was performed, we verified that all combinations result in acceptable levels of THD_V. The 3 best allocations are shown in Table 5.5, where the option with three equal braches is also shown in the last row. This table shows that the branch tuned to the highest frequency will perform a little better if the most available reactive power is allocated to it. The branch tuned to the central frequency should be the one with less allocated reactive power. Although this second sensitivity study shows that the best way to associate the available filter banks is to adopt small single-tuned filters for low order harmonics and larger branches for the higher order, one can also see that the option of three equal branches also performs very well (last row of Table 5.5).

Table 5.5. Effect of Changing the Filter Sizes

THD_V	1st branch [MVAr]	2nd branch [MVAr]	3rd branch [MVAr]
3.0773	1.2	1.2	2.7
3.094	1.3	1.2	2.6
3.1195	1.4	1.2	2.5
3.4832	1.7	1.7	1.7

5.6 Conclusions

In this chapter, appropriate filter topologies have been identified through the use of several indices to measure technical and economic performances. A general configuration of medium-voltage industrial system was used to properly calculate the indices and evaluate the filter associations. The investigation was conducted by exhaustive search.

The investigation on the filter quality factor provided further information in order to obtain the best topology, by efficiently refining the results. It was found that, when the target is to find the most appropriate combination of three filter branches of the same size, the combination composed by a set of 3 single-tuned filters is in general effective enough to decrease the THD_V levels to acceptable results without overloading, whereas other combinations may exhibit component overloading or ineffectiveness. The presented methodology considers all the filter design requirements and is able to eliminate the major uncertainty of the filter design.

Sensitivity studies dealing with the number of single-tuned branches were carried out and they show that 3 or 4 filter branches are the best solutions. Three branches are less expensive and have higher margin for stress. Further studies showed that although the best reactive power distribution is to install small single-tuned branches tuned to low order harmonics and a large single-tuned branch tuned to the highest order harmonic, the option of three equal branches also performs very well.

The next chapter of this thesis is concerned with the measurement and source determination of interharmonics. Interharmonics are another power utility concern of utility companies, especially in systems where power electronic loads are widely employed.

Chapter 6

Methods for Measurement and Identification of Interharmonic Sources[3]

Power electronic converters such as adjustable speed drives, which are harmonic-generating loads, can also generate interharmonics. Since large ASDs are commonly employed in industrial systems, interharmonics have become prevalent in medium-voltage distribution systems. Like harmonics, interharmonics are another power quality concern due their many hazardous effects. Today, one important concern from the utilities' standpoint is to determine the source of the interharmonics in systems where the problem is present.

This chapter proposes a new method for identifying the interharmonic source location in power systems. The method is based on the interharmonic impedances measured at the metering points, and is inspired by the fact that the impedance of interharmonic-generating loads at that frequency is much higher than that of the utility system. This method represents an improvement over the traditional power-direction method, as the new method is more robust and less prone to erroneous identification. Issues associated with the reliability of the recorded data are addressed, and a set of data reliability criteria is presented. The effectiveness of the new method has been verified through simulation studies and field measurements.

6.1 Introduction

Power System interharmonics are spectral components with a frequency that is a non-integer multiple of the supply fundamental frequency. For several reasons, these

[3] A version of this chapter has been submitted for publication: A. B. Nassif, J. Yong, H. Mazin, X. Wang, W. Xu, "An Impedance-Based Approach for Identifying Interharmonic Sources," *IEEE Transactions on Power Delivery.*

components are more troublesome and harmful than harmonics. Firstly, in contrast to harmonic components, interharmonics do not manifest themselves in known and/or fixed frequencies, for their frequencies can vary with the operating conditions of the interharmonic-producing load. This variation presents a hazard for control and protection signals, which may suffer interference from interharmonics. Secondly, interharmonics can cause flicker in addition to distorting the waveforms. Thirdly, interharmonics are more complex to analyze than harmonics, as they are related to the problem of waveform modulation.

Recently, many studies of interharmonic measurement and characterization in the frequency domain [16], [71]-[74] and mitigation techniques [17]-[18] have been published. The identification of the interharmonic source has also become a concern, as a utility company has the responsibility to provide customers with a power supply of a fixed quality. The cause of a problem cannot be identified, and mitigation schemes cannot be designed until the interharmonic source has been identified. Practical and reliable methods for identifying the interharmonic polluters are needed to accelerate the mitigation process.

References [75] and [76] use the interharmonic active power direction as a method for identifying the source of interharmonics. This method succeeds in identifying the source in the case study presented in [75] and in the simulation studies presented in [76]. However, the main limitation of this method is that its index is typically very small. This problem may lead to unreliable conclusions when the suspected spectral components have active power small enough to be difficult to measure, but a magnitude large enough to be a potential cause of interference with control signals.

Other studies have proposed techniques for tackling the problem of flicker source detection [77]-[79]. Since interharmonics cause waveform fluctuations, these methods can be applied for identifying interharmonic polluters. Reference [77] compares the fluctuations in the feeders' load level in order to identify the feeders that are contributing to the flicker level. This method can identify whether a feeder is contributing to the fluctuation, but cannot determine the direction to an interharmonic source. References [78] and [79] present a solution that relies on the flicker's active power and is able to detect the side of a metering point where the dominant generating-flicker load is located.

However, this solution cannot identify the interharmonic direction because if interharmonic (even of different frequencies) sources are in both sides of the PCC, the method cannot determine the direction to the source of each frequency. This limitation is a problem because in some applications (such as interharmonics causing interference with control signals), the interest is in identifying which customer is generating the specific interharmonic frequency(ies) that is(are) interfering with the control signals.

The method presented in this chapter is based on the measured interharmonic impedance at a metering point. The main idea behind this method is that the interharmonic impedance of the system is much smaller than that of an interharmonic-generating load. This method can identify the source of each interharmonic component without having to rely solely on the active power measurement and requires only an approximate value for the interharmonic impedance measured at the metering point.

6.2 Interharmonic Source Identification

In harmonic analysis, many polluters are usually present in a power distribution system for each harmonic order because power system harmonics always occur in fixed frequencies, i.e., integer multiples of the fundamental frequency. All harmonic loads usually generate all harmonic orders, and therefore, it is common to try to determine the harmonic contribution of each load rather than the harmonic sources. As opposed to harmonics, interharmonics are almost always generated by a single polluter. This property of interharmonics can be explained as follows.

The main interharmonic sources are adjustable speed drives (ASDs) with a p_1-pulse rectifier and a p_2-pulse inverter and periodically varying loads such as arc furnaces. Their interharmonic generation characteristics can be expressed as in equation (6.1) for ASDs [18] and (6.2) for periodically varying loads [16], respectively:

$$f_{IH} = \left| \left(p_1 m \pm 1 \right) f \pm p_2 n f_z \right|, \quad m = 0,1,2...; \quad n = 1,2,3..., \tag{6.1}$$

where f and f_z are the fundamental and drive-operating frequency.

$$f_{IH} = \left| f \pm n f_v \right|, \quad n = 1, 2, 3..., \tag{6.2}$$

where f_v is the load-varying frequency. According to equations (6.1) and (6.2), the interharmonic frequency depends on many factors such as the number of pulses of the converter and inverter, the drive-operating frequency, or the load-varying frequency. Therefore, the same frequency of interharmonics is rarely generated by more than one customer.

Based on the above analysis, for interharmonic source determination, we can restrict the analysis to the case of a single source for each of the interharmonic components. The most popular method currently being used to identify the interharmonic sources is based on the active power index. Figure 6.1 helps to explain the power direction method. For this problem, the polluter side is usually assumed to be represented by its respective Norton equivalent circuit. Figure 6.1 shows two different scenarios at the metering point between the upstream (system) and the downstream (customer) sides. Figure 6.1a and Figure 6.1b show the case where the interharmonic components come from the upstream side and the downstream side, respectively. The circuits presented in Figure 6.1 are used for each frequency.

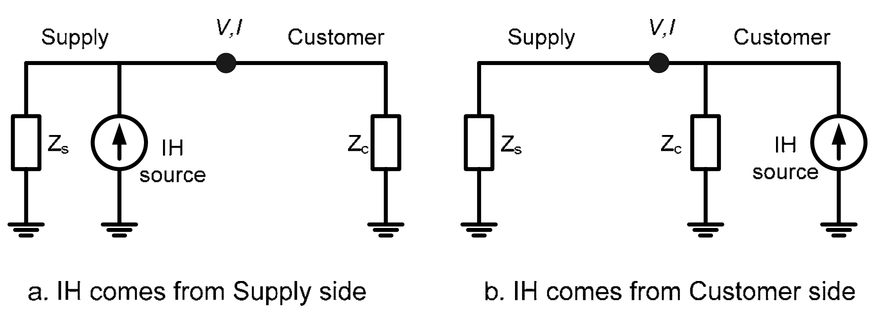

Figure 6.1. Determination of interharmonic source – two different scenarios.

The interharmonic active power can be obtained from the voltage and current measurements at a metering point as

$$P_{IH} = \mathrm{Re}\left\{ V_{IH} \times I_{IH}^{*} \right\} = \left| V_{IH} \right| \left| I_{IH} \right| \cos\left(\phi_{IH} \right), \tag{6.3}$$

where $|V_{IH}|$ and $|I_{IH}|$ are the interharmonic voltage and current magnitudes, respectively, and φ_{IH} is the angle displacement between the interharmonic voltage and current.

The conclusion of the power direction method, therefore, is the following:

- If $P_{IH} > 0$, the interharmonic component comes from the upstream side.
- If $P_{IH} < 0$, the interharmonic component comes from the downstream side.

If this criterion is extended to a multi-feeding system like that shown in Figure 6.2, the interharmonic source for each interharmonic can be identified. In such a case, monitoring equipment should be placed at each feeder suspected of injecting interharmonics into the system. For the system side measurements (point A), if the measured $P_{IH} > 0$, the interharmonic component comes from the system. For the customer side measurements (points B and C), if the measured $P_{IH} < 0$, the interharmonic component comes from the measured customer.

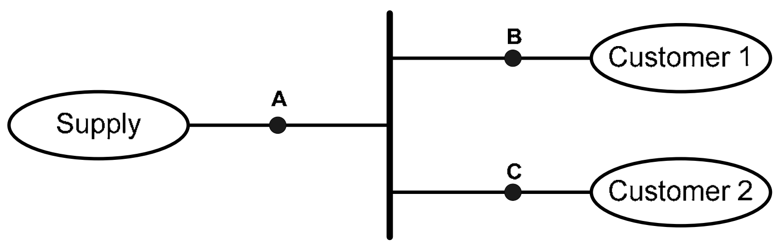

Figure 6.2. System diagram for locating the interharmonic source.

As a given interharmonic frequency has only one source, the power direction method (in theory) could always reveal the interharmonic source correctly. In reality, as the active power of the interharmonics is typically very small [80], the measured data may not be reliable, so this index may not provide reliable conclusions. On the other hand, the angle φ_{IH} can be very close to either $\pi/2$ or $-\pi/2$, oscillating around these angles because of measurement errors, and resulting in the measured active power index swinging its sign and potentially causing misjudgment. The drifting nature of interharmonics in frequency and the supply fundamental frequency variation also influence this inaccuracy. A more reliable method for identifying the interharmonic source location is proposed in the next section.

6.3 The Interharmonic Impedance-Based Method

6.3.1 The Proposed Method

The motivation for proposing this method can also be explained by using Figure 6.1 and Figure 6.2. The interharmonic impedance measured at each metering point can be obtained by using (6.4):

$$Z_{IH} = \frac{V_{IH}}{I_{IH}} = \frac{|V_{IH}|}{|I_{IH}|}\cos(\varphi_{IH}) + j\frac{|V_{IH}|}{|I_{IH}|}\sin(\varphi_{IH}) = R_{IH} + jX_{IH}. \tag{6.4}$$

The main idea behind this method is that the interharmonic impedance is essentially either the upstream or downstream impedance relative to the metering point. Figure 6.1 can be used to help explain how this information can be used to find the interharmonic source: if the source of interharmonics is in the upstream side of the metering point (Figure 6.1a), the measured impedance is the downstream impedance. On the other hand, if the source is in the downstream of the metering point (Figure 6.1b), the measured impedance is the upstream impedance. The above impedance-based directional identifier offers several unique advantages.

6.3.1.1 Magnitude of the measured impedance $|Z_{IH}|$

The system impedance is generally much smaller than the load side impedance, so the magnitude of $|Z_{th}|$ can be used to check if the impedance is the system-side impedance or load-side impedance and, in turn helps to determine the location of the interharmonic source. In fact, the fault MVA of the metering location is usually known approximately and can be used as a gauge to compare the values of $|Z_{th}|$. The range of the load-side impedance can be estimated by using V_1/I_1, which gives another comparative value for $|Z_{th}|$. For example, if $|Z_{IH}|$ and the system impedance $|Z_s|$ (after adjusting the impact of frequency) are **not** of comparable values, the measured impedance is likely to be the downstream impedance, and, consequently, the system is the interharmonic source. For customer side measurements, such as point B and C in Figure 6.2, if $|Z_{IH}|$ and $|Z_s|$ are of comparable sizes, then the measured impedance is the upstream impedance. Therefore, the measured customer is the interharmonic source. The adjustment of system side impedance to account for interharmonic frequency can be done as follows:

$$Z_s\left(f_{IH}\right) = R_s + j\frac{f_{IH}}{f_1}X_s \approx j\frac{f_{IH}}{f_1}X_s, \tag{6.5}$$

where R_s and X_s are system short-circuit impedance that can be determined from the fault MVA at the metering point.

The above comparative analysis does not require the accurate evaluation of the system or load interharmonic impedances. All that needs to be known is whether the measured impedance is of a value comparable to that of the system or the load. Since the impedance can be obtained by using the magnitudes of the interharmonic voltage and current, fluctuation of the angle displacement between the voltage and the current of the low-magnitude interharmonic components does not affect the accuracy of the method.

6.3.1.2 The sign of R_{IH}

A comparison of equations (6.3) and (6.4) reveals that the real part sign of the measured impedance is the same as the sign of the measured active power. Therefore, all the functionality featured by the power direction method is included in the impedance-based method. If the φ_{IH} is far away from $\pi/2$ and $-\pi/2$, this index can also be used to identify interharmonic sources independently. As a result, both $|Z_{IH}|$ and sign(R_{IH}) can be used either independently or together to support the reliability of each other's results.

6.3.1.3 The sign of X_{IH}

Together, the sign(R_{IH}) and sign(X_{IH}) can indicate whether the impedance is inductive or capacitive. If sign(R_{IH}) and sign(X_{IH}) have opposite signs, then the measured impedance is capacitive, and vice versa. It is well known that the system (especially the distribution system) impedance is typically inductive, whereas loads can have inductive or capacitive behavior. Therefore,

- If sign(R_{IH}) is positive but sign(X_{IH}) is negative, the implication is that the measured impedance is the capacitive downstream impedance. In this case, the measured downstream impedance may also be comparable to the system impedance since the capacitive reactance is inversely proportional to the frequency. In this case, sign(X_{IH}) is very helpful in identifying the measured impedance as downstream impedance.

- If sign(R_{IH}) is negative, but sign(X_{IH}) is positive, then the interharmonic comes from downstream, and the measured upstream impedance is capacitive. As this situation is unusual in distribution feeders, it indicates that the data may be not reliable.

Thus, the impedance index offers three unique attributes for interharmonic source identification. These attributes can be used to complement each other to enhance the reliability of the findings.

In addition to the above index, the pairing characteristic of interharmonics can also be utilized to provide additional confidence in the accuracy of the direction-finding results. Equations (6.1) and (6.2) show that interharmonics always appear in pairs. For the dominant pair of interharmonics (m = 0 and n = 1), the frequencies can be expressed as

$$f_{IH} = \left| f \pm f_w \right|, \tag{6.6}$$

where f_w is $p_2 f_z$ or f_v.

As a result, the summation or difference of the frequencies of a pair of interharmonic is $2f$. This result means that if the summation or difference of two interharmonic frequencies is $2f$, they can be regarded as coming from the same source. Since interharmonics drift in frequency, the pair relationship of interharmonics can be checked by using the correlation test. This process is discussed in section 6.5.

Associating two interharmonics with one source is very important in identifying the inharmonic source because even with the information redundancy provided by the impedance index about the interharmonic source, some measured data are not reliable and therefore cannot be trusted. In this case, the pair characteristic of interharmonics may be able to reveal where these interharmonics are coming from. One of the field tests results in section 6.5 presents an example.

The other application of this index is that for an interharmonic pair, if $|X_{IH}|$ decreases when the interharmonic frequency increases or if the sign(X_{IH}) of a pair of interharmonics are opposite, the measured impedance has capacitive behavior, and is, therefore, the downstream impedance. This information can also be used to support the results.

In conclusion, the indices presented in this subsection are derived from the measured impedance. They can be used either alone or to support each other. Therefore, the impedance-based method is more powerful and less prone to errors than the power direction method.

6.3.2 Simulation Results

The system in Figure 6.3, simulated by using PSCAD, is composed by a supply and two customers. Customer 2 generates a pair of interharmonics as shown in Figure 6.3. The fundamental frequency in this case is 50Hz, so that the interharmonic orders are 4.4 and 6.4 of the fundamental frequency.

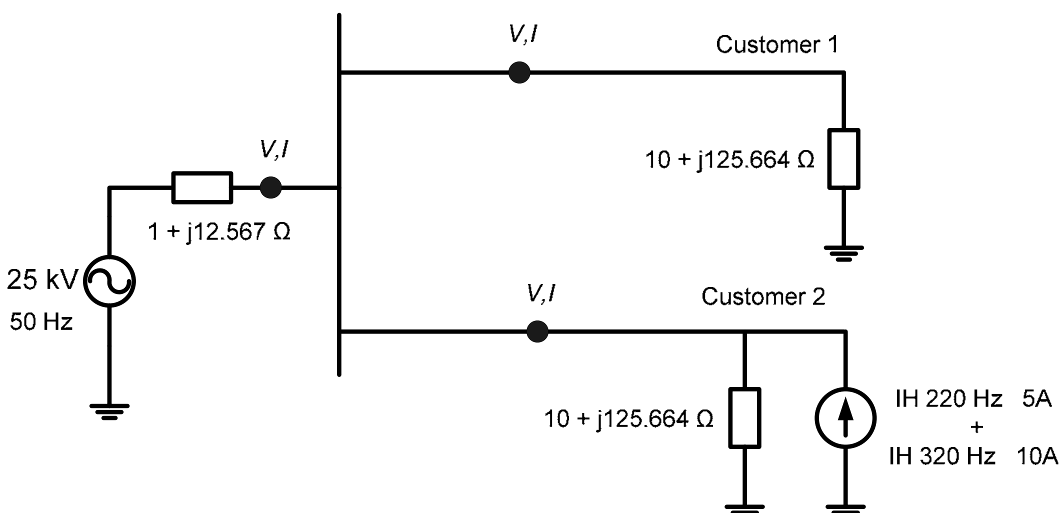

Figure 6.3. One line diagram of the simulated system

The results for the impedance-based method are presented in Table 6.1. It shows that the impedance $|Z(IH)|$ measured at customer 2 metering point is comparable to the calculated system interharmonics impedance $|Z_s(IH)|$. This finding implies that customer 2 is the interharmonic source. The sign of R and X for customer 2 and the system are both negative because of the direction of the current flow. The sign of R leads to the same conclusion, i.e., that the interharmonics are flowing from downstream of their metering points, and the sign of X implies that the load is inductive.

Table 6.1. Measured impedance of the loads

Location of measurements	**IH frequency [Hz]**	R_{IH} **[Ω]**	X_{IH} **[Ω]**	$\|Z_{IH}\|$ **[Ω]**	**Calculated** $\|Z_s(IH)\|$ **[Ω]**
Customer 1	220	10	553	553	55
	320	10	805	805	81
Customer 2	220	-1	-50	50	55
	320	-1	-73	73	81
System	220	-1	-55	55	55
	320	-1	-81	81	81

Simulation studies can be generally used to test a method under ideal conditions. For measurement studies, however, the data can be unreliable. A set of reliability criteria for the data is needed to be able to identify which data are reliable. These criteria are presented in the next section, before the measurement results, in order to facilitate reference as the results are presented.

6.4 On the Reliability of the Interharmonic Data

Actual interharmonic recorded data may be unreliable due to the typically low-magnitude interharmonic components and to their varying-frequency characteristics. A set of reliability criteria is proposed to assess the interharmonic data. It is based on interharmonic fundamentals and measurements issues. After the interharmonic data have been found to be reliable, they can be analyzed, and the reliability of the source identification results will increase.

6.4.1 Quantization Error Criterion

An ideal Continuous-to-Discrete converter converts a continuous-time signal into a discrete-time signal, where each sample is known with infinite precision. Quantizers for digital signal processing convert an analog signal into a digital signal as a sequence of finite-precision quantized samples. As the conversion is not instantaneous, high-performance Analog-to-Digital systems typically include a sample-and-hold, completing a conversion every time step. As the number of bits of data acquisition equipments is finite (the equipment used in this present study is a high-resolution device that has 12 bits), a coder is part of the A/D converter [81]. The equipment used in this study features a uniformly spaced, bipolar coder, and the number of quantization steps is 2^{12}.

The quantization step is a determining factor in defining a value for a threshold for the minimum magnitude of the measured interharmonics. As the energy of current signals drops to a level comparable to that of quantization noises, the signal may be corrupted, and the data will, therefore, be unreliable. For this reason, if the interharmonics are of a magnitude lower than that of the quantization error, they should not be trusted. This criterion is developed as:

1. The step size of the quantizer is

$$\Delta = \frac{V_{in}}{2^n}, \tag{6.7}$$

   where n is the number of bits, and V_{in} is the input range.

2. The current probe ratio is k_{probe}, which is the ratio V/A. This ratio is used because the data acquisition device uses voltage as an analog input, whereas the measurements are currents.

3. Therefore, the step size in amps is

$$\Delta_I = \frac{\Delta}{k_{probe}}. \tag{6.8}$$

4. Finally, the maximum quantization error will be half of the step size.

The input range, number of bits and current probe ratio will depend on the data-acquisition equipment and measurement set-up. All measurements presented in the field-test section were taken with an input range of 10 V (-5V to 5V). The probe ratio was always set as 10 mV/A. In addition, this threshold must be accordingly scaled for the values of the CT (current transformation) of the metering points.

6.4.2 Current and Voltage Spectra Correlation Criterion

If genuine interharmonics do exist, voltage and current spectra should show a correlation [22] because an interharmonic injection will result in a voltage across the system impedance, and therefore both the voltage and current should show similar trends at that frequency. As many measurement snapshots are taken, the variation over time of the interharmonic voltage and current trends are observed, and their correlation is analyzed. In order to quantify this similarity, the correlation coefficient is used [70]:

$$r[\%] = 100 \times \frac{n \times \sum_{i=1}^{n} I_{IH}(i) \times V_{IH}(i) - \sum_{i=1}^{n} I_{IH}(i) \times \sum_{i=1}^{n} V_{IH}(i)}{\sqrt{\left[n \times \sum_{i=1}^{n} I_{IH}^2(i) - \left(\sum_{i=1}^{n} I_{IH}(i) \right)^2 \right] \left[n \times \sum_{i=1}^{n} V_{IH}^2(i) - \left(\sum_{i=1}^{n} V_{IH}(i) \right)^2 \right]}}, \quad (6.9)$$

where I_{IH} and V_{IH} are the interharmonic frequency current and the voltage magnitudes of the n-snapshot interharmonic data, respectively.

The threshold for this coefficient is defined according to the experience gained when working with interharmonic data: 0.80. Frequencies that have a coefficient lower than the 0.80 threshold may not be reliable, as they may not be genuine interharmonics.

6.5 Field Test Results

In this section, the instrument set-up and two field test verifications are presented.

6.5.1 Instrument Set-up

The national instrument NI-6020E 12-bit data acquisition system with a 100 kHz sampling rate controlled by a laptop computer was used for the recording. Using this data-acquisition system, we obtained 256 samples per cycle for each waveform. As mentioned above, measurements were taken at the substation feeders and at the loads suspected to be the interharmonic sources. For the substation feeders, the captured waveforms were three phase voltages and currents at the point of metering in the load serving substations. For both systems (feeders and customer loads), all the measuring points were at 25 kV load serving substations; therefore CTs and PTs were used to step down the current and voltages, respectively, to measurable values. The measurements were taken for five seconds per minute, so that in every minute, a five-second snapshot of the three phase voltages and currents was captured.

6.5.2 Interharmonic Study at System #1

Interharmonic problems were experienced in an oilfield area of Alberta, Canada. Measurements were taken at three customers, codenamed Customer 1, Customer 2, and Customer 3, which were operating big oil extraction ASD drives and were suspected interharmonic sources. The system diagram is shown in Figure 6.4. The measurements at the metering points revealed that the interharmonic detected frequencies were present throughout the system.

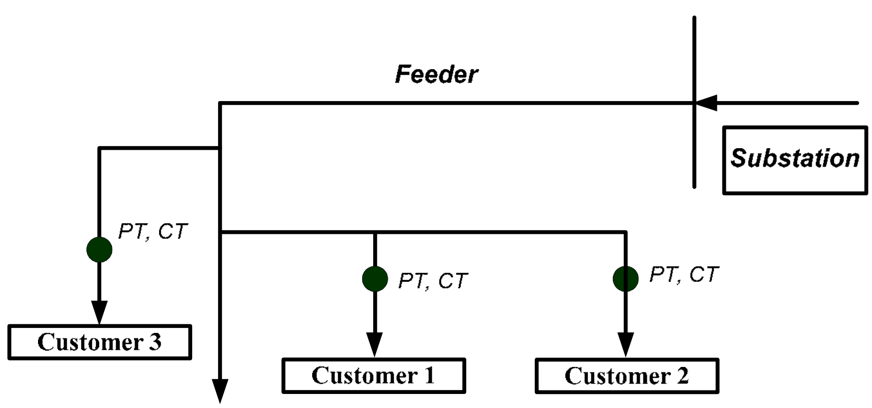

Figure 6.4. Field measurement locations at system #1

Figure 6.5 shows a sample contour plot of the spectrum calculated for the three Customers' currents in order to obtain the frequencies of the interharmonic components present in this system. Two main interharmonics are identified: 151 Hz and 271 Hz.

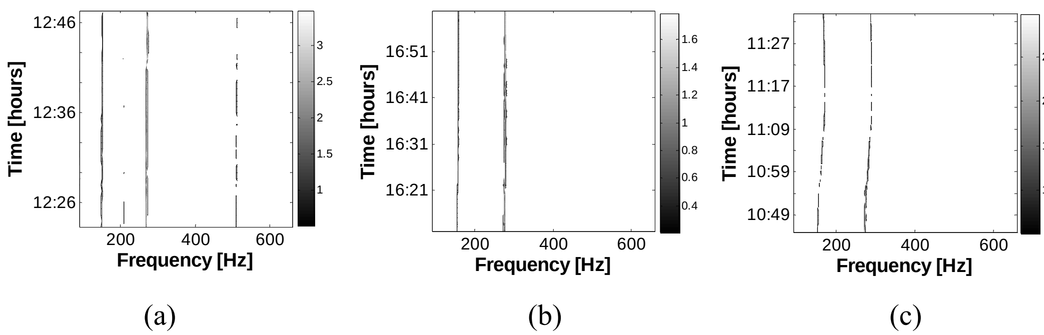

Figure 6.5. Contour plot of the interharmonic data recorded at the three Customers (phase A): (a) customer 1, (b) customer 2, (c) customer 3.

6.5.2.1 Criteria for determining the reliability of the data

Table 6.2 shows the percentage of reliable snapshots obtained by using the quantization error criterion. Only snapshots with an energy level higher than the quantization error could be used. All the data were reliable in this case due to the high magnitude of the interharmonic components.

Table 6.2. Reliable snapshots [%] according to the quantization error criterion for system #1

IH freq (Hz)	Customer 1	Customer 2	Customer 3
151 Hz	100	100	100
271 Hz	100	100	100

Table 6.3 shows the correlation results for the locations, revealing that the interharmonic voltage and current had a high degree of correlation at the three customer loads.

Table 6.3. Correlation results for system #1

IH freq (Hz)	Customer 1	Customer 2	Customer 3
151 Hz	0.93	0.88	0.98
271 Hz	1.00	1.00	1.00

6.5.2.2 Results

In this case, only customer side measurements were taken. Using the real fault data recordings from the PML meters at the substation, the short circuit impedance at the substation was calculated to be 0.928 + j2.913. Because no metering point was installed at the substation, we calculated a value for the system impedance at each location. According to the length and the size of the supplying line, the system impedances at locations 1 to 3 were calculated to be 5.712 + j8.125 Ω, 5.712 + j8.1250, and 9.3 + j12.02 Ω (at 60 Hz) respectively. These values are approximate because the length of the distribution feeders from the substation to each load was not known exactly.

The related system interharmonic impedances and the measured impedances are shown in Table 6.4, which shows that the calculated system interharmonic impedance has comparable value to the measured impedance at Customer 3. This result means that Customer 3 was the source of both frequencies.

Table 6.4. Impedance comparison at 25 kV level for system #1

Location of measurements	IH frequency [Hz]	Sign(R_{IH}) (R_{IH} [Ω])	Sign(X_{IH}) (X_{IH} [Ω])	$\lvert Z_{IH}\rvert$ [Ω]	Calculated $\lvert Z_s (IH)\rvert$ [Ω]
Customer 1	151	+ (40)	- (72)	82.7	21.23
	271	+ (54)	+ (220)	227.13	37.14
Customer 2	151	+ (207)	+ (128)	244.25	21.23
	271	+ (56)	+ (245)	252.19	37.14
Customer 3	151	- (6.7)	- (35)	35.2	32
	271	- (3)	- (56)	56.59	55

The information for sign(R_{IH}) reveals that the sign(R_{IH}) of Customer 3 is negative, so that Customer 3 was the source. This index was used as a "cross-check" to support the identification. In this case, the angle displacement between the voltage and current was not observed to fluctuate at around $\pm\pi/2$ radians. As well, with the data reliability verification, the sign(R_{IH}) alone also provides the correct result.

The sign(R_{IH}) and sign(X_{IH}) of Customer 1 are opposite at 151 Hz, indicating that the measured impedance at the Customer 1 metering point was capacitive downstream impedance. Therefore, we can confirm that Customer 1 was not an interharmonic source as well.

6.5.3 Interharmonic Study at System #2

Figure 6.6 shows the measurement set-up for the field measurement at this system. The substation feeder supplied three large oil-extracting customers located in Alberta, Canada. The three customers, codenamed Customer 1, Customer 2 and Customer 3, and the feeder were measured. The feeder could be regarded as system side. The three customers operated oil-extracting ASD drives and, therefore, were a potential source of interharmonics.

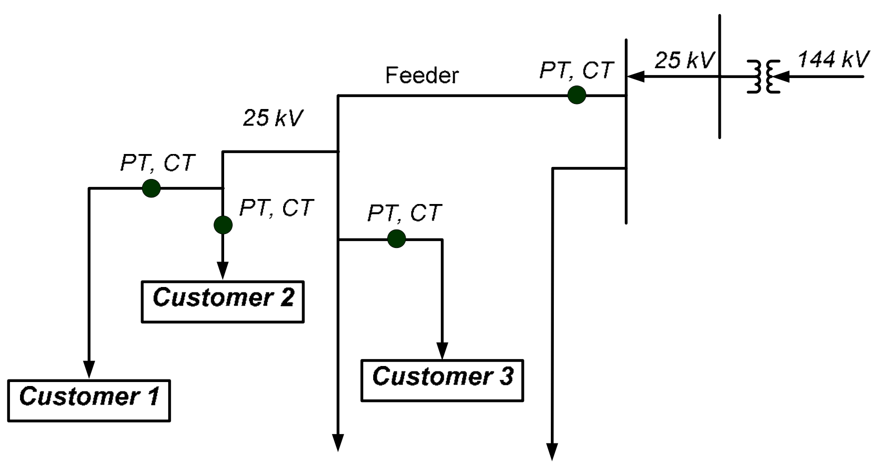

Figure 6.6. Single line diagram of system #2

After processing all the data snapshots taken at the four metering points, we obtained the contour plot of the spectrum calculated from the feeder current present in this system and shown in Figure 6.7. This figure reveals that the four interharmonic components, according to $2f$ index, seem to be two pairs around 228 Hz and 348 Hz, and 264 Hz and 384 Hz, respectively. These components drift in frequency due to the change of the drive operation conditions, but each exists within a narrow range of frequencies. The harmonic components were omitted from Figure 6.7 in order to improve the visualization of the interharmonics (the interharmonics are of much lower magnitude than the harmonics). The interharmonic components correlation results are shown in Figure 6.8, which also shows the same conclusion.

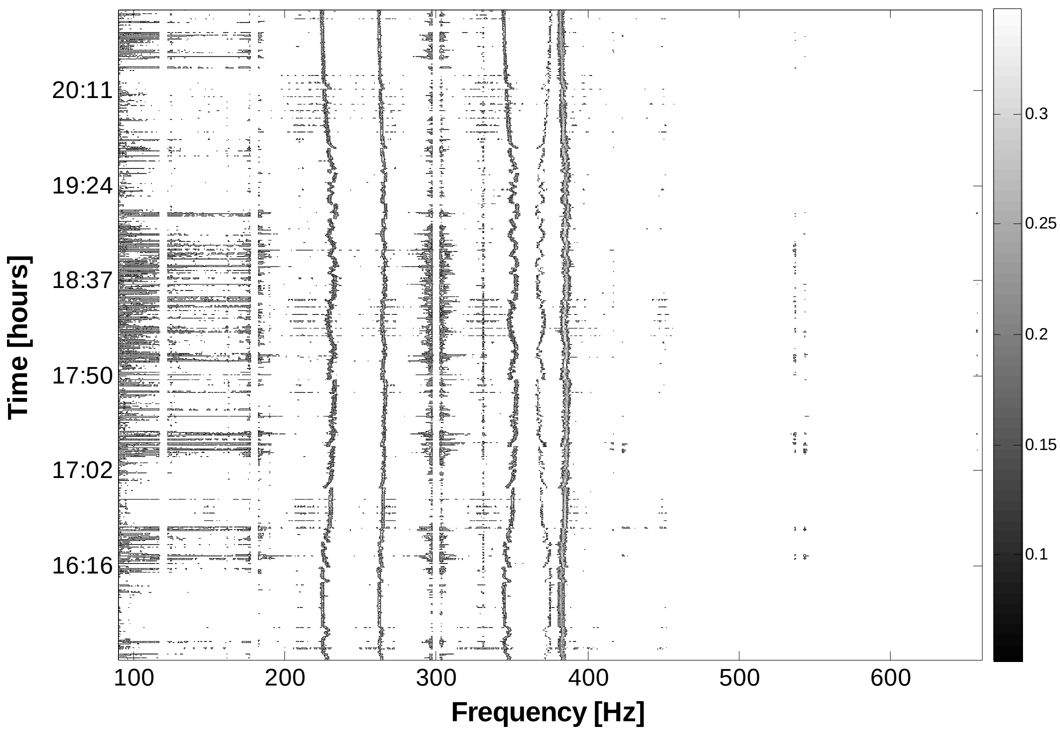

Figure 6.7. Contour plot of the interharmonic data recorded at the feeder (phase A)

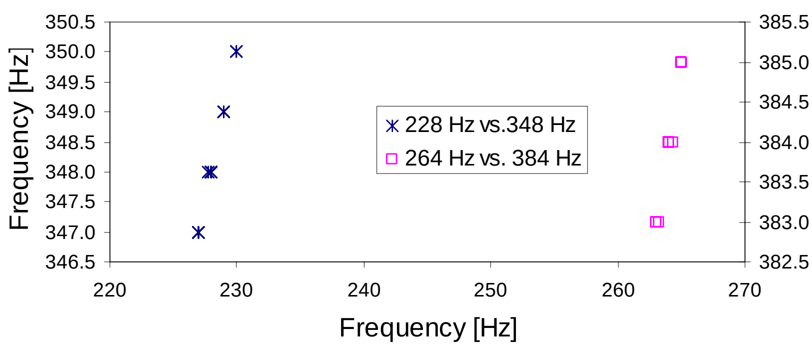

Figure 6.8. Correlation of interharmonic components for system #2

6.5.3.1 Criteria for determining the reliability of the data

The reliable snapshots (according to the energy level criterion) and correlation results are shown in Table 6.5 and Table 6.6, respectively. All the frequencies measured at the feeder, as well as the 3 measurements at the customer side, are unreliable. Therefore, much of the data should be rejected, and this requirement increases the difficulty of interharmonic source identification.

Table 6.5. Reliable snapshots [%] according to the quantization error criterion for system #2

IH freq [Hz]	Feeder	Customer 1	Customer 2	Customer 3
228	0.00	19.44	100.00	91.84
264	0.00	0.00	77.19	81.63
348	0.00	0.00	3.51	0.00
384	0.00	100.00	100.00	100.00

Table 6.6. Correlation results for system #2

IH freq [Hz]	Feeder	Customer 1	Customer 2	Customer 3
228	0.68	0.98	0.96	0.98
264	0.31	0.96	0.59	0.92
348	0.55	0.96	0.92	0.96
384	0.77	0.99	0.98	0.97

6.5.3.2 Results

The impedance comparison results are shown in Table 6.7. The crossed cells are considered unreliable according to the data reliability criteria (the feeder data are omitted since all are unreliable). The system impedance at the substation was calculated to be 0.623 + j2.582 by using the real fault data recordings from the PML meters at the substation. After adding the line impedance between the substation and the metering points, the system impedance at each metering point could be obtained, and then the related system interharmonic impedances, shown in Table 6.7, were calculated. As in the previous case study, the calculated value of $|Z_s|$ is an approximation.

Since less information from the available data was considered reliable, more indices were necessary to determine the interharmonic sources. Firstly, the comparison of the index $|Z_{IH}|$ with $|Z_s\ (IH)|$ reveals that the measured impedances of 228Hz and 384Hz at Customer 2 are comparable to the related system impedances, respectively, so that both measured impedances came from Customer 2. Since the measured impedance at 264Hz at Customer 3 is not comparable to the related system impedance, the former did not come from Customer 3. For the 348Hz interharmonic, it is hard to determine whether it is comparable to the related system impedance.

Secondly, the index sign(R_{IH}) was used to extract more information. The sign(R_{IH}) confirmed that both the 228Hz and 384Hz interharmonics came from Customer 2 since they had a negative sign. This result also indicates that the 348Hz interharmonic came from Customer 2 and that the 264Hz interharmonic came from Customer 3. These results contradict the result from index $|Z_{IH}|$.

Thirdly, both sign(R_{IH}) and sign(X_{IH}) were considered. It was found that for the 264 Hz interharmonic, the sign(R_{IH}) was negative but the sign(X_{IH}) was positive. This result implies that this data either indicated a capacitive load or might not have been reliable, so we cannot trust the result from sign(R_{IH}) for the 264 Hz interharmonic at Customer 3.

So far, based on the above analysis, we can confirm that the 228 Hz and 384 Hz interharmonics came from Customer 2. Finally, by using the pair characteristic, the 264Hz and 384Hz interharmonics can be associated with Customer 2. Therefore, the conclusion is that Customer 2 produced all the interharmonics.

This case demonstrates that the power direction method alone is not adequate for identifying the interharmonic source and may even provide a false determination, such as that at the 264 Hz interharmonic, even when using the reliability criteria. Through further investigation of the voltage-current angle displacement of each interharmonic frequency at each location, it was observed that the interharmonic frequency 264 Hz at Customer 2 location oscillated at around $-\pi/2$ radians, causing the power to fluctuate around zero. This result is shown in Figure 6.9 and provides a final confirmation that the power direction method alone cannot detect the source for this frequency at this customer location.

Table 6.7. Impedance comparison at 25 kV level for system #2

Location of measurements	**IH frequency [Hz]**	**Sign(R_{IH}) (R_{IH} [Ω])**	**Sign(X_{IH}) (X_{IH} [Ω])**	**$\lvert Z_{IH}\rvert$ [Ω]**	**Calculated $\lvert Z_s\ (IH)\rvert$ [Ω]**
Customer. 1	228	+ (41)	+ (516)	518	81.2
	348	+ (101)	+ (903)	909	123
	264	+ (39)	+ (550)	551	94
	384	+ (90)	+ (992)	996	135
Customer 2	228	- (100)	- (96)	140	81.2
	348	- (275)	- (50)	318	123
	264	+ (9)	- (193)	196	94
	384	- (185)	- (120)	220	135
Customer 3	228	+ (150)	+ (320)	354	81.2
	348	- (166)	+ (951)	968	123
	264	- (200)	+ (328)	389	94
	384	+ (585)	+ (940)	1106	135

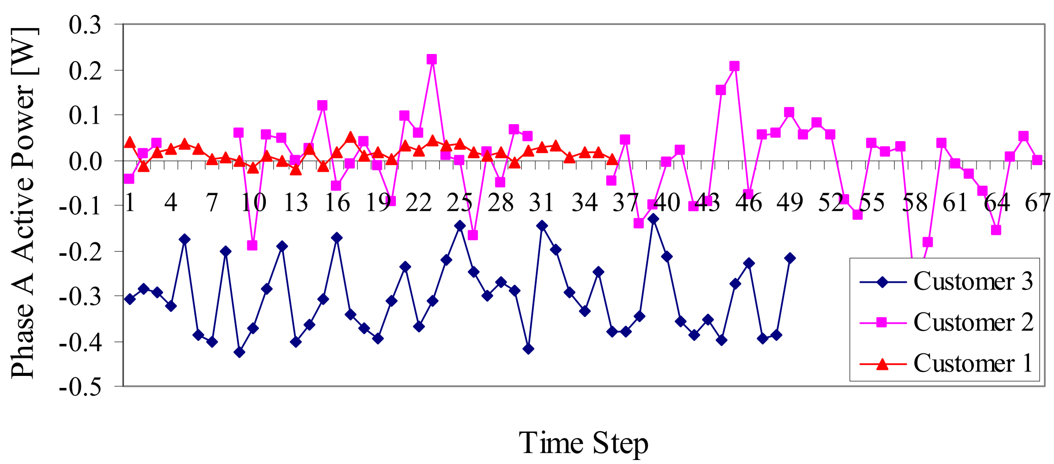

Figure 6.9. Phase A 264 Hz interharmonic active power for the three locations

6.6 Conclusions

This chapter proposed an interharmonic impedance-based method to approach the interharmonic source detection problem. The method was effective in simulation studies and studies using field-recorded data.

It can be concluded that:

- Four indices are included in the proposed method, which provide information from different perspectives. The absolute value of the measured impedance indicates the interharmonic source directly. The resistive part of the measured impedance provides the same information as that provided by using the power direction method, whereas the reactive part reveals information about the load. The pair characteristic of the interharmonics provides the frequency relationship.
- The presented case studies have shown that this proposed method is more robust than the power direction method.
- This method overcomes the limitations caused by the interharmonic current low magnitudes and the voltage-current angle displacement, which often render the traditional power direction method ineffective.

A set of criteria for determining the data reliability, which rely on the energy levels and the interharmonic current and voltage correlation, was also presented. These criteria reveal when one should not trust the interharmonic data when attempting to identify the source.

Chapter 7

Conclusions and Future Work

7.1 Thesis Conclusions and Contributions

This thesis has approached topics related to the modeling, measurement, and mitigation of power system harmonics. An extensive investigation of the harmonic characteristics of harmonic-generating home appliances was conducted. The attenuation/amplification effects for some of the power electronic-based home appliances were analyzed, and a modeling technique that takes the effects into consideration was proposed. The mitigation schemes for harmonics were investigated. The problem of interharmonics in distribution systems was also studied.

The main conclusions and contributions of this thesis are summarized as follows:

- An extensive investigation of the harmonic currents of harmonic-generating home appliances was conducted to fully characterize these devices. Two approaches were used:
    - A harmonic currents magnitude-based study, which determines the relative severity of the harmonics from home appliances, was performed. The Equivalent-CFL index was introduced for this purpose. From this study, it was possible to draw conclusions such as that one PC desktop injects a comparable amount of harmonics to that of 7 CFLs, and that microwave ovens and laundry washers are the most harmonic-polluting appliances inside modern households. The investigation of the current harmonics decline ratio was useful to approximate the characteristics of nonlinear appliances.
    - A harmonic currents phase angle-based study, which determines the harmonic compatibility of the harmonics from home appliances, was also carried out. The harmonic compatibility index was introduced for this

purpose. From this study, it was possible to draw conclusions about the harmonic cancellation that occurs when appliances are connected together. The indices led to conclusions such as that the amount of cancellation that occurs at the 3rd harmonic is smaller than those at higher-order harmonics. The indices also presented results that show that pulsed-shape current waveforms drawn by loads such as those of CFLs and computers have higher harmonic compatibility (and consequently less harmonic cancellation) with most of other appliances than the current waveforms from appliances such as fridges, washers and furnaces.

- Extensive characterization of the harmonic current attenuation and amplification effects was conducted. The current harmonics from home appliances can be attenuated or amplified depending on the waveshape of the applied voltage, as compared to the typical spectrum obtained when the appliance is supplied by undistorted supply. It was found that harmonic amplification can frequently occur under realistic conditions of voltage supply. Sensitivity studies were carried out by using an analytical model derived from the circuit topology employed in most power electronic-based appliances. By using many of the recorded supply voltage conditions, the findings obtained through measurements were confirmed.

- In order to consider the harmonic current attenuation/amplification effect, a frequency-domain measurement-based modeling technique was introduced. The model obtained through this technique can be easily incorporated into harmonic power flow programs. To obtain the harmonic models, the least squares-based data fitting method was used. The obtained harmonic models were evaluated, and their accuracies were assessed. It was found that the proposed models represented the harmonic attenuation or amplification that occurred under test conditions. The model was verified for CFLs, PC desktops and LCD monitors.

- Power system harmonic mitigation also received attention in this thesis. Harmonic mitigation is generally performed at medium-voltage level, and the harmonic mitigation techniques proposed in this thesis focused on medium-voltage distribution systems. Utilities can employ the presented solution to mitigate harmonics in residential feeders. Appropriate filter topologies were identified by using of several indices to measure technical and economic performances. A general configuration of a medium-voltage industrial system was used to properly calculate the indices and evaluate the filter associations. The investigation was conducted by making an exhaustive search. The main finding is that the configuration of three single-tuned filter branches had a very good performance in mitigating the harmonics at a desirable cost. Several sensitivity studies were carried out, and it was found that it was best to tune small-rating filter branches at the 5^{th} and 7^{th} harmonics and large-rating branches at the 11^{th} harmonic.

- For utilities, interharmonics have become another important power quality concern. The problems relating to power system interharmonics were investigated in the oilfields of Alberta. Techniques for measuring and identifying interharmonic sources were introduced. Four indices were included in the proposed method, which provided reliable information for determining the interharmonic source. The absolute value of the measured impedance indicates the interharmonic source directly. The resistive part of the measured impedance provides the same information as that provided by using the power direction method, whereas the reactive part reveals information about the load. The pair characteristic of the interharmonics provides the frequency relationship. This method overcomes the limitations caused by the interharmonic current low magnitudes and the voltage-current angle displacement, which often render the traditional power direction method ineffective. A set of reliability criteria was also introduced to determine the reliability of the interharmonic data. The method was shown to be effective in identifying the interharmonic source by using field measurement data of real case studies.

7.2 Suggestions for Future work

As with any study, something can always be done to extend the research. Several extensions and modifications of this thesis can be explored as follows:

- The appliances characterized in Chapter 2 can be combined in order to develop a representative house model. This model should also include the probabilistic aspect of appliance usage. The model for residential houses can then be used for feeder-wide harmonic impact studies. Finally, the harmonic and power factor impact of the large-scale adoption of electronic appliances, such as the CFL, can be thoroughly assessed.

- The harmonic amplification effect analysis similar to that conducted in Chapter 3 can be developed for three-phase ASDs. Harmonic amplification is expected to also occur for those large loads. A theory on why the harmonic amplification effect occurs can be further developed. The response of the single-phase capacitor-filtered diode bridge circuitry can be further analyzed in order to extract more information from the supply voltage waveform and to determine the reasons for amplification.

- The modeling technique introduced in Chapter 4 can be extended to consider the random behavior of the home appliances' usage patterns. This extension could be used for evaluating the level of harmonic distortion in distribution grids.

- More sophisticated and effective harmonic mitigation techniques can be developed by using tunable and switchable filters. Tunable filters can be based on the selected topology combination obtained in Chapter 5 in order to perform real-time harmonic mitigation. Tunable filters can also be designed to mitigate power system interharmonics. The concept of switchable filters can be used to optimize power factor correction and harmonic/interharmonic mitigation.

- The interharmonic source detection method can be implemented in power quality monitoring devices that can be eventually installed for many large customers. Due to its simplicity and practicality, this method can provide results in real time when interharmonics are present. The proposed method can also be applied to more field measurement case studies, and the findings can be used to write a survey of the main interharmonic polluters in today's systems.

Chapter 8

References

[1] W. E. Reid, "Power Quality Issues-Standards and Guidelines", *IEEE Transactions on Industry Applications*, vol. 32, no. 3, May/June 1996.

[2] Dugan, R. C., McGranaghan, M. F., Beaty, H. W., Electrical Power Systems Quality, 1996, McGraw-Hill.

[3] *IEEE Recommended Practices and Requirements for Harmonic Control in Electrical Power Systems,* IEEE Standard 519-1992.

[4] Task Force on Harmonics Modeling and Simulation, "Modeling and Simulation of the Propagation of Harmonics in Electric Power Networks, Part I: Concepts, Models, and Simulation Techniques", *IEEE Transactions on Power Delivery*, vol. 11, no. 1, January 1996.

[5] Arrillaga, J., Neville, R. W., Power System Harmonics, 2nd Edition, 2003, *John Wiley & Sons*.

[6] Nagle, Saff, and Snider, "Fundamentals of Differential Equations", *Addison Wesley Longman*, fifth edition.

[7] IEEE Working Group on Nonsinusoidal Situations: Effects on Meter Performance and Definitions of Power, "Practical Definitions for Powers in Systems with Nonsinusoidal Waveforms and Unbalanced Loads: a Discussion", *IEEE Transactions on Power Delivery*, vol. 11, no. 1, January 1996, pp. 79-101.

[8] IEEE Trial-Use Standard Definitions for the Measurement of Electric Power Quantities under Sinusoidal, Nonsinusoidal, Balanced or Unbalanced Conditions, IEEE Standard 1459-2000.

[9] Wakileh, G. J., Power Systems Harmonics, Fundamentals, Analysis and Filter Design, 2001, *Springer*.

[10] Kimbark, E. W., Direct Current Transmission, vol. 1, 1971, John Wiley & Sons.

[11] Das, J. C., Power System Analysis, Short Circuit Load Flow and Harmonics, 2001, *Marcel Dekker*.

[12] E. F. Fuchs, D. J. Roesler, F. S. Alashhab, “Sensitivity of Electrical Appliances to Harmonics and Fractional Harmonics of the Power System Voltage. Part I: Transformers and Induction Machines”, *IEEE Transactions on Power Delivery*, vol. 2, no. 2, April 1987, pp. 437-444.

[13] E. F. Fuchs, D. J. Roesler, K. P. Kovacs, “Sensitivity of Electrical Appliances to Harmonics and Fractional Harmonics of the Power System Voltage. Part II: Television Sets, Induction Watthour Meters and Universal Machines”, *IEEE Transactions on Power Delivery*, vol 2, no. 2, April 1987. pp. 445-453.

[14] CEI/IEC 1000-2-1, “Electromagnetic Compatibility”, Part 2: Environment, Section 1: Description of the environment – Electromagnetic Environment for Low-Frequency Conducted Disturbances and Signaling in Public Power Supply Systems, 1st ed., 1990.

[15] IEC 61000-2-2, Compatibility Levels for Low-Frequency Conducted Disturbances and Signaling in Public Low-Voltage Power Supply Systems, 2nd ed., 2000.

[16] IEEE Task Force on Harmonics Modeling and Simulation, “Interharmonics: Theory and Measurement”, *IEEE Transactions on Power Delivery*, vol. 22, no. 4, Oct. 2007.

[17] Interharmonic in Power System IEEE Interharmonic Task Force, Cigre 36.05/CIRED2, WG2/UIEPQ/CC02 Voltage Quality Working Group [Online]. Available: http://grouper.ieee.org/groups/harmonic/iharm/docs/

[18] R. Yacamini, “Power System Harmonics: Part 4 Interharmonics”, *IEE Power Engineering Journal*, pp. 185-193, Aug. 1996.

[19] Cigré 36.05/CIRED 2 CCO2 Voltage Quality Working Group and IEEE Interharmonic Task Force, et al., “Interharmonics in Power Systems,” pp.3-8, Jan. 1997.

[20] C. Li and W. Xu, “On the Ambiguity of Defining and Measuring Inter-Harmonics”, *IEEE Power Engineering Review*, July 2001.

[21] M. Hernes, and B. Gustavsen, “Simulation of shaft vibrations due to interaction between turbine-generator train and power electronic converters at the Visund Oil platform,” *Proceedings of the Power Conversion Conference 2002*, vol. 3, pp.1381-1386, Osaka, April 2-5, 2000.

[22] C. Li, W. Xu, T. Tayjasanant, "Interharmonics: Basic Concepts and Techniques for their Detection and Measurement", *Electric Power System Research*, vol. 66, pp. 39-48, July 2001.

[23] S. T. Mak, D. L. Reed, "TWACS, A New Viable Two-Way Automatic Communication System for Distribution Networks. Part I: Outbound Communication", *IEEE Transactions on Power Apparatus and Systems*, PAS-101, no. 8, Aug. 1982, pp. 2941-2949.

[24] A. Mansoor, W. M Grady, A. H. Chowdhury, M. J. Samotyj, "An Investigation of Harmonic Attenuation and Diversity among Distributed Single-Phase Electronic Loads", *IEEE Transactions on Power Delivery,* vol. 10, no. 1, Jan 1995.

[25] J. C. Das, "Passive Filters – Potentialities and Limitations", *IEEE Transactions on Industry Applications*, vol. 40, no. 1, January/February 2004.

[26] D. Bohaichuk, C. Muskens, W. Xu, "Mitigation of Harmonics in Oil Field Electric Systems Using a Centralized Medium Voltage Filter", *Proceedings of the 9th IEEE ICHPQ*, October 2000, pp. 614-618.

[27] C. Muskens, D. Bohaichuk, W. Xu, "Mitigation of Harmonics in Oil Field Electric Systems Using Multiple Low Voltage Filters", *IEEE PES Summer Meeting*, July 2000, pp. 748-752.

[28] C. Kawann, A. E. Emanuel, "Passive Shunt Harmonic Filters for Low and Medium Voltage: a Cost Comparison Study", *IEEE Transactions on Power Systems*, vol. 11, no. 4, November 1996, pp. 1825-1831.

[29] S. Alyasin, S. Hoffman, R. Sasaki, "The identification of the true energy savings realized from high efficiency electronic loads", *Proceedings of the IEEE PES T & D*, April 10-15, 1994 pp. 79-85.

[30] A. Domijan, O. Hancock, C. Maytrott, "A study and evaluation of power electronic based adjustable speed motor drives for air conditioners and heat pumps with an example utility case study of the Florida Power and Light Company", *IEEE Transactions on Energy Conversion*, vol. 7, no. 3, Sept. 1992, pp. 396-404.

[31] L. E. Sulfstede, "Applying Power Electronics to Residential HVAC – The Issues", *IEEE Transactions on Industry Applications*, vol. 29, no. 2, March/April 1993, pp. 300-305.

[32] A. M. Jungreis, A. W. Kelley, "Adjustable Speed Drive for Residential Applications", *IEEE Transactions on Industry Applications*, vol. 31, no. 6, Nov./Dec. 1995, pp. 1315-1322.

[33] IEA International Energy Agency, “Cool Appliances – Policy Strategies for Energy Efficient Homes”, 2003.

[34] Compact Fluorescent Lights: What you should know, available online at: http://www.clean.ns.ca/default.asp?mn=1.377.389.391.430.

[35] R. R. Verberder, O. C. Morse, W. R. Alling, “Harmonics from Compact Fluorescent Lamps”, *IEEE Transactions on Industry Applications*, vol. 29, no. 3, May 1993, pp. 670-674.

[36] NEMA, CFL Share of Household Lamps Reaches New High, Nov. 10, 2008, available online on January 23, 2009 at: http://www.nema.org/media/pr/20081110a.cfm

[37] D. J. Pileggi, E. M. Gulachenski, C. E. Root, T. J. Gentile, A. E. Emanuel, “The Effect of Modern Compact Fluorescent Lights on Voltage Distortion”, *IEEE Transactions on Power Delivery*, vol. 8, no. 3, July 1993, pp. 1451-1459.

[38] R. Dwyer, A. K. Khan, M. McGranaghan, L. Tang, R. K. McCluskey, R. Sung, T. Houy, “Evaluation of Harmonic Impacts from Compact Fluorescent Lights on Distribution Systems”, *IEEE Transactions on Power Systems*, vol. 10, no. 4, Nov. 1995, pp. 1772-1779.

[39] A. E. Emanuel, J. A. Orr, D. Cyganski, E. M. Gulachenski, “A Survey of Harmonic Voltages and Currents at the Customer’s Bus”, *IEEE Transactions on Power Delivery*, vol. 8, no. 1, Jan 1993, pp. 411-421.

[40] A. E. Emanuel, J. Janczak, D. J. Pileggi, E. M. Gulachenski, C. E. Root, M. Breen, T. J. Gentile, “Voltage Distortion in Distribution Feeders with Nonlinear Loads”, *IEEE Transactions on Power Delivery*, vol. 9, no. 1, Jan 1994, pp. 79-87.

[41] N. Browne, S. Perera, P. F. Ribeiro, “Harmonic Levels and Television Events”, *Proceedings of the IEEE PES General Meeting 2007*, June 24-28, 2007.

[42] V. Katic, B. Dumnic, S. Mujovic, J. Radovic, “Effects of Low Power Electronics & Computer Equipment on Power Quality at Distribution Grid-Measurements and Forecast, *Proceedings of the IEEE International Conference on Industrial Technology,* 2004, pp. 585-589.

[43] T. Rasmussen, K. Gaffney, R. Rubin, “Illuminating Current CFL Usage Patterns: Results from a CFL Metering Study”, *International Energy Efficiency in Domestic Appliances & Lighting Conference ‘06*, EEDAL’06, 21-23 June 2006, London.

[44] E. Swan, RLW Analytics, “What Type of Appliances and Lighting are being used in California Residences?”, California Lighting and Appliance Efficiency

Saturation Study (CLASS), Available at: www.calmac.org/events/CLASS-05_CALMAC_Presentation.ppt

[45] Z. Wei, N. R. Watson, L. P. Frater, "Modeling of Compact Fluorescent Lamps", *Proceedings of the IEEE ICHQP 2008*, Wollongong, Australia, Sept 28- Oct 1 2008.

[46] Statistics Canada, Selected dwelling characteristics and household equipment, available online at: http://www40.statcan.gc.ca/l01/cst01/famil09b-eng.htm.

[47] R. Yacamini, "Power System Harmonics. Part 1. Harmonic Sources.", *Power Engineering Journal*, vol. 8, no. 4, Aug. 1994, pp. 193-198.

[48] Y. G. Hegazy, M. M A. Salama, "Calculations of Diversified Harmonic Currents in Electric Distribution Systems", *IEE Proceedings Generation and Distribution*, vol. 150, no. 6, November 2003, pp. 651-658.

[49] A. Mansoor, W. M. Grady, P. T. Staats, R. S. Thallam, M. T. Doyle, and M. J. Samotyj, "Predicting the Net Harmonic Currents Produced by Large Numbers of Distributed Single-Phase Computer Loads", *IEEE Transactions on Power Delivery*, vol. 10, no. 4, Oct. 1995, pp. 2001-2006.

[50] E. F. El-Saadany, M. M. A. Salama, "Reduction of the Net Harmonic Current Produced by Single-Phase Non-Linear Loads due to Attenuation and Diversity Effects", *Electrical Power & Energy Systems*, vol. 20, no. 4, pp. 259-268, 1998.

[51] E. E. Ahmed, "Assessment of Harmonic Distortions for Systems with Distributed Harmonic Sources", Ph.D. Thesis, University of Alberta, 2003.

[52] A. Prudenzi, U. Grasselli, "IEC Std. 61000-3-2 Harmonic Current Emission Limits in Practical Systems: Need of Considering Loading Level and Attenuation Effects", *IEEE PES Summer Meeting 2001*, pp. 277-282.

[53] A. Testa, R. Langella, "Harmonic Pollution in Italian Distribution Networks in Coincidence with Important Sport Events", *IEEE Power Engineering Society General Meeting*, June 24-28, 2007.

[54] M-T. Chen, C-M. Fu, "Characteristics of Fluorescent Lamps under Abnormal System Voltage Conditions", *Electric Power System Research*, no. 41, 1997, pp.99-107.

[55] A. B. Nassif, J. Acharya, "An Investigation on the Harmonic Attenuation Effect of Modern Compact Fluorescent Lamps, *Proceedings of the ICHQP 2008*, Sept 28-Oct 1, 2008.

[56] A. B. Nassif, W. Xu, "Characterizing the Harmonic Attenuation Effect of Compact Fluorescent Lamps", *IEEE Transactions on Power Delivery*, vol. 24, no. 3, July 2009, pp. 1748-1749.

[57] A. Mansoor, W. M. Grady, R. S. Thallam, M. T. Doyle, S. D. Krein, M. J. Samotyj, "Effect of the Supply Voltage Harmonics on the Input Current of Single-Phase Diode Bridge Rectifier Loads", *IEEE Trans Power Delivery*, vol. 10, no. 3, July 1995, pp. 1416-1422.

[58] R. Arseneau, M. Ouellette, "The Effects of Supply Harmonics on the Performance of Compact Fluorescent Lamps", *IEEE Transactions on Power Delivery,* vol. 8, no. 2, April 1993, pp. 473-479.

[59] P. S. Knight, "Electrical Code Simplified – House Wiring Guide", Based on the 20^{th} edition of the Canadian Electrical Code, Book 1 (2006-2010).

[60] D. O. Koval, C. Carter, "Power Quality Characteristics of Computer Loads", *IEEE Transactions on Industry Applications*, vol. 33, no. 3, May/June 1997, pp. 613-621.

[61] J. Yong, A. B. Nassif, W. Xu, "A Frequency-Domain Harmonic Model for Compact Fluorescent Lamps", *IEEE Transactions on Power Delivery*, submitted for publication.

[62] T. M. Gruzs, "A Survey of Neutral Currents in Three-Phase Computer Power Systems", *IEEE Transactions on Industry Applications*, vol. 26, no. 4, July/August 1990, pp. 719-725.

[63] E. Embriz-Santander, A. Domijan, C. W. Williams, "A Comprehensive Harmonic Study of Electronic Ballasts and their Effect on a Utility's 12kV, 10MVA Feeder", *IEEE Trans. Power Delivery*, vol. 10, no. 3, July 1995, pp. 1591-1599

[64] P. N. Korovesis, G. A. Vokas, I. F. Gonos, F. V. Topalis, "Influence of Large-Scale Installation of Energy Saving Lamps on the Line Voltage Distortion of a Weak Network Supplied by Photovoltaic Station", *IEEE Transactions on Power Delivery*, vol. 19, no. 4, Oct 2004, pp. 1787-1793.

[65] J. C. Sola, M. Salichs, "Study and Characterization of Waveforms from Low-Watt (<25 W) Compact Fluorescent Lamps with Electronic Ballasts", *IEEE Transactions on Power Delivery*, vol. 22, no. 4, Oct 2007, pp. 2305-2311.

[66] J. G. Mayordomo, L. F. Beites, R. Asensi, F. Orzaez, M. Izzediine, L. Zabala, "A Contribution for Modeling Controlled and Uncontrolled AC/DC Converters in

Harmonic Power Flows", *IEEE Transactions on Power Delivery*, vol. 13, no. 4, Oct 1998, pp. 1501-1508.

[67] Y. Sun, G. Zhang, W. Xu, J. Mayordomo, "A Harmonically Coupled Admittance Matrix Model for AC/DC Converters", *IEEE Transactions on Power Systems*, vol. 22, no. 4, Nov 2007, pp. 1574-1582.

[68] M. Fauri, "Harmonic Modelling of Non-Linear Load by means of Crossed Frequency Admittance Matrix", *IEEE Transactions on. Power Systems*, vol. 12, no. 4, Nov 1997, pp. 1632-1638.

[69] E. Thunberg, L. Soder, "A Norton Approach to Distribution Network Modeling for Harmonic Studies", *IEEE Transactions on Power Delivery*, vol. 14, no. 1, Jan 1999, pp. 272-277.

[70] R. A. Johnson, G. K. Bhattacharyya, "Statistics: Principles and Methods", 5th Ed. New York, John Wiley, 2005.

[71] T. X. Zhu, "Exact Harmonics/Interharmonics Calculation Using Adaptive Windows Width", *IEEE Transactions on Power Delivery*, vol. 22, no. 4, October 2007, pp. 2279-2288.

[72] M. K. Ghartemani, M. R. Iravani, "Measurement of Harmonics/Interharmonics of Time-Varying Frequencies", *IEEE Transactions on Power Delivery*, vol. 20, no. 1, January 2005, pp. 23-31.

[73] Z. Liu, J. Himmel, K. W. Bonfig, "Improved Processing of Harmonics and Interharmonics by Time-Domain Averaging", *IEEE Transactions on Power Delivery*, vol. 20, no. 4, October 2005, pp. 2370-2380.

[74] T. Tarasiuk, "Hybrid Wavelet-Fourier Spectrum Analysis", *IEEE Transactions on Power Delivery*, vol. 19, no. 3, July 2004, pp. 957-964.

[75] T. Tayjasanant, W. Xu, "A Case Study of Flicker/Interharmonic Problems Caused by a Variable Frequency Drive", in *Proceedings of the ICHQP 2004*, Lake Placid, NY, Sept. 12-15, 2004, pp. 72-76.

[76] T. Kim, E. J. Powers, W. M. Grady, A. Arapostathis, "Real and Reactive Power Analysis for Interharmonics", *IEEE Electric Ship Technologies Symposium 2005*, pp. 244-247.

[77] A. M. Dan, "Identification of a flicker source," in *Proceedings of the ICHQP 1998*, Athens, Greece, Oct. 14-16, 1998, pp. 1179-1181.

[78] P. G. V. Axelberg, M. J. Bollen, "An Algorithm for Determining the Direction to a Flicker Source", *IEEE Transactions on Power Delivery*, vol. 21, no. 2, April 2006, pp. 755-760.

[79] P. G. V. Axelberg, M. J. Bollen, I. Y. Gu "Trace of Flicker Sources by Using the Quantity of Flicker Power", *IEEE Transactions on Power Delivery*, vol. 23, no. 1, January 2008, pp. 465-471.

[80] M. B. Rifai, T. H. Ortmeyer, W. J. McQuillan, "Evaluation of Current Interharmonics from AC Drives", *IEEE Transactions on Power Delivery*, vol. 15, no. 3, July 2000, pp. 1094-1098.

[81] A. Oppenheim, R. Schafer, J. Buck, "Discrete-Time Signal Processing", *Prentice Hall*, 2nd edition.

[82] C. J. Chou, C. W. Liu, J. Y. Lee, "Optimal Planning of Large Passive-Harmonic-Filters Set at High Voltage Level", *IEEE Transactions on Power Systems*, vol. 15, no. 1, pp. 433-441, Feb. 2000.

[83] Y. P. Chang, C. J. Wu, "Optimal Multi-objective Planning of Large-Scale Passive Harmonic Filters Using Hybrid Differential Evolution Method Considering Parameter and Loading Uncertainty", *IEEE Transactions on Power Delivery*, vol. 20, no. 1, pp. 408-416, Jan. 2005.

[84] A. F. Zobaa, "The Optimal Passive Filters to Minimize Voltage Harmonic Distortion at a Load Bus", *IEEE Transactions on Power Delivery*, vol. 20, no. 2, pp. 1592-1597, Apr. 2005.

[85] G. W. Chang, H. L. Wang, S. Y. Chu, "Strategic Placement and Sizing of Passive Filters in a Power System for Controlling Voltage Distortion", *IEEE Transactions on Power Delivery*, vol. 19, no. 3, pp. 1204-1211, July 2004.

[86] G. W. Chang, S. Y. Chu, H. L. Wang, "A New Method of Passive Harmonic Filter Planning for Controlling Voltage Distortion in a Power System", *IEEE Transactions on Power Delivery*, vol. 21, no. 1, pp. 305-312, Jan. 2006.

[87] Y. Y. Hong, W. F. Huang, "Interactive Multi-objective Passive Filter Planning with Fuzzy Parameters in Distribution Systems Using Genetic Algorithms", *IEEE Transactions on Power Delivery*, vol. 18, no. 3, pp. 1043-1050, July 2003.

[88] X. Yao, "The Method for Designing the Third Order Filter", *Proceedings of the IEEE ICHQP 1998*, Oct. 1998, pp. 139-142.

[89] Y. Xiao, J. Zhao, S. Mao, "Theory for the Design of C-type Filter", *Proceedings of the IEEE ICHQP 2004*, Sept. 2004, pp. 11-15.

[90] *IEEE Standard for Shunt Power Capacitors*, IEEE Standard 18-2002, Oct. 2002.

[91] *IEEE Guide for Application and Specification of Harmonic Filters*, IEEE Standard 1531-2003, Nov. 2003.

[92] J. D. Ainsworth, “Filters, Damping Circuits and Reactive Volt-Amps in HVDC Convertors”, *High-Voltage Direct Current Convertors and Systems*, Macdonald London, chapter 7, 1965.

[93] T. Hiyama, M. S. A. A. Hammam, T. H. Ortmeyer, “Distribution System Modeling with Distributed Harmonic Sources”, *IEEE Transactions on Power Delivery*, vol. 9, no. 4, April 1989, pp. 1297-1304.

[94] T. H. Ortmeyer, T. Hiyama, “Distribution system harmonic filter planning”, *IEEE Transactions on Power Delivery*, vol. 11, no. 4, October 1996, pp. 2005-2012.

[95] J. A. Pomilio, S. M. Deckmann, “Characterization and Compensation of Harmonics and Reactive Power of Residential and Commercial Loads”, *IEEE Transactions on Power Delivery*, vol. 22, no. 2, April 2007, pp. 1049-1055.

Appendix A

Measurement Results of Home Appliances

The appendix presents the data of various home appliances that were referred through this thesis. The data are categorized in four types: lighting loads, computing equipment, home electronics, and household appliances. The home appliances were mainly studied in Chapter 2.

A.1 Data Processing Methods

Measurements were generally conducted for one than one device within the same appliance type. Each device will yield a set of harmonic spectra data. From these data, a representative harmonic characteristic of the devices were derived by using a weighted average of the individual device data according to the following steps:

1. Compute the per-watt (pw) waveform data for each device *i* of the same appliance type:

$$I_{pw-i} = \frac{I_i}{P_i} \tag{A.1}$$

   where P_i is the measured operating power of the device.

2. Average the above per-watt waveform data over the number of devices measured within the same brand:

$$I_{pw-brand-b} = \frac{\sum_{i=1}^{N_{brand}} I_{pw-i}}{N_{brand}} \tag{A.2}$$

where N_{brand} is the number of devices of the same brand

3. Average the above per-watt waveform data over the numbers of brands measured:

$$I_{pw} = \frac{\sum_{b=1}^{B} I_{pw-brand-b}}{B} \tag{A.3}$$

4. Select a representative operating power level for the type of applications whose data is being processed, $P_{typical}$. Some of the representative operating power levels are determined from the survey data and others are based on common sense estimates using the measurement results.

5. The representative harmonic waveform for the type of appliances under study is finalized determined as:

$$I_{appliance} = I_{pw} \times P_{typical} \tag{A.4}$$

The above data have two applications. One is to establish the harmonic current source model, which is obtained by calculating the spectra of the obtained waveforms, for the appliance type. The other application is to compute the Equivalent-CFL and harmonic compatibility indices.

A.2 Lamps (CFLs, Fluorescent tubes and incandescent lamps)

Twelve (12) compact fluorescent lamps commonly available in the Canadian retail stores were selected for investigation. They are all designed to operate at 60Hz, 120V, and have power consumption ratings of 5W to 30W. The lamps are listed in Table A-1. Note that the lamps are assigned with a code for easy identification. These codes were also used in the results of Chapter 4. The lamps' powers are the last two numeric digits of their names and codes.

Table A-1. The twelve measured CFLs

No.	Code	CFL Make/Name
1	CFL P 15	Compact Phillips 15W
2	CFL G 13	Compact Greenlight 13W
3	CFL N 09	Compact NOMA 9W
4	CFL G 23	Compact Globe 23W
5	CFL S 13	Compact Sylvania 13W
6	CFL S 27	Compact Sylvania 27W
7	CFL S 30	Compact Sylvania 30W
8	CFL G 10	Compact GE 10W
9	CFL G 26	Compact GE 26W
10	CFL P 05	Compact Phillips 5W
11	CFL P 27	Compact Phillips 27W
12	CFL P 14	Compact Phillips 14W

The waveform and spectra (which are normalized by the fundamental frequency value) are presented in Table A-2 and Figure A-1.

Table A-2. Detailed harmonic currents [A] absorbed by the measured CFLs

H	CFL P 15	CFL G 13	CFL N 09	CFL G 23	CFL S 13	CFL S 27	CFL S 30	CFL G 10	CFL G 26	CFL P 05	CFL P 27	CFL P 14
1	0.159	0.134	0.095	0.260	0.110	0.288	0.287	0.087	0.271	0.047	0.239	0.131
3	0.127	0.095	0.067	0.172	0.088	0.205	0.207	0.066	0.190	0.037	0.188	0.101
5	0.089	0.061	0.042	0.095	0.064	0.124	0.129	0.044	0.119	0.028	0.133	0.067
7	0.069	0.052	0.034	0.051	0.054	0.079	0.085	0.037	0.102	0.021	0.100	0.057
9	0.050	0.038	0.023	0.028	0.051	0.031	0.037	0.033	0.072	0.016	0.070	0.051
11	0.030	0.019	0.012	0.049	0.041	0.031	0.027	0.023	0.034	0.010	0.038	0.036
13	0.023	0.020	0.010	0.044	0.029	0.036	0.038	0.015	0.032	0.007	0.027	0.024
15	0.019	0.018	0.009	0.039	0.026	0.036	0.036	0.016	0.024	0.005	0.024	0.023
17	0.014	0.010	0.007	0.034	0.027	0.036	0.037	0.013	0.023	0.004	0.021	0.019
19	0.012	0.013	0.009	0.029	0.024	0.028	0.031	0.010	0.026	0.003	0.023	0.014
21	0.013	0.009	0.009	0.027	0.022	0.027	0.027	0.009	0.023	0.004	0.025	0.013
23	0.014	0.014	0.009	0.034	0.022	0.016	0.016	0.007	0.028	0.003	0.027	0.011
25	0.016	0.016	0.011	0.039	0.020	0.015	0.011	0.006	0.029	0.006	0.030	0.008
27	0.017	0.014	0.008	0.034	0.017	0.021	0.016	0.006	0.024	0.004	0.027	0.008
29	0.017	0.015	0.007	0.026	0.017	0.022	0.021	0.005	0.025	0.003	0.022	0.006

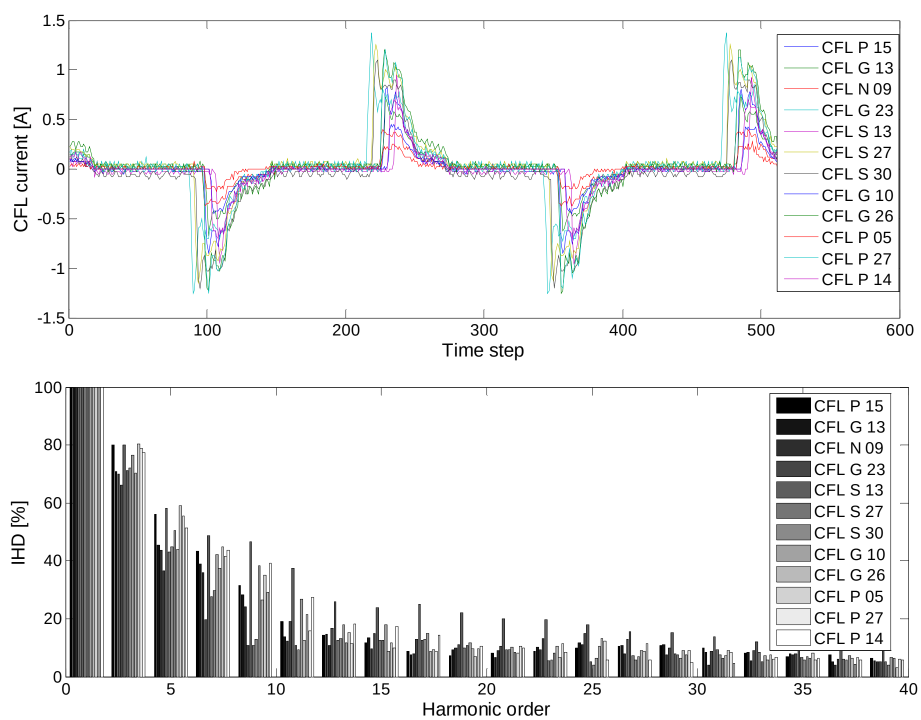

Figure A-1. Waveforms and normalized spectra of the measured CFLs

Figure A-2 shows the representative CFL model.

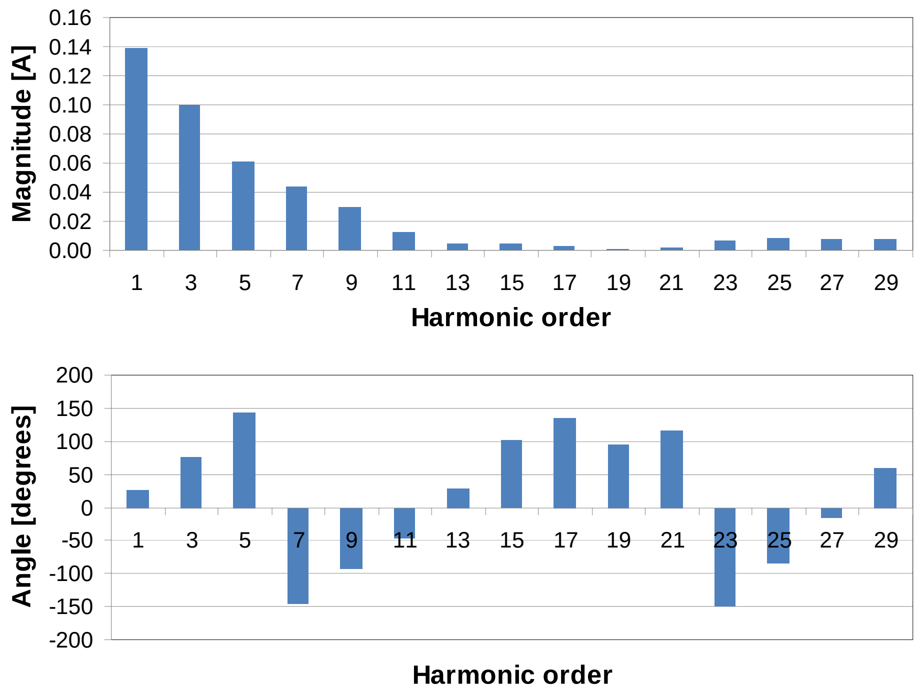

Figure A-2. Harmonic spectra of a representative 15W CFL

The following traditional lamps were selected for measurements:

- Electronic Ballast Tube Phillips cool white 15W – EBc P 15
- Electronic Ballast Tube Phillips ALTO 15W – EBa P 15
- Electronic Ballast Tube Phillips soft white 15W – EBs P 15
- Magnetic Ballast Tube Phillips ALTO 15W – MBa P 15
- Incandescent Phillips 60W – Inc P 60

Table A-3 shows the magnitude characteristics of the five measured lamps. This table also provides information such as THD_I, brand, model and measured input total rms power. The corresponding waveforms and spectra are shown in Figure A-3.

Table A-3. Characteristics of the five measured lamps

Manufacturer	Phillips		Phillips		Phillips		Phillips		Phillips	
Model	EBc P 15		EBa P 15		EBs P 15		MBa P 15		Inc P 60	
Operating Power [W]	17		17		16		33		59	
***THD_I* [%]**	145.36		133.70		138.22		7.86		3.73	
	Mag. [A]	**Angle [deg]**	**Mag. [A]**	**Angle [deg]**	**Mag. [A]**	**Angle [deg]**	**Mag. [A]**	**Angle [deg]**	**Mag. [A]**	**Angle [deg]**

H1	**0.153**	**21.2**	**0.154**	**21.7**	**0.143**	**21.1**	**0.731**	**-67.4**	**0.494**	**-0.05**
H3	0.124	53.9	0.123	56.6	0.117	53.7	0.057	144.0	0.012	-128.9
H5	0.087	105.5	0.088	106.7	0.083	101.5	0.004	178.7	0.011	-162.5
H7	0.069	169.4	0.068	170.2	0.067	165.1	0.005	-131.3	0.003	147.9
H9	0.067	-134.8	0.067	-132.4	0.066	-134.4	0.002	-46.2	0.002	143.3
H11	0.054	-84.2	0.053	-82.7	0.055	-80.1	0.003	-40.9	0.003	-47.4
H13	0.039	-21.8	0.039	-24.0	0.039	-25.3	0.001	18.7	0.002	70.1
H15	0.031	51.1	0.032	49.7	0.025	31.8	0.000	79.3	0.003	-78.4
H17	0.031	118.6	0.032	115.3	0.027	87.4	0.001	90.3	0.001	173.9
H19	0.026	-172.7	0.026	174.5	0.029	165.2	0.001	163.7	0.001	74.4
H21	0.019	-95.7	0.022	-118.1	0.025	-132.6	0.000	163.4	0.002	-112.6
H23	0.024	-31.5	0.023	-52.0	0.015	-87.8	0.001	-42.7	0.001	62.0
H25	0.025	61.8	0.020	14.9	0.023	-19.7	0.001	-56.8	0.001	-44.1
H27	0.025	142.1	0.016	82.3	0.012	37.7	0.001	117.6	0.001	-29.0
H29	0.020	-124.9	0.015	163.1	0.012	77.2	0.002	-7.9	0.001	-38.2

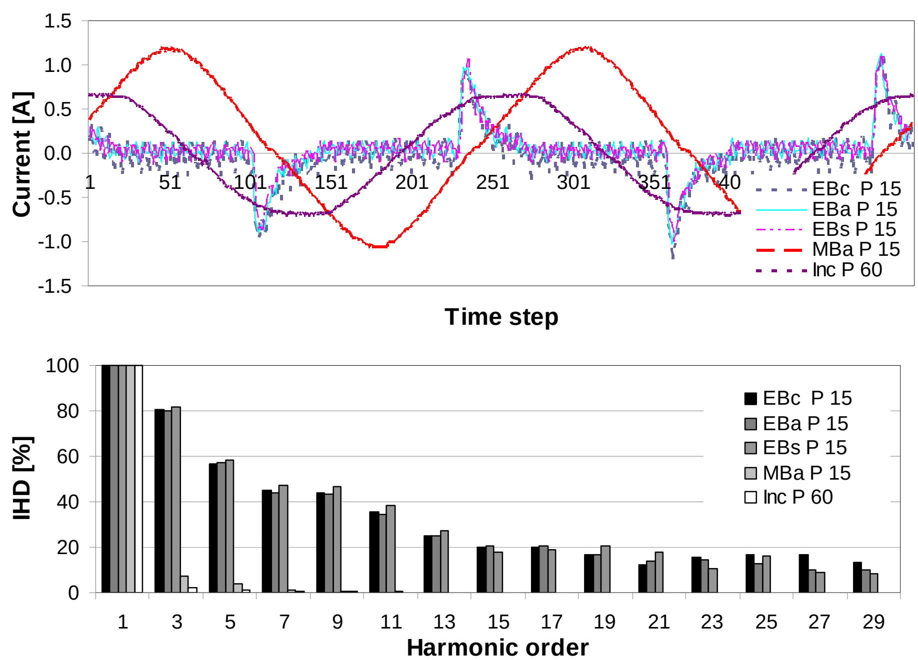

Figure A-3. Measured waveform and spectra of five traditional lamps

A.3 Computing Equipment – Computers and Monitors

Desktop PCs

The following three desktop computers, which were measured for this project, are presented in this section. Results of two PCs are omitted due to high resemblance to the presented results.

- PC1: Intel Core 2 quad with dedicated video card and 4GB ram;
- PC2: Intel Pentium IV HT, with 2 GB ram;
- PC3: Intel Pentium IV, with 1 GB ram.

PCs were measured under many typical conditions (reading DVDs, browsing internet, executing software, idling, etc – gaming and 3D tasks were not recorded). It was observed that, among the recorded conditions, the operating power did not vary significantly. Therefore, a random operating condition was selected to be presented here. Table A-4 presents detailed information of the measured computers. Figure A-4 shows the waveforms and spectra.

Table A-4. Characteristics of three measured PCs

Manufacturer	**HP**		**Acer**		**Dell**		**Model**	
Model	Pavilion a1034n		AM5620-E5301A		Dimension 3100			
Operating Power [W]	94.0		87.7		71.9		100	
***THD_I* [%]**	99.5		106		105		108	
	Mag. [A]	**Angle [deg]**	**Mag. [A]**	**Angle [deg]**	**Mag. [A]**	**Angle [deg]**	**Mag. [A]**	**Angle [deg]**
H1	**0.823**	**0.5**	**0.759**	**4.1**	**0.623**	**9.6**	**0.876**	**4.7**
H3	0.650	1.6	0.633	12.7	0.514	16.1	0.739	10.1
H5	0.407	3.6	0.425	23.5	0.338	28.3	0.513	18.5
H7	0.161	8.6	0.202	42.7	0.157	61.1	0.268	37.5
H9	0.099	58.1	0.033	116.6	0.058	148.0	0.085	107.6
H11	0.120	168.7	0.074	-172.9	0.089	-160.0	0.062	-175.0
H13	0.118	178.0	0.084	-148.5	0.085	-133.0	0.097	-155.0
H15	0.050	-170.2	0.045	-116.5	0.045	-79.7	0.063	-122.0
H17	0.050	-64.8	0.012	-28.2	0.025	10.4	0.029	-148.0
H19	0.070	-17.7	0.038	20.5	0.037	32.2	0.036	131.7
H21	0.041	-7.9	0.036	46.9	0.034	80.5	0.036	159.9
H23	0.025	12.6	0.015	89.4	0.020	145.5	0.023	82.5
H25	0.031	144.6	0.013	166.2	0.023	-154.0	0.014	172.3
H27	0.031	161.6	0.022	-154.7	0.027	-104.0	0.020	-152.0
H29	0.011	171.0	0.017	-127.7	0.018	-75.8	0.019	-130.0

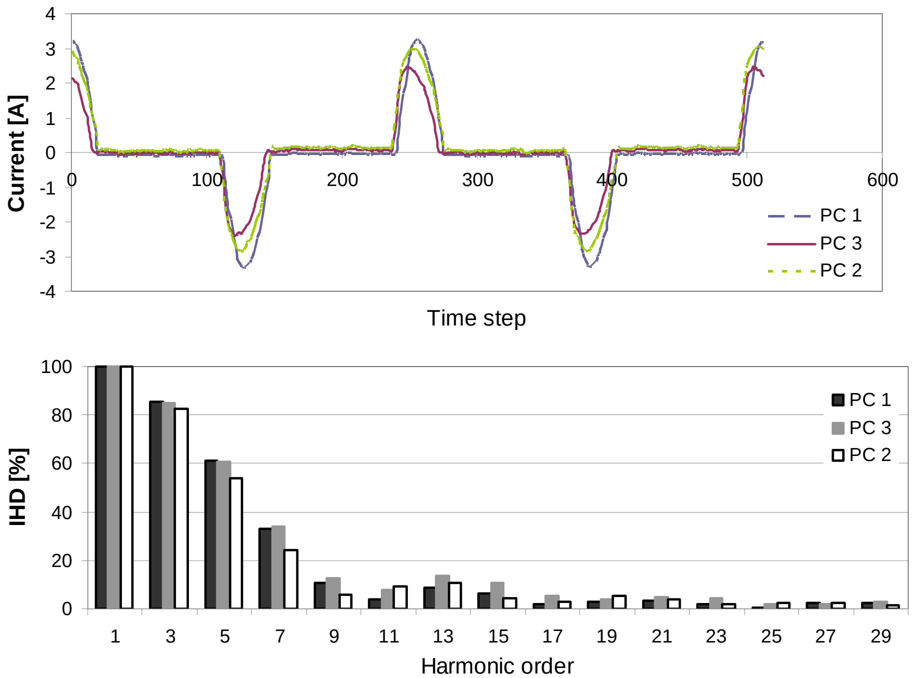

Figure A-4. Measured waveform and spectra of three desktop PCs

Computer LCD Monitors

Three of the five measured LCD monitors are presented in this section. They are:

- 22” wide-screen
- 19” full-screen
- 17” full-screen

Table A-5 shows the characteristics of three devices. Their waveforms and spectra are shown in Figure A-5.

Table A-5. Characteristics of three measured LCD monitors

Manufacturer	**Acer**		**NEC**		**HP**		**Model**	
Model	AL2216W		Multisync 1940CX		F1703			
Operating Power [W]	31.2		24.9		38.8		40	
***THD_I* [%]**	118		104		96		102	
	Mag. [A]	**Angle [deg]**	**Mag. [A]**	**Angle [deg]**	**Mag. [A]**	**Angle [deg]**	**Mag. [A]**	**Angle [deg]**
H1	**0.279**	**14.4**	**0.218**	**15.0**	**0.260**	**16.8**	**0.334**	**15. 4**
H3	0.22975	34.7	0.170239	32.7	0.20115	40.5	0.271	36.0

H5	0.15893	63.5	0.104987	59.6	0.11485	75.9	0.174	66.3
H7	0.09960	108.7	0.051427	103.5	0.04194	135.6	0.084	115.9
H9	0.07275	167.6	0.043937	163.3	0.03515	-156.2	0.044	178.2
H11	0.06833	-141.7	0.047486	-142.5	0.03936	-104.8	0.040	-129.6
H13	0.06523	-105.5	0.040823	-100.7	0.02485	-65.4	0.037	-90.5
H15	0.04662	-59.8	0.023884	-40.6	0.01727	-5.37	0.024	-35.2
H17	0.03141	1.2	0.022469	35.2	0.02560	57.1	0.022	31.2
H19	0.03197	44.0	0.024233	74.9	0.01617	104.9	0.017	74.6
H21	0.02624	88.5	0.017244	117.6	0.01084	151.6	0.011	119.2
H23	0.01825	139.6	0.010277	175.5	0.01437	-138.4	0.013	178.7
H25	0.01160	-167.6	0.010581	-120.6	0.01317	-69.7	0.010	-119.3
H27	0.01076	-97.8	0.011409	-64.4	0.00856	-16.7	0.009	-59.5
H29	0.00945	-55.2	0.007076	4.7	0.00881	69.7	0.008	126.4

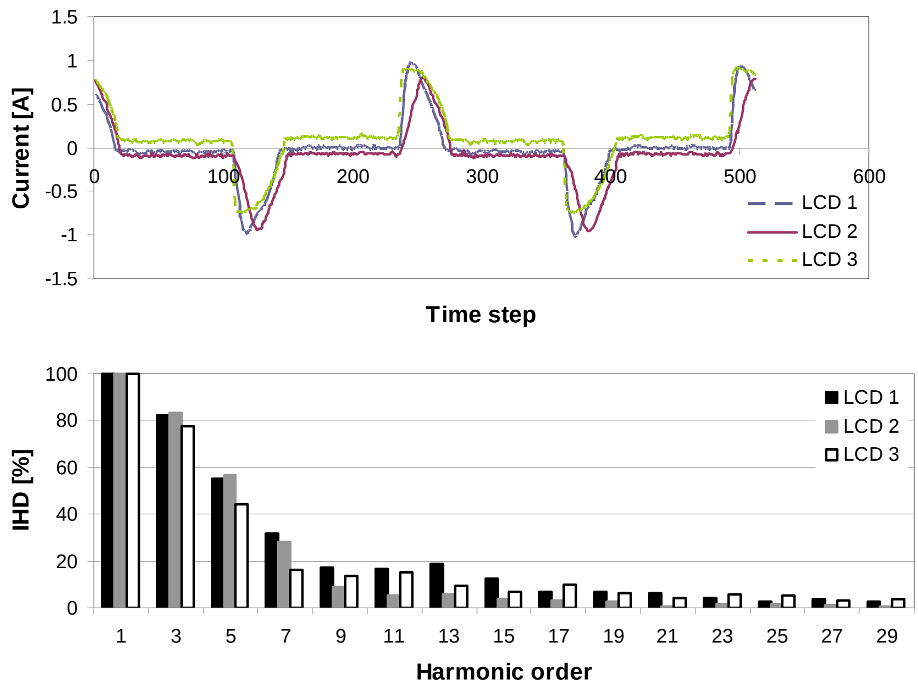

Figure A-5. Measured waveform and spectra of three LCD monitors

Laptop Computers

All the five laptop computers measured for this project can operate in two conditions, as described below. Condition 1 is a condition of higher power consumption, higher harmonic generation, and typically more time in operation. Therefore, the calculated indices were obtained for this condition.

1. Condition 1: turned on and charging;
2. Condition 2: turned off and charging.

Table A-6 shows the characteristics of three measured laptop computers. The current waveforms and normalized spectra are shown in Figure A-6.

Table A-6. Characteristics of three measured laptops

Manufacturer	**IBM**		**IBM**		**Toshiba**		**Model**	
Model	2531-6EU		7664-16U		PSU34C-NS108C			
Condition	On + charging		On + charging		On + charging			
Operating Power [W]	55.5		68.9		70.7		75	
***THD_I* [%]**	127		133		151		136	
	Mag. [A]	**Angle [deg]**	**Mag. [A]**	**Angle [deg]**	**Mag. [A]**	**Angle [deg]**	**Mag. [A]**	**Angle [deg]**
H1	**0.496**	**16.2**	**0.614**	**16.4**	**0.647**	**20.6**	**0.675**	**17.7**
H3	0.3970	47.1	0.5016	51.6	0.5122	65.7	0.542	54.8
H5	0.2559	89.1	0.3427	97.6	0.3456	125.5	0.362	104.1
H7	0.1730	154.1	0.2527	161.9	0.2922	-158.1	0.273	172.6
H9	0.1715	-135.9	0.2504	-136.4	0.3128	-92.4	0.279	-121.5
H11	0.1775	-82.9	0.2402	-86.5	0.2983	-34.2	0.273	-67.9
H13	0.1490	-37.4	0.1971	-36.9	0.2637	27.3	0.232	-135.7
H15	0.1237	21.3	0.1564	20.4	0.2448	90.4	0.199	44.1
H17	0.1156	77.4	0.1354	78.0	0.2251	150.3	0.181	101.9
H19	0.0947	134.0	0.1101	131.9	0.1920	-149.1	0.151	158.9
H21	0.0808	-171.7	0.0831	-169.5	0.1638	-84.8	0.124	-142.0
H23	0.0671	-110.1	0.0671	-105.0	0.1454	-21.8	0.106	-78.9
H25	0.0630	-50.6	0.0599	-43.9	0.1228	38.9	0.094	-138.5
H27	0.0554	6.11	0.0464	13.5	0.0974	102.4	0.076	40.6
H29	0.0428	68.3	0.0349	83.4	0.0785	168.2	0.060	106.6

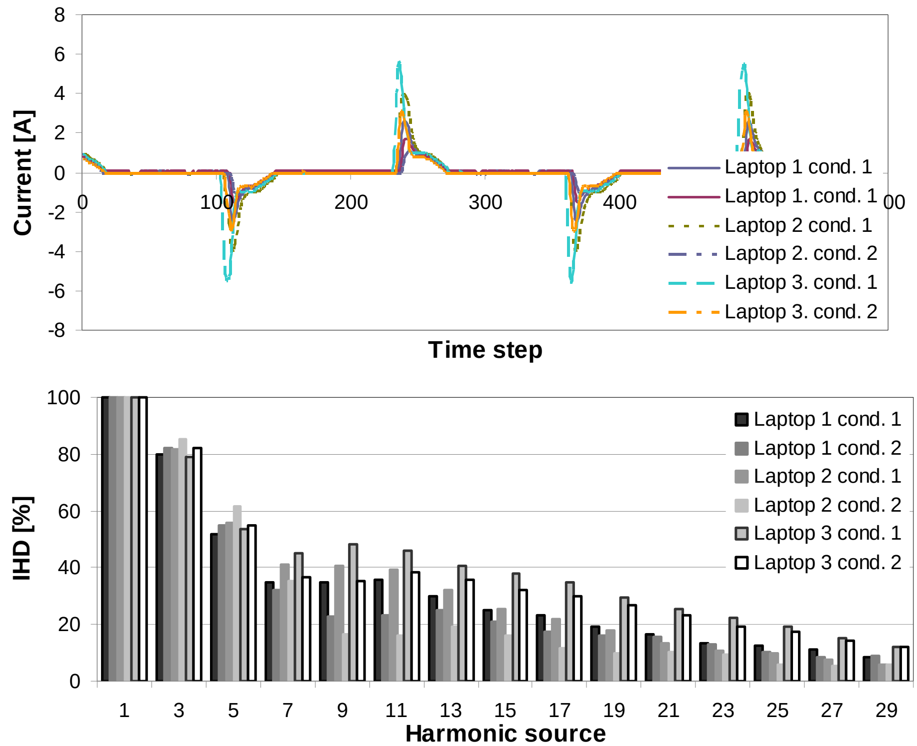

Figure A-6. Measured waveform and spectra of three laptops operating in two conditions

A.4 Home Electronics – TVs and Microwaves

High-Definition LCD Television Sets

There is a variety of TVs available in the market today, e.g. LCD, Plasma, and CRT. All technologies are available in different resolutions (from 480i to 1080p). LCD TVs were measured because they are becoming the most popular technology in the Canadian market nowadays. Three of the measured LCD HDTVs are listed below, and their waveforms are presented in Figure A-7 and Table A-7. It was observed that their operating power almost does not change as the TV operates continuously, and therefore a random condition was chosen for analysis.

1. 26” 720p LCD HDTV
2. 42” 1080i LCD HDTV
3. 52” 1080p LCD HDTV

Table A-7. Characteristics of three measured TVs

Manufacturer	**Insigna**		**SamSung**		**Sony**		**Model**	
Model	NSLCD26F		LNS4051DX/XAA		KDL-46s3000			
Operating Power [W]	95.3		207		293		300	
***THD_I* [%]**	6.24		5.27		10.61		7	
	Mag. [A]	**Angle [deg]**	**Mag. [A]**	**Angle [deg]**	**Mag. [A]**	**Angle [deg]**	**Mag. [A]**	**Angle [deg]**
H1	**0.797**	**4.0**	**1.74**	**9.5**	**2.64604**	**6.1**	**2.581**	**6.5**
H3	0.02653	-22.2	0.06681	47.4	0.21846	51.4	0.135	25.5
H5	0.01904	-155.6	0.05446	-133.5	0.15621	-150.2	0.100	-146.4
H7	0.01705	-24.3	0.01983	-161.9	0.04589	-172.9	0.043	-119.7
H9	0.02159	-148.5	0.00522	-92.0	0.01823	3.1	0.031	160.9
H11	0.00367	3.75	0.00522	26.6	0.02096	14.4	0.014	14.9
H13	0.00853	-162.0	0.00348	175.6	0.02759	179.7	0.020	-175.5
H15	0.00892	56.2	0.00400	25.5	0.02994	3.5	0.022	28.4
H17	0.00167	146.7	0.00331	-147.6	0.01613	-168.3	0.009	-176.3
H19	0.00327	40.5	0.00679	10.2	0.00672	-31.4	0.009	126.4
H21	0.00526	-61.4	0.00974	-73.2	0.00834	-143.1	0.013	-92.6
H23	0.00446	-99.3	0.00679	34.8	0.00742	9.1	0.010	101.5
H25	0.00223	-81.6	0.00383	-79.8	0.00294	152.4	0.005	-123.0
H27	0.00279	148.3	0.00539	-178.8	0.00845	59.0	0.008	129.5
H29	0.00422	124.0	0.00226	-146.5	0.00900	-89.5	0.009	-157.3

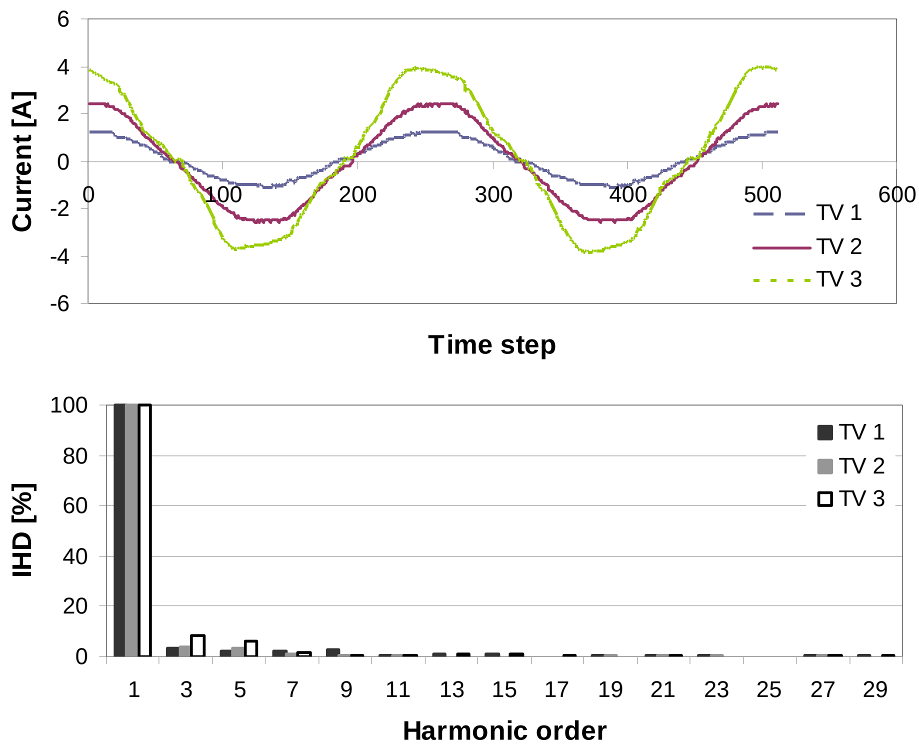

Figure A-7. Measured waveform and spectra of three LCD HDTVs

Standard-Definition CRT Television Sets

One CRT TV was measured for obtaining the results presented in Chapter 2. The production of CRT TVs is currently being superseded by the production of TVs of newer technologies, such as Plasma, LCD and LED. This device was studied because it is still in use in many typical residences, but it is likely that it will no longer be available in the future. The waveform and spectrum information for a 20” model are presented in Figure A-8 and Table A-8, respectively.

Table A-8. Characteristics of the CRT TV

Manufacturer	Venture	
Model	Q2035A	
Operating Power [W]	48.5	
***THD_I* [%]**	145.80	
	Mag. [A]	**Angle [deg]**
H1	**0.398**	**5.2**
H3	0.356	10.8

H5	0.309	18.4
H7	0.246	26.0
H9	0.184	33.5
H11	0.123	43.1
H13	0.066	55.2
H15	0.022	81.1
H17	0.011	-174.5
H19	0.022	-136.2
H21	0.024	-118.5
H23	0.018	-112.9
H25	0.008	-101.1
H27	0.001	-112.5
H29	0.007	84.6

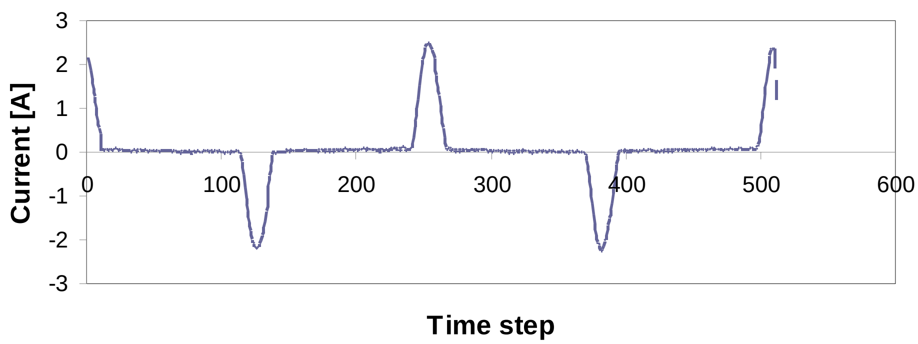

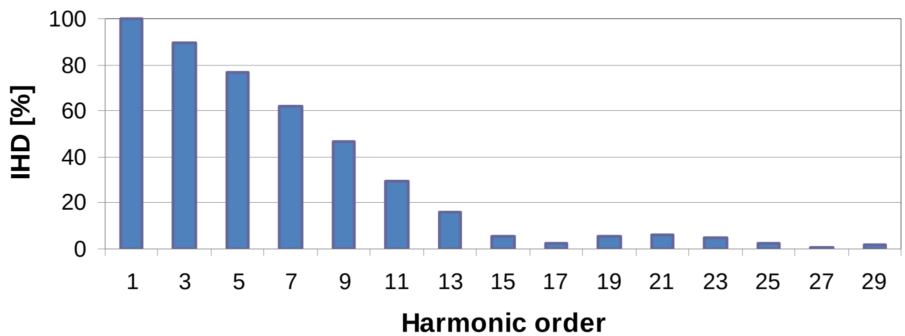

Figure A-8. Measured waveform and spectra of the CRT TV

Microwave Ovens

During the measurement of microwave ovens, it was observed that they exhibit primarily two states: on and off. What makes a difference among the different power levels is the time they are on; for example, when they are performing at 100%, their magnetron is on all the time; for lower power levels, the time when the magnetron operates is adequately timed. Three microwave ovens were measured. Table A-9 shows the characteristics of two of them, and Figure A-9 shows their waveform and spectra.

Table A-9. Characteristics of two measured microwave ovens

Manufacturer	**Danby**		**GoldStar**		**Model**	
Model	DMW607W		N/A			
Condition	100%		100%			
Operating Power [W]	1097		999		1200	
***THD_I* [%]**	41.3		26.6		34	
	Mag. [A]	**Angle [deg]**	**Mag. [A]**	**Angle [deg]**	**Mag. [A]**	**Angle [deg]**
H1	**9.77**	**-11.4**	**8.57**	**0.7**	**10.492**	**-5.3**
H3	3.8082	43.4	2.09667	39.8	3.342	41.6
H5	1.1299	-72.6	0.75230	-64.1	1.070	-68.3
H7	0.4174	156.3	0.36587	132.3	0.448	144.3
H9	0.2571	85.0	0.18593	50.9	0.252	68.0
H11	0.1310	-4.9	0.12510	-63.9	0.147	-34.4
H13	0.0714	-102.8	0.07969	-167.0	0.087	-134.9
H15	0.0606	-169.2	0.05227	98.1	0.065	-35.5
H17	0.0371	75.1	0.04541	-4.4	0.048	35.3
H19	0.0411	-21.1	0.03427	-121.2	0.043	-71.1
H21	0.0391	-123.4	0.02656	133.9	0.037	5.3
H23	0.0332	131.8	0.02228	30.0	0.032	80.9
H25	0.0303	50.9	0.02056	-75.4	0.029	-12.2
H27	0.0283	-42.6	0.01971	179.0	0.027	68.2
H29	0.0254	-138.3	0.01457	70.6	0.023	-33.8

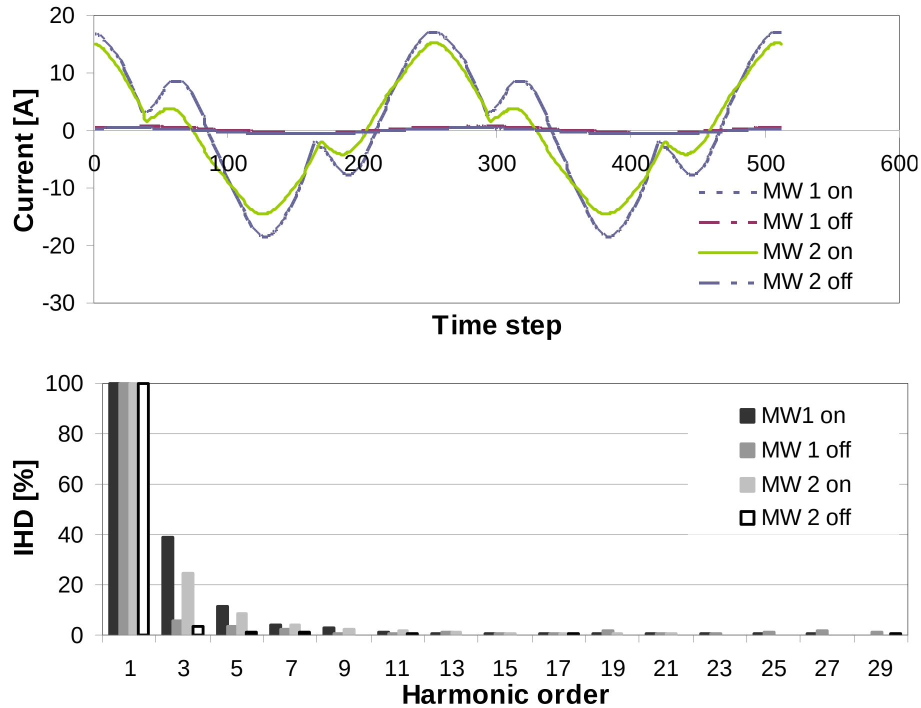

Figure A-9. Measured waveform and spectra of two microwave ovens over two duty cycles

A.5 Household Appliances – Fridges, Washers, Dryers and Furnace

ASD-Driven Refrigerators

Three ASD-based high-end refrigerators were measured. They were measured for over 6 hours in order to capture their whole operating cycle. It was observed that they show typically 4-5 duty cycles, and that they repeat every 2-3 hour periods when no human interaction with the device exists. Table A-10 shows the characteristics of the three measured refrigerators. Their waveforms and normalized spectra are shown in Figure A-10.

Table A-10. Characteristics of three ASD-based measured fridges

Manufacturer	**LG 1**		**LG 2**		**Whirlpool**		**Model**	
Model	LFX25960ST		LFC22760ST		GX5SHTXTS			
Condition	100%		100%		100%			
Operating Power [W]	1100		1300		1100		1200	
***THD_I* [%]**	5.8		6.5		7.19		6.3	
	Mag. [A]	**Angle [deg]**	**Mag. [A]**	**Angle [deg]**	**Mag. [A]**	**Angle [deg]**	**Mag. [A]**	**Angle [deg]**
H1	**2.32**	**-7.0**	**2.27**	**-0.9**	**2.95**	**-12.0**	**2.27**	**-0.9**
H3	0.09	-131.3	0.08	-118.2	0.14	-128.6	0.08	-118.2
H5	0.06	-131.1	0.12	-134.6	0.07	-123.2	0.12	-134.6
H7	0.08	64.4	0.06	100.8	0.11	97.2	0.06	100.8
H9	0.02	-3.0	0.01	172.2	0.03	54.5	0.01	172.2
H11	0.01	-88.5	0.01	-101.9	0.01	45.6	0.01	-101.9
H13	0.03	-4.2	0.01	51.6	0.03	64.4	0.01	51.6
H15	0.01	-51.5	0.01	-111.0	0.01	71.9	0.01	-111.0
H17	0.00	-44.6	0.00	-13.4	0.01	137.5	0.00	-13.4
H19	0.00	1.2	0.01	167.9	0.01	147.9	0.01	167.9
H21	0.00	-12.9	0.01	-41.5	0.01	165.4	0.01	-41.5
H23	0.00	32.52	0.00	124.5	0.01	176.0	0.00	124.5
H25	0.00	-55.8	0.01	-99.5	0.00	-154.5	0.01	-99.5
H27	0.00	52.6	0.00	93.0	0.00	-113.3	0.00	93.0
H29	0.00	47.9	0.00	-149.5	0.00	-50.7	0.00	-149.5

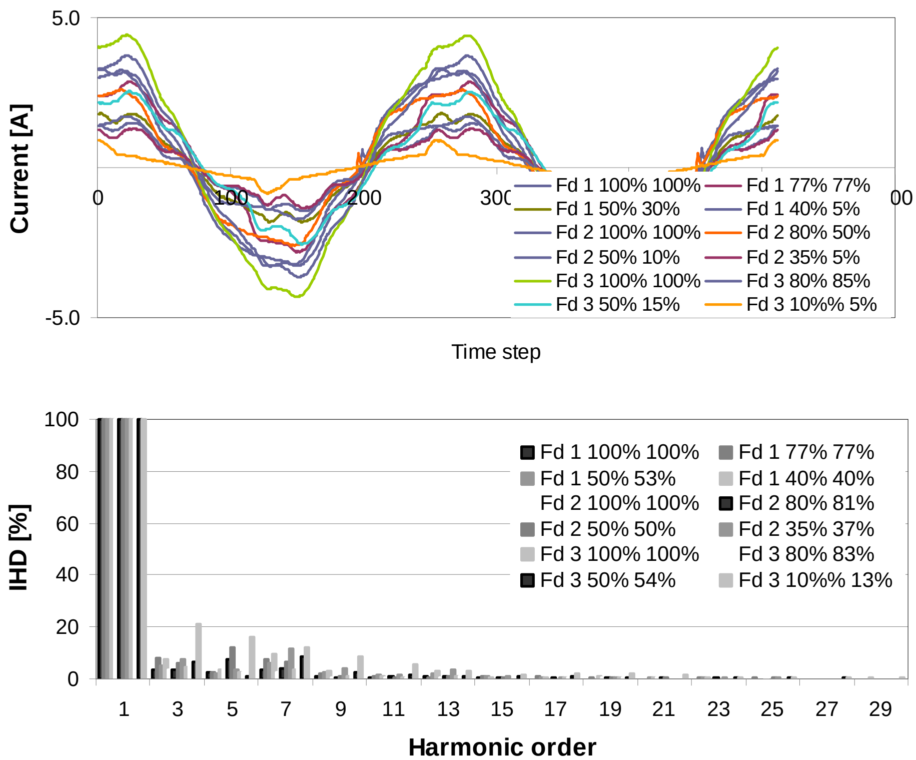

Figure A-10. Measured waveform and spectra of three refrigerators operating in 4 conditions

Regular Refrigerators

Sample results of one of the measured regular refrigerators are presented in this subsection. The regular refrigerators are, however, will be reduced in production to give place to the newer technology ASD-based refrigerators [30]-[32]. Today, they still represent the majority of refrigerator loads in most typical customers.

Regular refrigerators were observed to have only two states: "on" and "off". Normally, they are "off" about 2/3 of the times [95]. Table A-11 and Figure A-11 show the harmonic characteristics and waveforms and normalized spectra of one sample unit of this appliance type, respectively.

It was expected that this kind of load would not exhibit significant current distortion. Figure A-11 also presents the voltage of this waveform to show that the current distortion is not caused by the applied voltage.

Table A-11. Characteristics of the regular fridge

Manufacturer	**GE**	
Model	GTM14XETACS	
Condition	100%	
Operating Power [W]	150	
***THD_I* [%]**	18	
	Mag. [A]	**Angle [deg]**
H1	**1.275**	**-19.7**
H3	0.060	-131.6
H5	0.170	173.5
H7	0.076	34.4
H9	0.007	5.0
H11	0.034	-129.0
H13	0.022	76.0
H15	0.004	145.1
H17	0.012	-37.9
H19	0.007	146.0
H21	0.002	-155.3
H23	0.004	34.4
H25	0.002	-126.1
H27	0.001	-100.6
H29	0.002	179.2

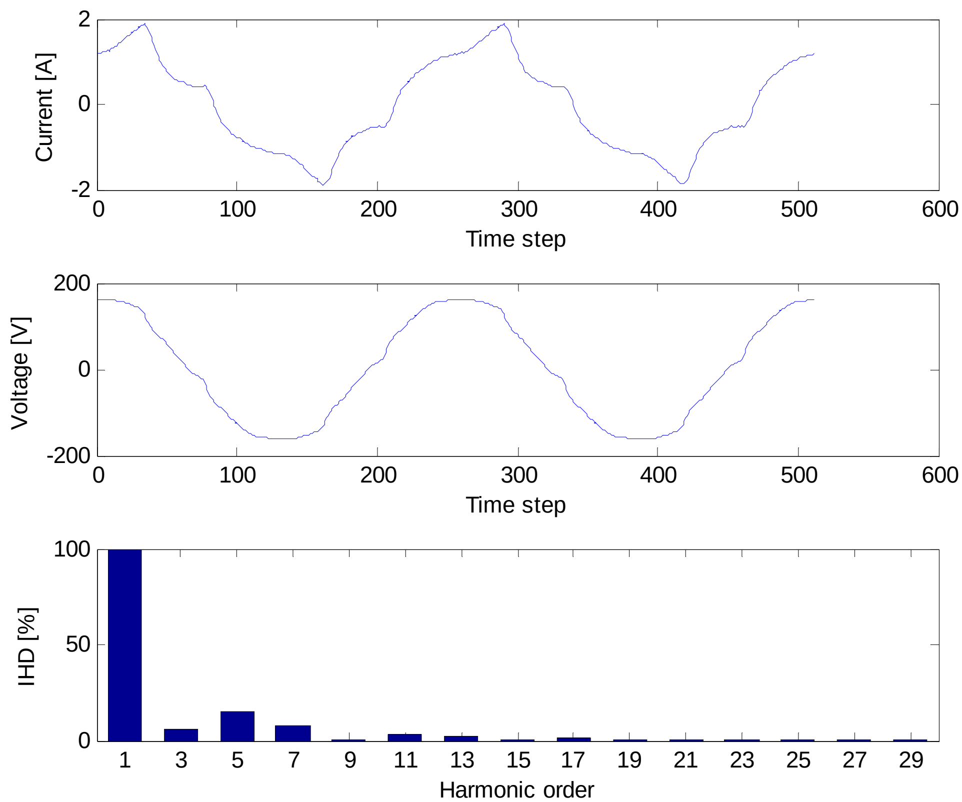

Figure A-11. Measured waveform and spectra of the regular refrigerator

ASD-Driven Laundry Washers

Among the two measured ASD-driven washers, one of them is presented in this section as representative. It has been measured in different operating conditions: filling water, washing, rinsing, rinsing off, spinning, and fast spinning. It has been observed that the "rinsing" condition is the one that consumes the highest amount of power and it is as well the condition where the highest amount of harmonics is injected. The measured waveforms and normalized spectra are shown in Figure A-12, and Table A-12 shows the characteristics of one measured washer.

Table A-12. Characteristics of the measured washer

Manufacturer	**SamSung**
Model	P801
Condition	**Rinsing**
Operating Power [W]	189
***THD_I* [%]**	75.4

	Mag. [A]	Angle [deg]
H1	**2.31**	**-63. 6**
H3	1.5377	164.5
H5	0.5284	19.2
H7	0.2892	126.1
H9	0.3796	-19.7
H11	0.1176	174.3
H13	0.1795	-76.5
H15	0.1918	147.5
H17	0.0418	-91.1
H19	0.1222	88.6
H21	0.1051	-41.1
H23	0.0213	25.6
H25	0.0818	-101.9
H27	0.0566	-63.5
H29	0.0187	164.4

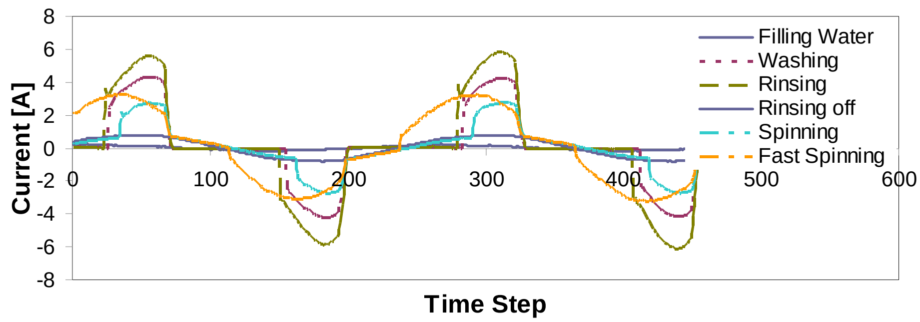

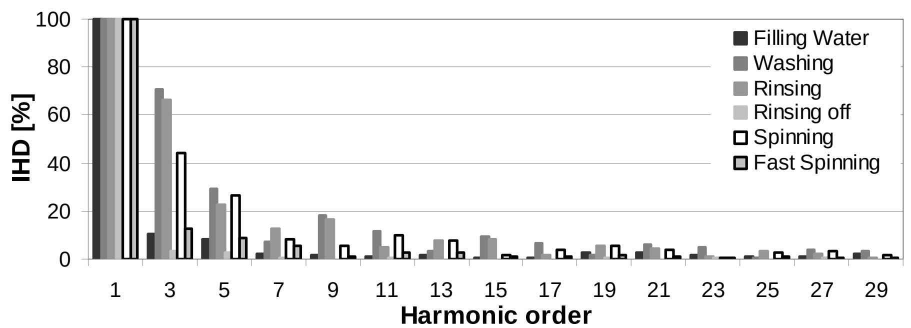

Figure A-12. Measured waveform and spectra of the washer operating at 6 different cycles

ASD-Driven Laundry Dryers

Table A-13 shows the characteristics of an ASD-based laundry dryer. Figure A-13 shows the waveform and normalized spectra results. The input voltage for the dryer is 240V, for this device is connected between the two hot conductors of the single-phase distribution transformers typically used in North America.

Table A-13. Characteristics of the ASD-based laundry dryer

Manufacturer	**LG**	
Model	DLEV833W	
Operating Power [W]	3600	
Condition	53%	
THD_I **[%]**	1.55	
	Mag. [A]	**Angle [deg]**
H1	**4.235**	**-168.5**
H3	1.293	-65.7
H5	1.141	11.2
H7	0.988	88.2
H9	0.796	166.8
H11	0.590	-113.4
H13	0.415	-30.2
H15	0.259	57.7
H17	0.163	155.0
H19	0.120	-96.3
H21	0.104	8.3
H23	0.091	101.5
H25	0.070	-169.9
H27	0.044	-78.7
H29	0.023	32.8

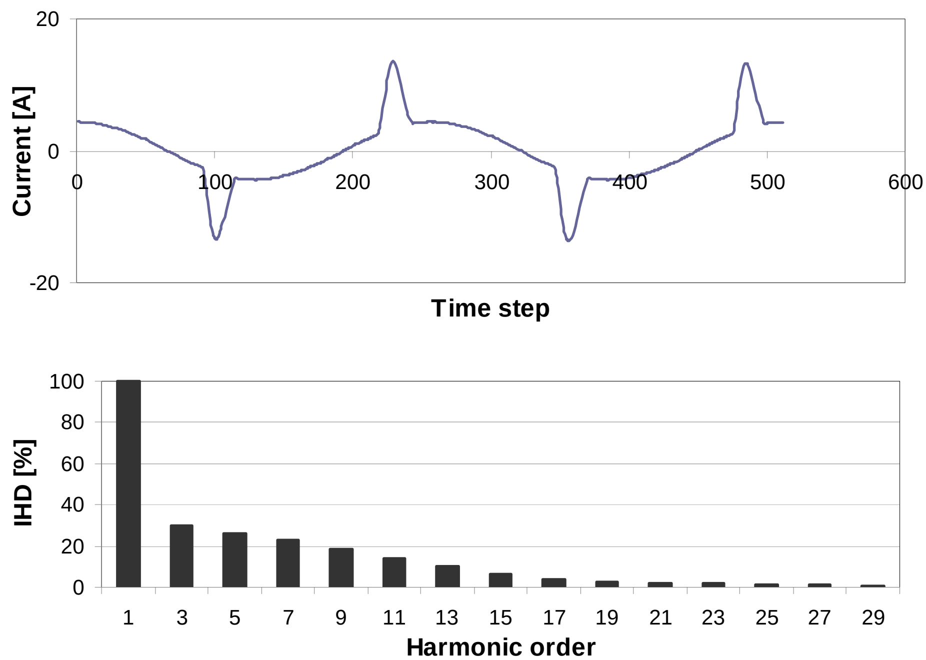

Figure A-13. Measured waveform and spectra of the ASD-based laundry dryer

Regular Laundry Dryers

Table A-14 shows the characteristics of two measured dryers. For washer 1, we were unable to record the voltages, and therefore the current phase angle is unavailable as well. As a consequence, only the phase angles of washer 2 were used. Figure A-14 shows the waveform and normalized spectra results for two measured dryers. Differently from the ASD-based case, the regular dryers do not have an ASD, and no significant harmonics were noticed in their measurements.

Table A-14. Characteristics of two measured dryers

Manufacturer	**GE**		**GE**		**Model**	
Model	PSXH43		PVXR363ED			
Operating Power [W]	3600		4180		4500	
Condition	100%		100%			
***THD_I* [%]**	1.55		1.37		1.4	
	Mag. [A]	**Angle [deg]**	**Mag. [A]**	**Angle [deg]**	**Mag. [A]**	**Angle [deg]**
H1	**17.3**		**20.2**	**38.7**	**21.683**	**38.7**
H3	0.1629		0.1936	110.1	0.206	110.1
H5	0.1941		0.1673	-176.1	0.211	-176.1

H7	0.0537		0.0504	-101.7	0.061	-101.7
H9	0.0069		0.0060	-26.6	0.008	-26.6
H11	0.0260		0.0544	49.9	0.046	49.9
H13	0.0416		0.0464	129.9	0.051	129.9
H15	0.0069		0.0060	-145.7	0.008	-145.7
H17	0.0139		0.0181	-51.4	0.018	-51.4
H19	0.0087		0.0121	52.6	0.012	52.6
H21	0.0052		0.0101	153.6	0.009	153.6
H23	0.0087		0.0121	-115.3	0.012	-115.3
H25	0.0069		0.0121	-30.8	0.011	-30.8
H27	0.0017		0.0121	57.1	0.008	57.1
H29	0.0087		0.0101	157.9	0.011	157.9

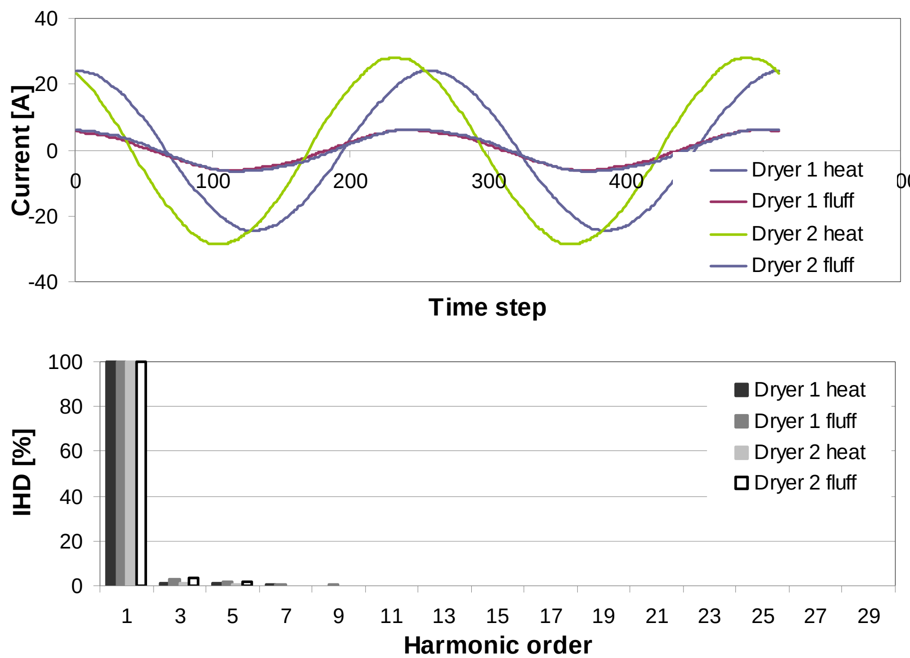

Figure A-14. Measured waveform and spectra of two dryers operating in two duty cycles

Heat-Pump Furnace

One installed fully-operating heat pump was measured at the service panel of one house. Its waveform and normalized spectra are shown in Figure A-15. It can be seen that this device operates at similar conditions when it is either heating or cooling the house environment. Table A-15 shows its characteristics. The presented results are for the condition that it consumed the largest observed amount of power.

Table A-15. Characteristics of the measured furnace

Manufacturer	**Unknown**	
Model	N/A	
Condition	100%	
Operating Power [W]	535	
***THD_I* [%]**	10.5	
	Mag. [A]	**Angle [deg]**
H1	**5.16**	**-33.0**
H3	0.50480	-159.4
H5	0.19938	78.6
H7	0.04851	141.5
H9	0.02654	-30.8
H11	0.01957	-131.7
H13	0.00636	-78.7
H15	0.00393	125.7
H17	0.00645	-0.1
H19	0.00167	-179.2
H21	0.00115	45.0
H23	0.00342	-120.9
H25	0.00149	94.1
H27	0.00372	55.0
H29	0.00083	-3.1

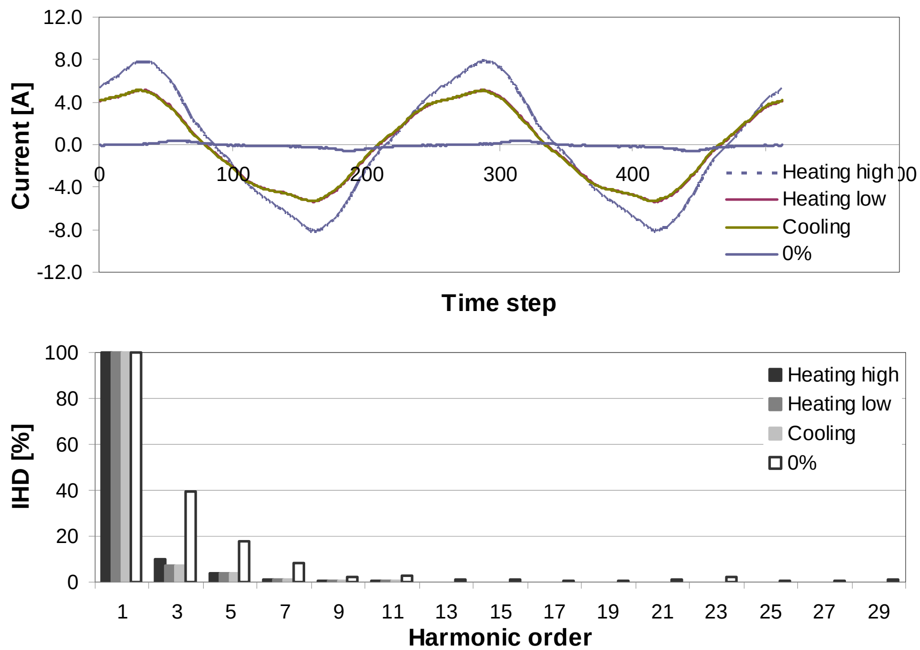

Figure A-15. Measured time-domain waveform of the furnace operating at 4 different cycles

Appendix B

Numerical Issues Encountered in Chapter 4

Numerical difficulties were encountered when performing the least-squares solution presented in chapter 4. This appendix explains the main numerical problems.

B.1 Matrix Conditioning

Numerical problems may arise when inverting the normal matrix. Such problems were observed for the Full Model and coupled *Y* model. The cause of these problems was the ill-conditioning of the normal matrix. The condition number was monitored and observed to be always very high. This factor can measure the conditioning of a matrix: the closer to 1, the better conditioned the matrix is. To try to overcome the numerical instability, a decomposition technique was used. In the application of least-squares, the matrix to be inverted, called the normal matrix, is often ill-conditioned, and a singular-value-decomposition (SVD) was an attempt to improve the results. This decomposition allows the inverse to be obtained by using equation (B.1):

$$\left[V_{h,m}V_{m,h}^{T}\right]^{-1} = VD^{-1}U^{T}, \; where \; D^{-1} = diag\left(\frac{1}{\sigma_1}, \frac{1}{\sigma_2}, \ldots \frac{1}{\sigma_n}\right). \tag{B.1}$$

If the matrix is ill-conditioned, SVD can be used to approximate its inverse by using the following matrix:

$$\left[V_{h,m}V_{m,h}^{T}\right]^{-1} = UDV^{T} \approx VD_0^{-1}U^{T}. \tag{B.2}$$

$$D_0 = \begin{cases} \dfrac{1}{\sigma_i}, & if\, \sigma_i > \varepsilon \;\; (\varepsilon\, is\, a\, small\, threshold). \\ 0, & otherwise. \end{cases} \tag{B.3}$$

This technique slightly improved the solution when the coupled models were being obtained, but was not able to completely overcome the numerical instability. Therefore, the results were not satisfactory. The decoupled model, which does not suffer from this numerical instability, is theoretically immune to this problem, and, as shown in the results, seems to be accurate in predicting the CFL harmonic current injections.

B.2 Improving the Diversity of the Measurements

The choice of using the measurements from twelve CFLs has been shown to be of great usefulness in performing the least squares optimization. CFLs of the most popular brands are used to estimate a model that, in theory, can fit all CFLs. By using such a model, the diversification of the related voltages-currents increased the degree of independence of the measurements, and the results were improved. In order to obtain the model by using different CFLs, their currents were normalized by the rated current of each CFL, and the voltages were normalized by the rated voltage. The same diversification technique was adopted for estimating the PCs' and LCD monitors' models. For these last cases, however, fewer measured units were used – 6 PCs and 3 LCD monitors.

Appendix C

Instrumentation Accuracy

For all measurements presented in this thesis, the same set of instruments was used. This appendix describes the accuracy of the data recorded by the instruments used in this thesis.

C.1 Characteristics of Instruments

The voltage probes used are the Differential Probe for Power Management, Model 4232, manufactured by ProbeMaster. This type of probes has the following specification:

Bandwidth:	DC to 25 MHz (-3dB)
Accuracy:	±2%
Attenuation Ratio:	1:10 and 1:100
Input Voltage:	±70V (DC + Peak AC) or 50Vrms for 1/10
Max. Differential:	±700V (DC +Peak AC) or 500Vrms for 1/100
Max. Common Mode	±700V (DC + Peak AC) or 500Vrms
<u>Output Voltage</u>	
Max. Amplitude:	±7V (into 2K OHM load)
Offset (Typical):	<+5mV, -10°C to 40°C
Noise (Typical):	1.5 to 2mV

The current probes used are the Fluke 80i-110s AC/DC Current Clamp, manufactured by Fluke. This type of probes has the following specification:

Current Range:	0.1 to 100A DC or 0.1 to 70A AC

Basic Accuracy (DC to 1kHz):	100mV/A setting: 50mA to 10A +/- 3% of reading + 50mA 10mV/A setting: 50mA to 40A +/- 4% of reading + 50mA 40A to 80A +/- 12% of reading + 50mA 80 to 100A +/- 15% of reading
Output Signal:	10A range: 100mV/A | 100A range: 10mV/A
Bandwidth:	1Hz to 20kHz

The data were collected using the National Instruments' **NI DAQPad-6020E USB** data acquisition system, which has the following characteristics:

- **Inputs:** 8 differential BNC analog inputs (12-bit),
- **Sampling Rate:** 100 KS/s

C.2 Measurement Accuracy

The A/D conversion introduces quantization error. The data collected are in the form of digital values while the actual data are in analog form. So the data are digitalized with an A/D converter. The error associated with this conversion is the quantization step. As the energy of current signals drops to a level comparable to that of quantization noises, the signal may be corrupted, and the data will, therefore, be unreliable. For this reason, if the harmonic currents are of magnitude lower than that of the quantization error, they should not be trusted. This criterion was developed as follows:

1. The step size of the quantizer is

$$\Delta = \frac{V_{in}}{2^n} = \frac{1}{2^{12}}, \tag{C.1}$$

where n is the number of bits, and V_{in} is the input range. All measurements presented in this report were taken with an input range of 1 V (-0.5V to 0.5V).

2. The current probe ratio is k_{probe}, which is the ratio V/A. This ratio is used because the data acquisition device uses voltage as an analog input, whereas the measurements are currents.

3. Therefore, the step size in amps is

$$\Delta_I = \frac{\Delta}{k_{probe}}. \tag{C.2}$$

4. Finally, the maximum quantization error will be half of the step size.

For the measurement of individual appliances (Chapter 2), the probe ratio was set to 100 mV/A. The step size is, therefore,

$$\Delta_I = \frac{\Delta}{k_{probe}} = \frac{1}{k_{probe} \times 2^{12}} = 0.00244A. \tag{C.3}$$

The maximum quantization error is 0.00122A.

For all measurements related to the attenuation effects (Chapter 3), the probe ratio was always set as 10 mV/A. The step size is

$$\Delta_I = \frac{\Delta}{k_{probe}} = \frac{1}{k_{probe} \times 2^{12}} = 0.0244A. \tag{C.4}$$

The maximum quantization error is 0.0122A.

For all measurements related to the appliances modeling (Chapter 4), the probe ratio was set as 10 mV/A. The step size is

$$\Delta_I = \frac{\Delta}{k_{probe}} = \frac{1}{k_{probe} \times 2^{12}} = 0.0244A. \tag{C.5}$$

In this case, the maximum quantization error is, therefore, 0.0122A.

For all measurements related to the interharmonics (Chapter 6), the probe ratio was set as 10 mV/A. The step size is

$$\Delta_I = \frac{\Delta}{k_{probe}} = \frac{1}{k_{probe} \times 2^{12}} = 0.0244A. \tag{C.6}$$

In this case, the maximum quantization error is, therefore, 0.0122A.

In summary, the quantization error encountered by this project is in the range of 0.00122A to 0.0122A. The implication is that if the corresponding current value is less than these errors, they cannot be trusted.